8-6-2021

Assessment and optimization of marsh terracing for wetland restoration in the northern Gulf of Mexico using remote sensing and a wave model approach

Raúl Jefferson Osorio Morillo
raulosoriomorillo@yahoo.es

Assessment and optimization of marsh terracing for wetland restoration in the northern Gulf of Mexico using remote sensing and a wave model approach

By

Raúl Jefferson Osorio Morillo

Approved by:

Anna C. Linhoss (Major Professor)
Adam Skarke
Padmanava Dash
Mohammadmehdi Armandei
Prem B. Parajuli
Steven H. Elder (Graduate Coordinator)
Jason M. Keith (Dean, Bagley College of Engineering)

A Dissertation
Submitted to the Faculty of
Mississippi State University
in Partial Fulfillment of the Requirements
for the Degree of Doctor of Philosophy
in Biological Engineering
in the Department of Agricultural and Biological Engineering

Mississippi State, Mississippi

August 2021

Name: Raúl Jefferson Osorio Morillo

Date of Degree: August 6, 2021

Institution: Mississippi State University

Major Field: Biological Engineering

Major Professor: Anna C. Linhoss

Title of Study: Assessment and optimization of marsh terracing for wetland restoration in the northern Gulf of Mexico using remote sensing and a wave model approach

Pages in Study: 121

Candidate for Degree of Doctor of Philosophy

Coastal Louisiana U.S. is facing wetland loss caused mainly by geologic subsidence and sea-level rise. These losses are accelerated by human activities such as the creation of canals and waterways for gas and oil extraction. Wetland loss in coastal Louisiana has encouraged to the implementation of various wetland restoration techniques. Marsh terraces are a one restoration technique consisting of segmented berms of soil that are built in inland coastal ponds. They are designed to increase marsh area, dissipate wind driven waves, encourage marsh expansion, and possibly reduce shoreline erosion. Marsh terraces have been implemented for almost 30 years; however, little research has been conducted to determine their effectiveness at reducing wave energy. Therefore, the overall goal of this research is to find the most optimal terrace design at reducing significant wave height, and therefore wave energy. The specific objectives of this study are to 1) assess terrace performance and longevity over time, 2) simulate wave climates in marsh terrace sites and determine the effectiveness of marsh terraces for the reduction of wave energy, and 3) assess the effectiveness of different terrace designs at reducing significant wave height during low winds and cold front passages in coastal Louisiana. These objectives were accomplished through remote sensing and numerical wave modeling. This study found that there

was more predominant deposition than erosion in 20 marsh terrace fields. The study also used a numerical model to simulate small, high frequency waves in two terrace sites, finding an agreement between modeled and observed data. Moreover, wave height was reduced in terrace sites compared to unterraced sites. Finally, it was found that the chevron design is the most optimal terrace design at reducing significant wave height in a variety of wind conditions. This study adds to our knowledge of marsh terrace performance. In this way, marsh terraces may be used as an effective restoration technique at reducing wave energy, not just in Louisiana, but throughout the Gulf Coast, the U.S., and other coasts worldwide that are facing wetland loss.

DEDICATION

This dissertation is dedicated to my beloved wife and best friend Claudia, who has supported and cheered me up me every day since the beginning of this journey. Her support and love through this degree and during the pandemic has been invaluable. To my sister Sabine, remember, the sky is the limit, follow your dreams but always remember where we come from. To my dad Eusevio, who always encouraged me to learn English and motivates me to keep going. To my role model, my mom Liliana, my personal and professional growth are the result of your decisions, mentoring, support, and all the love you give to me. Finally, to my grandmother and angel Clemen, who raised me and still protects me from above. This success is yours as well!

"Ser más, para servir mejor"

ACKNOWLEDGEMENTS

First, I would like to thank God and the Mother of sorrows for all the blessings. Thanks to this country, the U.S., who opened its doors and welcomed me and my wife, letting us to pursue and accomplish our dreams.

An immense and sincere thanks to my advisor and main professor Dr. Anna C. Linhoss, who believed in me since the beginning and gave me the opportunity to pursue my Ph.D. Her mentoring, support, and guidance has made me grow as a scientist. Anna, thank you for introducing me to the modeling world. I would also like to thank my committee members Dr. Skarke, Dr. Dash, Dr. Armandei and Dr. Parajuli for all the help and input provided to this dissertation. A special thanks to the marsh terracing team from Mississippi State and Ducks Unlimited during this project. I have learnt a lot from you during field work and during our meetings, it was great to being part of such a multidisciplinary team.

I would like to thank the National Academy of Sciences, Engineering and Medicine, Gulf Research Program, for providing the funding to conduct this project (grant number 2000008944). I would also like to thank the landowners in coastal Louisiana who let us conduct research in their properties, without their permission no data collection would have been possible. Thank you as well to the friends I made at ABE 330, your company and our lunches made this journey more fun. Ramin, thank you for your friendship and for your everyday kindness, as you always say, we can accomplish whatever we want to.

A special and deepest thanks to my wife Claudia, for your everyday support, motivation, and the love you give to me. Thank you for your patience while reviewing my manuscripts, I know you learned a lot about waves as well. Thank you for taking care of me during this journey and during the challenging times of the pandemic. I love you; brighter days are coming.

Last, but not least, I would like to thank my family, my mom, my dad, and my sister. Being far away from all of you has probably been one of the biggest challenges of this journey. Thank you for your support, motivation, love, and for always being there for me. I love you and miss you every day.

"Labor Omnia Vincit"

TABLE OF CONTENTS

LIST OF TABLES

LIST OF FIGURES

CHAPTER I

INTRODUCTION

The Gulf of Mexico has wetlands as major ecological features. Coastal ponds are depressions with open shallow water, usually unvegetated and commonly found on marsh platforms predominant in the coast of Louisiana [1, 2]. Wave–induced erosion, is the main process responsible for marsh pond creation, expansion, and pond depth increase [2]. This area undergoes a high percentage of wetland loss caused mainly by direct and indirect effects of natural erosive processes. In coastal Louisiana, the rate of wetland loss is exceptionally high due to the combined effect of subsidence (5–10 mm per year) [3–5] and sea level rise (12± 8 mm per year) [3]. To address wetland loss, many restoration programs have implemented wetland restoration techniques such as breakwaters, sediment retention structures, sediment diversions, saltwater barriers, levees, impoundments, and marsh terraces [6–8]. Marsh terracing is a wetland restoration technique involving linear segmented ridges of soil that are built in shallow, inland coastal ponds that were once marsh [6]. Marsh terraces have been implemented for almost 30 years to slow and potentially reverse coastal wetland loss by reducing marsh pond creation and shoreline erosion [1, 9]. The objectives of marsh terracing is to reduce wave energy, increase marsh area, and possibly reduce shoreline erosion [10]. However, further research is needed to determine the effectiveness of marsh terraces and to identify an optimal design to reduce wave energy [10].

Remote sensing methods have been applied successfully in several research projects to identify and assess many aspects of wetlands [11–13]. Marshes are considered a relatively easy

type of wetland to identify [14] along with marsh terraces. Even though terraces have a narrow shape and are small land features in coastal ponds, they are possible and easy to identify using aerial high-resolution imagery [15]. There is limited research using remote sensing to assess marsh terrace performance related to erosional and depositional processes. A few unpublished reports have assessed individual terrace performance during a short period of time [16–19]. Therefore, there was the need for a study assessing the performance of multiple marsh terrace sites over time using remote sensing techniques [15].

Hydrodynamic and wave modeling has been widely used to assess wave climates in wetlands under different weather conditions [20–22]. Also, wave modeling has proven effective in simulating wave conditions in shallow water environments that are semi-protected by an artificial or a natural marine structure [23–25]. However, very limited research has been conducted to assess hydrodynamics in marsh terrace environments using numerical modeling [19]. This study utilized the Simulating Waves Nearshore (SWAN) to better understand the effect of terraces on wave climate in marsh terrace environment. SWAN is a numerical third–generation phase–averaged model based on the spectrum concept that solves the energy balanced equation to simulate wave conditions in coastal and inland shallow water environments [26].

For the purposes of this study, terrace efficacy will be defined as the ability to reduce wave height and enhance sediment deposition. Therefore, it is necessary to identify which terrace designs factors (shape, spacing, orientation) are more important at reducing wave energy under different environmental conditions (geological processes, wind, and waves). Identifying an efficient terrace design and marsh terrace performance over time will help restoration agencies with the efficient implementation of this technique.

The central hypothesis of this dissertation is that some marsh terrace designs reduce wave energy and enhance deposition more efficiently than others. The main goal of this dissertation is to find the most optimal terrace design at reducing significant wave height, and therefore wave energy. To accomplish the main goal, the overall objectives of this study are to: 1) assess terrace performance over time related with erosional and depositional processes 2) simulate wave climates in marsh terrace sites, conduct wave model validation, and determine the effectiveness of marsh terraces for the reduction of significant wave height, and 3) assess the effectiveness of different terrace designs at reducing significant wave height during low winds and cold front passages in coastal Louisiana. Specific project objectives will be mentioned in the following chapters.

There is limited research related with terrace design, therefore, the current study will update and enhance our knowledge on marsh terraces design factors affecting the reduction of significant wave height. In this way, marsh terraces can be evaluated as an effective restoration technique in the Gulf Coast, encouraging their implementation in the U.S., and other coasts facing wetland loss worldwide.

REFERENCES

[1] Vinent, O. D.; Herbert, E. R.; Coleman, D. J.; Himmelstein, J. D.; Kirwan, M. L. Onset of Runaway Fragmentation of Salt Marshes. *One Earth*, **2021**.

[2] Mariotti, G. Revisiting Salt Marsh Resilience to Sea Level Rise: Are Ponds Responsible for Permanent Land Loss? *J. Geophys. Res. Earth Surf.*, **2016**, *121* (7), 1391–1407.

[3] Jankowski, K. L.; Törnqvist, T. E.; Fernandes, A. M. Vulnerability of Louisiana's Coastal Wetlands to Present-Day Rates of Relative Sea-Level Rise. *Nat. Commun.*, **2017**, *8*, 14792.

[4] Yuill, B.; Lavoie, D.; Reed, D. J. Understanding Subsidence Processes in Coastal Louisiana. *J. Coast. Res.*, **2009**, 23–36.

[5] Morton, R. A.; Bernier, J. C. Recent Subsidence-Rate Reductions in the Mississippi Delta and Their Geological Implications. *J. Coast. Res.*, **2010**, 555–561.

[6] Turner, R. E.; Streever, B. *Approaches to Coastal Wetland Restoration: Northern Gulf of Mexico*; Kugler Publications, 2002.

[7] Ducks Unlimited. Geodatabase of Existing Marsh Terraces, 2015.

[8] O'Connell, J. L.; Nyman, J. A. Marsh Terraces in Coastal Louisiana Increase Marsh Edge and Densities of Waterbirds. *Wetlands*, **2010**, *30* (1), 125–135.

[9] Smith, J. M.; Cialone, M. A.; Wamsley, T. V; McAlpin, T. O. Potential Impact of Sea Level Rise on Coastal Surges in Southeast Louisiana. *Ocean Eng.*, **2010**, *37* (1), 37–47.

[10] Brasher, M. G. Review of the Benefits of Marsh Terraces in the Northern Gulf of Mexico. **2015**, No. May.

[11] Guo, M.; Li, J.; Sheng, C.; Xu, J.; Wu, L. A Review of Wetland Remote Sensing. *Sensors*, **2017**, *17* (4), 777.

[12] Couvillion, B. R.; Barras, J. A.; Steyer, G. D.; Sleavin, W.; Fischer, M.; Beck, H.; Trahan, N.; Griffin, B.; Heckman, D. Land Area Change in Coastal Louisiana from 1932 to 2010. **2011**.

[13] Oliver-Cabrera, T.; Wdowinski, S. InSAR-Based Mapping of Tidal Inundation Extent and Amplitude in Louisiana Coastal Wetlands. *Remote Sens.*, **2016**, *8* (5), 393.

[14] FGDC. *Application of Satellite Data for Mapping and Monitoring Wetlands*; Washington, DC, 1992.

[15] Osorio, R. J.; Linhoss, A. Evaluation of Marsh Terraces for Wetland Restoration: A Remote Sensing Approach. *Water*, **2020**, *12* (2), 336.

[16] Good, B.; Peele, H.; Bourgeois, R. Aerial Growth of the Sabine Marsh Terracing Project over a Ten-Year Period. *Rep. to Louisiana Dep. Nat. Resour. Interag. Agreem.*, **2005**, 2505–2512.

[17] Castellanos, D.; Aucoin, S. *Operations, Maintenance, and Monitoring Report for Little Vermilion Bay Sediment Trapping (TV-12)*; 2004.

[18] Thibodeaux, C.; Guidry, M. *2009 Operations, Maintenance, and Monitoring Report for Pecan Island Terracing (ME-14)*; Lafayette, Louisiana, USA, 2009.

[19] Marie, M. Geomorphic Efectiveness of Marsh Terracing as a Coastal Restoration Technique in Southern Louisiana, Tulane University, 2020.

[20] Leonardi, N.; Carnacina, I.; Donatelli, C.; Ganju, N. K.; Plater, A. J.; Schuerch, M.; Temmerman, S. Dynamic Interactions between Coastal Storms and Salt Marshes: A Review. *Geomorphology*, **2018**, *301*, 92–107.

[21] Barbier, E. B.; Georgiou, I. Y.; Enchelmeyer, B.; Reed, D. J. The Value of Wetlands in Protecting Southeast Louisiana from Hurricane Storm Surges. *PLoS One*, **2013**, *8* (3).

[22] Mariotti, G.; Fagherazzi, S.; Wiberg, P. L.; McGlathery, K. J.; Carniello, L.; Defina, A. Influence of Storm Surges and Sea Level on Shallow Tidal Basin Erosive Processes. *J. Geophys. Res. Ocean.*, **2010**, *115* (C11).

[23] Cooper, A. H.; Mulligan, R. P. Application of a Spectral Wave Model to Assess Breakwater Configurations at a Small Craft Harbour on Lake Ontario. *J. Mar. Sci. Eng.*, **2016**, *4* (3), 46.

[24] Vona, I.; Gray, M. W.; Nardin, W. The Impact of Submerged Breakwaters on Sediment Distribution along Marsh Boundaries. *Water*, **2020**, *12* (4), 1016.

[25] Vieira, B. F. V; Pinho, J. L. S.; Barros, J. A. O.; Antunes do Carmo, J. S. Hydrodynamics and Morphodynamics Performance Assessment of Three Coastal Protection Structures. *J. Mar. Sci. Eng.*, **2020**, *8* (3), 175.

[26] Booij, N.; Ris, R. C.; Holthuijsen, L. H. A Third-generation Wave Model for Coastal Regions: 1. Model Description and Validation. *J. Geophys. Res. Ocean.*, **1999**, *104* (C4), 7649–7666.

CHAPTER II

EVALUATION OF MARSH TERRACES FOR WETLAND RESTORATION: A REMOTE SENSING APPROACH

Introduction

Marsh Terracing

Marsh terracing is a wetland restoration technique consisting of segmented and discontinuous ridges of sediment built in coastal marsh areas [1–3] aligned in a variety of patterns (chevron, squares, circles, checkerboard, etc.). Berm widths range from two to five meters. However, berm length and spacing vary depending on design pattern and location [4,5]. The goal of marsh terracing is to reduce wave energy, minimize fetch between ridges, increase marsh area, and possibly reduce shoreline erosion [6,7]. Marsh terraces are usually built in shallow ponds, where natural marshes have been converted to open water [6]. They are constructed at the same elevation of the surrounding marsh to allow periodic inundation of the terraces [3]. Usually, marsh vegetation is planted around the perimeter of the terrace and in the intertidal area to prevent terrace erosion, enhance stability, and ecosystem diversity [7].

Marsh terracing is a relatively new restoration technique. It was first implemented in the U.S. in 1990 at the Sabine National Wildlife Refuge in Cameron Parish, Louisiana [1,8]. Currently, marsh terraces have only been constructed along the northern Gulf of Mexico. If proven effective, this restoration technique could be established in other marshes or shallow water regions with similar sediments conditions [2]. In fact, marsh terracing has the same principles of many land

reclamation techniques where the main goal is to create new land from coastal shallow areas by drying, pumping water, or raising the elevation of the waterbed in ponds or coastal areas. Land reclamation has been used for a long time in many coastal countries in Europe and Asia [9]. However, the goal of marsh terracing is to create marsh area for wetland recovery purposes and not to convert land for human activities like agriculture, industry, and residential [10].

Study Definitions

For this study, several terms are defined below. A terrace field is defined as an area including a set of terraces following the same pattern or having common attributes (e.g., construction date and design) within the same contiguous water body (inland pond). A terrace field of study is referred to any of the 20 terrace fields analyzed in this study. A terrace field does not include the shorelines or surrounding marsh platforms. Cumulative land change refers to the entire period of land change analyzed for each of the 20 terrace fields of study. Predominant deposition or erosion is defined as the strongest or main long-term geological process quantified throughout the cumulative land change analysis within the terrace field of study. Channels refers to natural or artificial waterways (canals) surrounding or adjacent to the terrace fields of study that may serve as an external supply of water or sediment. High channel density refers to terrace fields of study surrounded or connected by channels. Low channel density refers to either few channels surrounding or connecting terrace fields of study or channels surrounding but not connecting to terrace fields of study, generally blocked by structural marsh management (SMM) such as levees or dikes.

Wetland Restoration Techniques

Many restoration programs have implemented wetland restoration techniques that encourage the creation of new, coastal emergent marsh and potentially reduces sediment erosion and wetland loss [7]. Some examples of these restoration techniques are: breakwater, sediment retention structures, freshwater and sediment diversions, saltwater barriers, vegetative plantings, use of dredged material, and SMM including levees and impoundments [2,3,7,11]. One of the biggest challenges that wetland restoration projects face is assessing success over time and applying new findings to future programs [12,13] and remote sensing technology provides a great potential for change detection analyses and thus very useful in assessing the success of these restoration projects.

Remote Sensing in Wetland Analysis

Remote sensing methods have been used widely for studying wetland in many areas, for example, to assess land use/cover changes and wetland mapping [14]. Marshes are considered a relatively easy type of wetland to identify [15] compared to marsh terraces, which may be more challenging because they are relatively small and narrow pieces of land. Aerial imagery has been successfully used in studies where small areas were analyzed [14]; thus, high-resolution aerial imagery is best for identifying marsh terraces via remote sensing.

Remote sensing methods have been applied successfully across a diversity of projects to identify and assess many aspects of wetlands in Louisiana. For example, Penland et al. (2002) [16] classified coastal land loss between 1932 and 1990 in the Mississippi River Delta Plain using topographic maps and aerial photography. Barras et al., (2003) assessed coastal land loss from 1932–2000 and projected additional losses until 2050 using satellite and aerial images. Couvillion et al., (2011) detected land area changed from 1932 to 2010 in coastal Louisiana employing

historical surveys, aerial and satellite data. Oliver-Cabrera & Wdowinski (2016) [19] detected tidal inundation zones and assessed the interaction between coastal wetlands and tidal currents utilizing Interferometric Synthetic Aperture Radar (InSAR) observations using satellite data. These studies demonstrate the successful application of remote sensing methods in coastal Louisiana and the need for implementing wetland restoration projects in this area.

Unsupervised Classification and Change Detection Analysis

Unsupervised classification is a widely used remote sensing technique in wetland land use/cover classification analysis[20,21]. It is a per-pixel method using K-means or ISODATA algorithms to cluster pixels with similar spectral values together. Then the analyst provides information to organize, classify, interpret, and label the clusters into meaningful classes. This method is recommended when field data or previous knowledge of the study area is unavailable [22]. Sometimes clusters do not correspond to the correct class information and accuracy assessments are recommended to verify and correct this issue. Unsupervised classification, also called clustering, is a less time-consuming method than the supervised classification in which the collection of training data is the first and main step [23,24]. According to a review by Ozesmi and Bauer (2002) [25], unsupervised classification is the most commonly applied method to classify land cover in wetland environments.

Once an area has been classified into different land use and land covers, change detection analysis is used to assess change over time in that area. Change detection analysis can be used for understanding relationships between human activities and natural events. Hence, change detection can be used to improve the management of natural resources and to help in decision-making processes [26–28]. Change detection is performed to assess and quantify the historical changes of Earth's features due human or natural phenomena over time with reference to multi-temporal

datasets [26,29,30]. Different change detection algorithms include: write function memory insertion, multi-date composite image, image algebra (e.g., band or image differencing), post-classification comparison, binary mask applied to date 2, ancillary data source used as date 1, spectral change vector analysis, chi-square transformation, cross-relation, visual on-screen digitization, and knowledge-based vision systems [31]. According to Klemas (2010) [24] image differencing is the most commonly used change detection technique for monitoring wetland changes. Moreover, an important factor to consider when performing change detection analysis is using imagery acquired at the same time or near the same time of the year for every year of analysis to avoid differences related with phenological state, season, and sun angle [24–26].

Previous Studies Assessing Marsh Terrace Performance

Very few projects, remote sensing or otherwise, and a few unpublished technical reports have assessed the performance of marsh terraces regarding erosion and deposition [7]. In fact, there have been more studies on the ecological impacts of marsh terraces [6,32–34] than the success and longevity of marsh terrace physical design. This lack of study on terrace design success has limited the implementation of this technique more widely [7]. The lack of analysis is particularly surprising considering the 980-linear km of marsh terraces (and 90 terrace fields) that have been constructed [35].

In one of the few studies on marsh terrace design success, Steyer (1993) [8] reported marsh gain at two terraced fields at the Sabine National Wildlife Refuge (NWR) after one year of construction. In this study, a total of 1.47 ha. of emergent marsh were mainly present on the terrace footprints. Two years post terrace construction, new vegetation covered adjacent areas of the terrace footprints resulting in 6.8 ha. of new marsh. In another study of marsh terrace design success, Good et al. (2005) [36] assessed change in land area of two terrace fields at the same

Sabine NWR using GIS methods and aerial photography. This study documented a 4.71 ha. (18%) total increase of emergent marsh within the terrace field and adjacent areas of non-terraced islands and shorelines over a period of ten years.

Castellanos and Aucoin (2004) [37] compared aerial photography of one recently constructed terrace field and a reference site with 2 years post-construction imagery in the Little Vermilion Bay. They documented 2.1 ha (7%) land loss of two terrace fields and surrounding marsh. Also, they reported a mudflat increase of 80.7 ha in the terrace field and an increase of 4.51 ha in the reference site. Land loss was mainly attributed to sacrificial terraces built in the southern area of the terrace field. Thibodeaux et al. (2009) [38] monitored two terrace fields three years post-construction. They reported a decrease of 16% in emergent vegetation outside the terrace footprints in the Pecan Island restoration terrace field in southwest Louisiana compared with a nearby reference site that decreased by 9% in emergent vegetation. Miller et al. (2011) [39] performed a land change analysis from 2004–2007 for eastern Little Vermilion Bay and Little White Lake terrace sites in south central Louisiana. This analysis showed land gain of 7.3 ha and 2.8 ha, respectively along terrace edges in both terrace fields. While these results are promising they mostly present short-term findings from five terrace fields.

Study Objectives

In order to broadly assess the efficacy of marsh terraces, a more comprehensive review of terrace performance in multiple sites over multiple years is needed. Therefore, the objective of this study is to assess the change in marsh terrace area over time, using classification of high-resolution aerial imagery and subsequent change detection analysis. Questions that will be addressed in this research include: (1) how do the terraces perform over time and space and (2) which marsh terrace design factors are related to terrace performance?

Materials and Methods

Data and Study Area

Marsh terrace change over time was analyzed by two databases: (1) a marsh terrace geodatabase in ArcGIS platform as shapefiles created by Ducks Unlimited (DU) [35] and (2) approximately 120 aerial images from the National Agriculture Imagery Program (NAIP) [40] from five parishes in coastal Louisiana from 2003–2017. Due to limitations in NAIP imagery and computational time, all terrace fields were not assessed. Three criteria were used to select a subset of terrace fields which includes terrace age, geopolitical location, and imagery cloud cover. These criteria are described below.

First, terrace fields of study that were at least ten years old (built between 2003 and 2007) were selected. Ten years of aerial imagery provided a time lapse, which could be considered as a sufficient time-period to evaluate moderately long-term terrace performance. Terraces built before 2003 were not included in the analyses because NAIP imagery was only available since 2003.

Second, specific fields of study were further randomly selected based on their geopolitical location. Coastal Louisiana is politically divided in eight parishes and geomorphologically divided in two regions, the Chenier Plain in the southwest and the Deltaic Plain of the Mississippi River in the southeast (Figure 2.1). Both regions differ in geologic processes, coastal morphology, and hydrological characteristics [6]. Furthermore, the rates of subsidence and relative sea-level rise are both greater in the Deltaic region (11.2 mm per year and 13.2 ± 8.8 mm per year, respectively) than in the Chenier Plain (7.5 mm per year and 9.5 ± 6.3 mm per year, respectively [41].

Third, after the terrace fields were screened based on the first two selection criteria, cloud free images were visually selected for unsupervised classification. The NAIP imagery with less than 10% cloud cover per quarter quad tile were selected [42].

According to the DU dataset [35], approximately 90 terrace fields have been built from 1990 until 2017 in Louisiana and Texas. Sixty out of these 90 terrace fields were built between 2003 and 2017, including 50 in the Chenier region and ten in Deltaic region. Most of the terrace fields were built in the Chenier Plain due to more suitable construction sites and substrates characteristics [43]. Based on the selection criteria, a total of 20 marsh terrace fields in coastal Louisiana were randomly selected. This resulted in six terrace study fields located in Cameron Parish, nine in Vermilion, one in Iberia, two in St. Mary, and two in Terrebonne. Thus, a total of seventeen terrace fields were from the Chenier region and three terrace fields were from the Deltaic region (Figure 2.1).

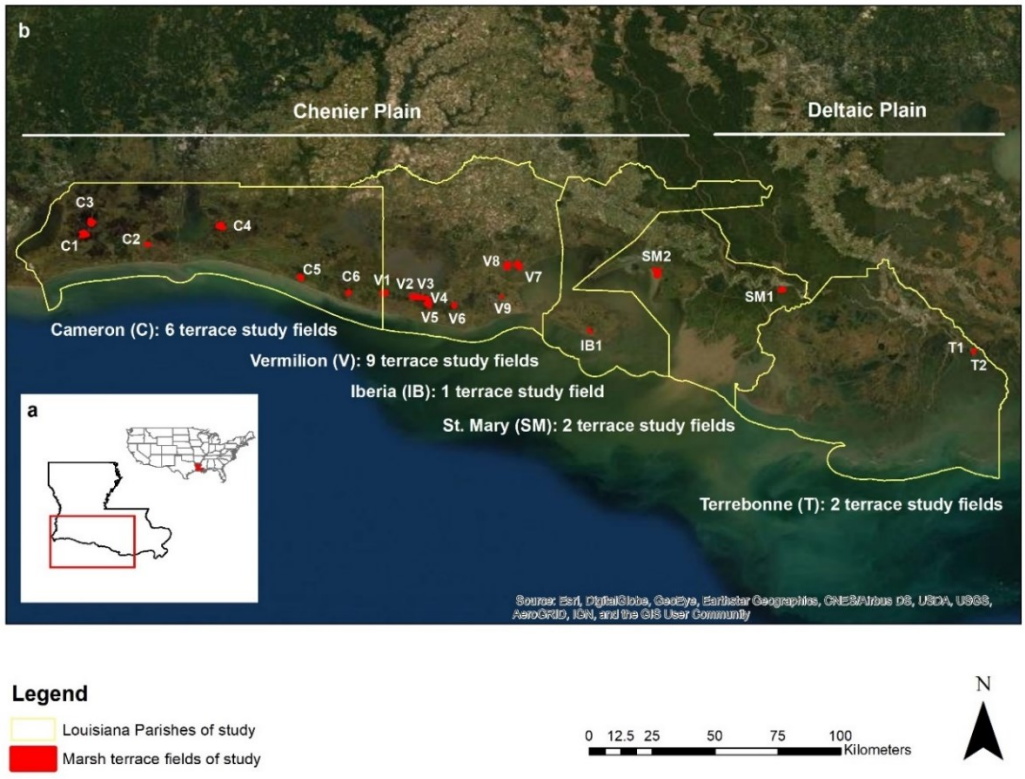

Figure 2.1 (a) Coastal Louisiana. U.S.; (b) Marsh terrace fields of study selected to assess performance over time in the Chenier Plain and Deltaic Plain Region in Coastal Louisiana.

NAIP aerial imagery has one-meter spatial resolution with three bands in the red, green, and blue wavelength region [42]. This imagery was used for three main reasons. First, it is freely available. Second, the one-meter spatial resolution is appropriate for this study. Third, NAIP imagery is already preprocessed by the federal program and is available in digital ortho-quarter quad tiles (DOQQs) or compressed in county mosaics (CCM) [42]. The imagery is already geometrically corrected to UTM coordinate system and are ortho-rectified for planimetric accuracy [44]. The remote sensing method applied standard photogrammetric techniques to the NAIP imagery.

Water level data was downloaded from the Louisiana's Coastwide Reference Monitoring system (CRMS) website [45] matching the time of imagery acquisition. This was done to identify potentially misleading results in the marsh terrace change in area due to water level fluctuations. It is important to mention that in some of the marsh terrace fields in the Chenier Plain, water levels are controlled by water control structures, which are managed by property owners. Structural marsh management (SMM) has been predominant in the Chenier Plain [46] since the middle of the 1950's, with the purpose of reducing saltwater intrusion, control water level, and reducing open water areas [47,48]. SMM techniques include levees, impoundments, and water control structures [49].

Data Analysis

ArcMap 10.5.1 [50] was used to create feature classes of the terrace fields of study. Polygons were drawn for delineating each of the terrace fields without including the shoreline or surrounding marsh platform. Imagery subsetting and remote sensing unsupervised classification were performed using ERDAS IMAGINE Software [51]. Imagery subsetting was done using the terrace field polygons created in ArcMap and the NAIP imagery from Louisiana Parishes. As a

result, a mask was created for each terrace field of study. The Iterative Self Organizing Data (ISODATA) algorithm [23] was used to derive information clusters based on a previous study [32]. This was done with the purpose of classifying the aerial imagery into land and water categories. A minimum distance algorithm was used in this study. Marsh terrace fields of study, where floating aquatic vegetation or submerged aquatic vegetation (SAV) were present in the aerial imagery, were classified using three categories (water, land, aquatic vegetation) instead of just 2 (water and land). Those fields were classified with utmost care by creating more classes after properly recoding them following suggestions given by Couvillion et al. (2011) [18]. This was done to achieve higher accuracy and to avoid misclassification.

ArcMap 10.5.1 and PythonWin 2.7.13 [52] were used to edit classified rasters, add fields, generate new categories in the rasters, create and reclassify difference maps, and generate land change detection maps for each terrace field of study. Post-classification image differencing was performed as change detection methods in this study. A class score was given to each classified land cover class (1 for water, 2 for land). Using the new class score value field, the classified image from the first chronological year of analysis or the year when the terrace was built (i.e., 2003) was subtracted from the other classified images (i.e., 2005, 2007… 2017), one by one. This analysis shows cumulative change over time for each image after the first image (i.e., 2003–2005, 2003–2007… 2003–2017). This post-classification difference map process separated the classified raster pixels in three categories: erosion, deposition, and no change. Post-classification image differentiation was performed to obtain the cumulative change in the erosion and deposition of the terrace fields of study.

Accuracy assessments were conducted from classified imagery. A confusion matrix [53,54] was computed using randomly chosen accuracy assessment points. These random points

were created using an equalized stratified random sampling strategy so that each class had the same number of points. A table was created where each random point had a record for ground truth and for the classified image value. The ground truth field was updated by visually comparing the classified value with the equivalent area in Google Earth Pro [55] and NAIP imagery. The confusion matrix calculated errors of omission and commission; and finally, a kappa index was derived denoting agreement and an overall accuracy. Kappa index ranges from 0 to 1. Coefficients higher than 0.7 are considered acceptable and those equal or lower than 0.4 indicate a low correlation between the classified image and the reference image of comparison [56,57]. This was conducted based on the importance of having high classification accuracy in the images to detect real changes and to avoid misleading classification results [25].

The change detection analyses were performed every two/three-years depending on the terrace field of study. Due to imagery limitations, the same years could not be analyzed for every terrace field of study. If the desired imagery had cloud cover or if it was not available, the previous or following year was assessed. Spatial measurements such as land change percentages and area in hectares, and accuracy assessments were calculated. Similar to the Good et al. (2005) [36] study, inferential statistics were not applied because treatment replication (between terrace fields and over time) is impractical [58].

The results from these analyses, predominantly erosional or depositional terrace fields, were related to the following independent terrace design factors: terrace location (Chenier or Deltaic region), terrace shape (linear, chevron, rectangular or other), terrace size (small <40 hectares, big >40 hectares), alignment of the terraces (north, south, east, west and diagonal), and finally a visual identification to determine if the terrace fields were surrounded or connected by channels, levees, or open water.

Due to computational time, the number of terrace study fields was limited to 20. This, in addition to the fact that treatment replications are impractical, made statistical analyses unfeasible. As such, results from this study should be considered descriptive rather than quantitative.

Results

Overall, in the marsh terrace fields of study, performance over time showed more predominant deposition (55%) than erosion (45%). A confusion matrix, summarizing the accuracy assessment results for the classified imagery, is shown in Table 2.1. The mean Kappa index of agreement was 0.86 (86%) with a standard deviation of 0.11. The Kappa coefficient is considered acceptable for imagery classification [56,57]. Therefore, there is a strong agreement and good accuracy between the classified imagery and reference imagery. The mean and standard deviation of the errors of omission and commission for each class of the classified imagery are also shown in Table 2.1.

Table 2.1 Confusion Matrix showing the accuracy assessment results for the classified imagery. The values correspond to the mean ± the standard deviation of the classified imagery.

	Water	**Land**	**Total**	**Errors of Commission**	**Kappa**
Water	28.85 ± 1.73	0.99 ± 1.29	30 ± 0	0.97 ± 0.04	
Land	2.85 ± 3.11	26.69 ± 3.91	30 ± 0	0.89 ± 0.13	
Total	31.82 ± 3.77	27.92 ± 4.03	60 ± 0		
Errors of omission	0.91 ± 0.08	0.96 ± 0.05		0.93 ± 0.06	
Total					0.86 ± 0.11

Figure 2.2 shows an example of an analyzed marsh terrace field of study (C3), located in Cameron Parish, that demonstrated predominant deposition. This terrace field was constructed in 2006. In this example, overall cumulative terrace deposition was more predominant than

cumulative erosion, in other words deposition is higher than erosion in each period of analysis. This trend was consistent across years (Table 2.2; Figure 2.3). In this example, deposition mostly occurred in the southern portion of the terrace field of study (Figure 2.2e).

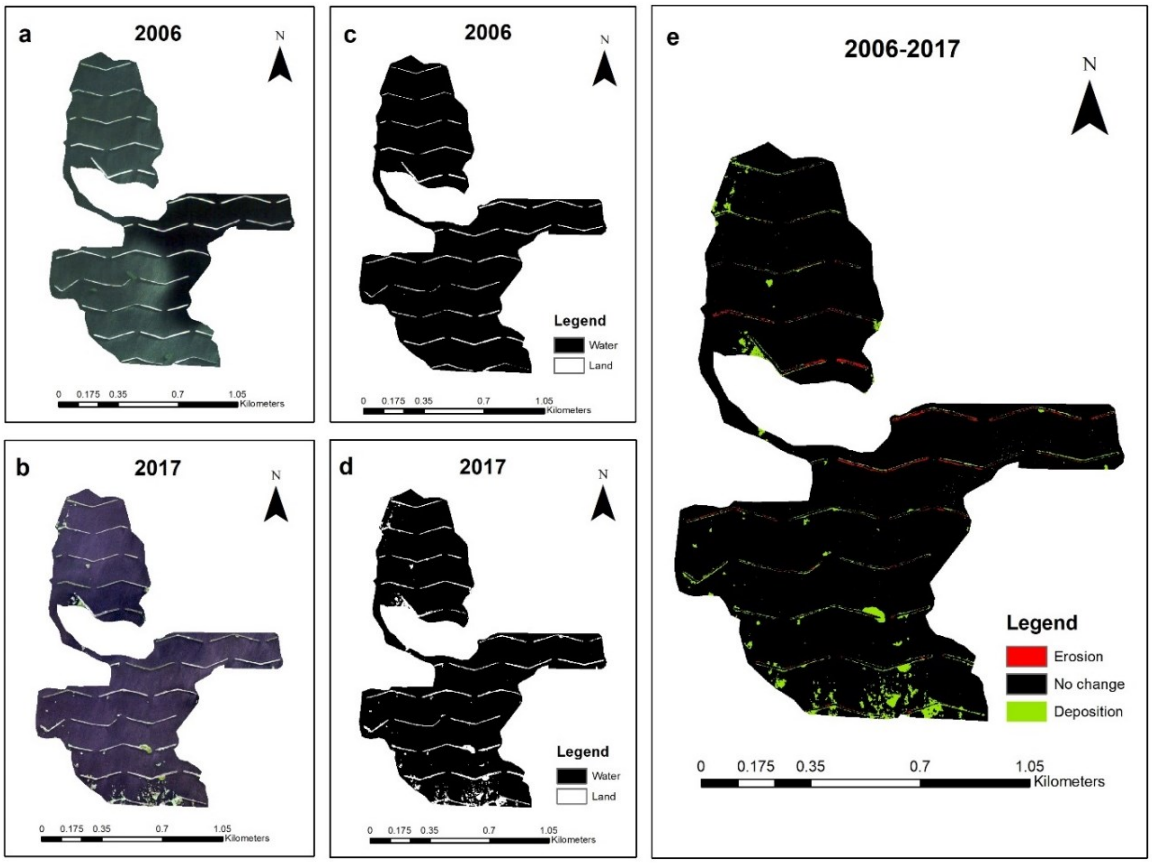

Figure 2.2 Analysis of a terrace field (C3) at Cameron Parish, LA. (a) Marsh terrace National Agriculture Imagery program (NAIP) imagery from 2006 showing the terraces recently built (where the white color is recently constructed and unvegetated terraces); (b) Marsh terrace NAIP imagery from 2017 showing the vegetated terraces (green color) after 11 years of establishment; (c) and (d) Marsh terrace land/water classified imagery from 2006 and 2017 respectively, where the white color represents the terraces and black color represents water within the polygon of analysis; (e) Change detection map from 2006–2017 where red color represents erosion, black is no change, and light green represent deposition.

Table 2.2 Cumulative land change % and area (ha) of C3 marsh terrace field at Cameron Parish LA.

	2006–2007		2006–2010		2006–2013		2006–2015		2006–2017	
	%	ha	%	ha	%	ha	%	ha	%	ha
Erosion	0.2	0.2	1.2	1.2	0.4	0.4	0.7	0.7	0.6	0.6
No Change	96.9	106.5	96.6	106.1	96.6	106.1	95.2	104.6	96.4	105.9
Deposition	2.9	3.1	2.3	2.5	3.1	3.3	4.1	4.5	3.1	3.3

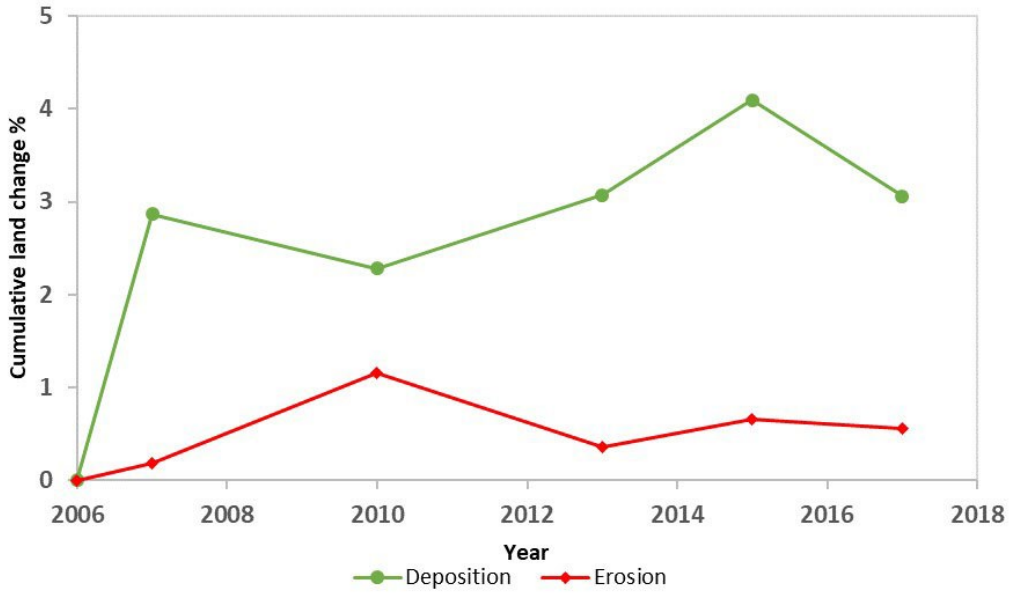

Figure 2.3 Trend graph showing cumulative marsh terrace performance from 2006–2017 of C3 terrace field of study.

The analysis described for terrace C3 was conducted for each of the remaining 19 terrace fields of study. The data for each of these analyses is too cumbersome to present in this publication. Thus, summary statistics are presented in Table 2.3.

Terrace fields of study showed predominant deposition in 11 (55%) terrace fields; eight of these depositional sites (47%) were located in the Chenier region, and three (100%) were located in the Deltaic region. Predominant erosion was found in nine (45%) of the terrace fields. All of

these erosional sites (53%) were located in the Chenier region (Table 2.3). In most cases, terrace fields that had high density of adjacent channels or relate to channels, thereby an external sediment source, displayed more predominant deposition (11) compared to terraces surrounded with a low density of channels (six; Table 2.3).

Table 2.3 Marsh terraces fields of study design factors and performance. Alignment definitions: west to east terrace alignment (W/E), north to south terrace alignment (N/S), arbitrary refers to a terrace alignment following different directions within a terrace field of study. Channel density definitions: high refers to channels surrounding or connecting with the terrace field of study; low refers to either few channels surrounding or connecting with the terrace field of study or presence of channels not connected with the terrace field of study blocked by levees or dikes. Performance refers to either predominant deposition or erosion in a field of study.

Terrace	Parish	Geological Region	Shape	Alignment	Area (Hectares)	Channel Density	Levees	Performance
C1	Cameron	Chenier	chevron	W/E	322.81	high	yes	deposition
C2	Cameron	Chenier	linear	W/E	12.61	low	yes	erosion
C3	Cameron	Chenier	chevron	W/E	109.54	high	yes	deposition
C4	Cameron	Chenier	chevron	diagonal	142.06	high	no	deposition
C5	Cameron	Chenier	rectangular	diagonal	54.82	high	yes	deposition
C6	Cameron	Chenier	linear	diagonal	11.78	high	no	erosion
V1	Vermilion	Chenier	chevron	W/E	98.58	high	yes	deposition
V2	Vermilion	Chenier	rectangular	W/E	312.69	low	yes	erosion
V3	Vermilion	Chenier	rectangular	N/S	218.83	low	yes	erosion
V4	Vermilion	Chenier	chevron	diagonal	279.27	low	yes	erosion
V5	Vermilion	Chenier	linear	arbitrary	25.03	high	yes	deposition
V6	Vermilion	Chenier	chevron	W/E	38.26	low	no	erosion
V7	Vermilion	Chenier	linear	arbitrary	169.11	high	no	deposition
V8	Vermilion	Chenier	linear	arbitrary	107.88	low	no	erosion
V9	Vermilion	Chenier	linear	diagonal	7.84	high	no	erosion
IB1	Iberia	Chenier	linear	N/S; W/E	29.53	high	no	erosion
SM1	St. Mary	Deltaic	chevron	diagonal	56.38	high	yes	deposition
SM2	St. Mary	Chenier	linear	arbitrary	430.23	high	no	deposition
T1	Terrebonne	Deltaic	linear	W/E	19.75	high	no	deposition
T2	Terrebonne	Deltaic	linear	W/E	22.95	high	no	deposition

In southwestern Louisiana, out of the six terrace fields of study in Cameron Parish, predominant deposition occurred in four and predominant erosion occurred in two terrace fields. Vermilion Parish had the highest number of predominant eroded terrace fields of study with a total of nine fields. In this parish, only three showed predominant deposition and the remaining six

showed predominant erosion. In Iberia Parish the single marsh terrace field that was analyzed showed predominant erosion over time. Both terrace fields of study in St. Mary showed predominant deposition. Finally, the two terrace fields of study located in Terrebonne showed predominant deposition. The results mentioned above are also spatially depicted in Figure 2.4.

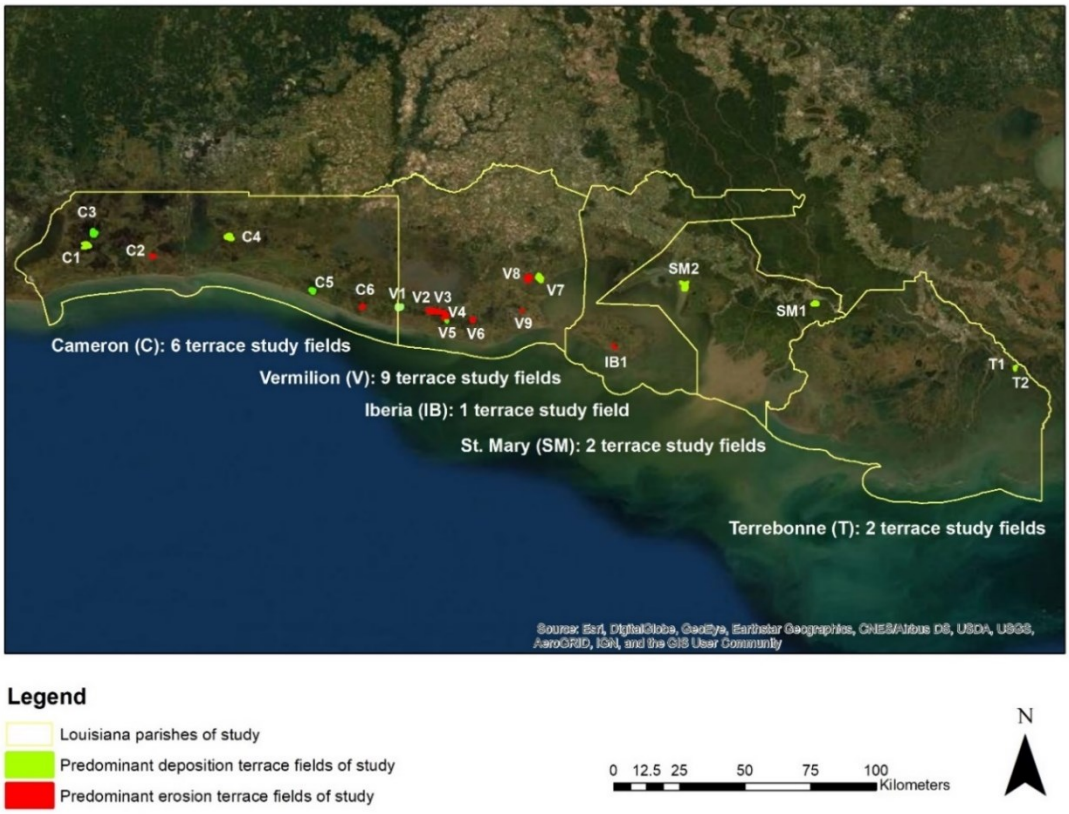

Figure 2.4 Marsh terrace fields of study performance over time in the Chenier Plain and Deltaic Plain Region in Coastal Louisiana. T1 and T2 are overlapping.

Figures 2.5 and 2.6 show trends of all the terrace fields' cumulative land change percentage over time. In most cases, trend lines do not cross, which means marsh terrace fields of study are either consistently erosional (seven fields of study, 35%) or depositional (seven fields of study, 35%).

One potential issue in this study was the fact that imagery was taken under varying hydrological and tidal regimes. This presented the threat of results reflecting changes in water elevation and not land loss. However, 70% of the results show consistent deposition or erosion. This consistency supports our conclusion that the change analysis represents changes in terraces area and not differences in water elevation. This conclusion was also supported by observing water level data at the date and time of the NAIP aerial imagery acquisition. In general water level fluctuated between 30 and 60 cm in terrace fields of study. Bolduc and Afton (2005) [49] also mentioned that water levels in ponds of managed marshes are between 29 and 39 cm on average. Imagery was observed for years with high (>60 cm) and low (<30 cm) water levels in the terrace fields of study. The absence of a halo effect surrounding the terraces and terraces design features, especially the slope and vegetation in the edges, confirmed that differences in water level did not affect the area of analysis.

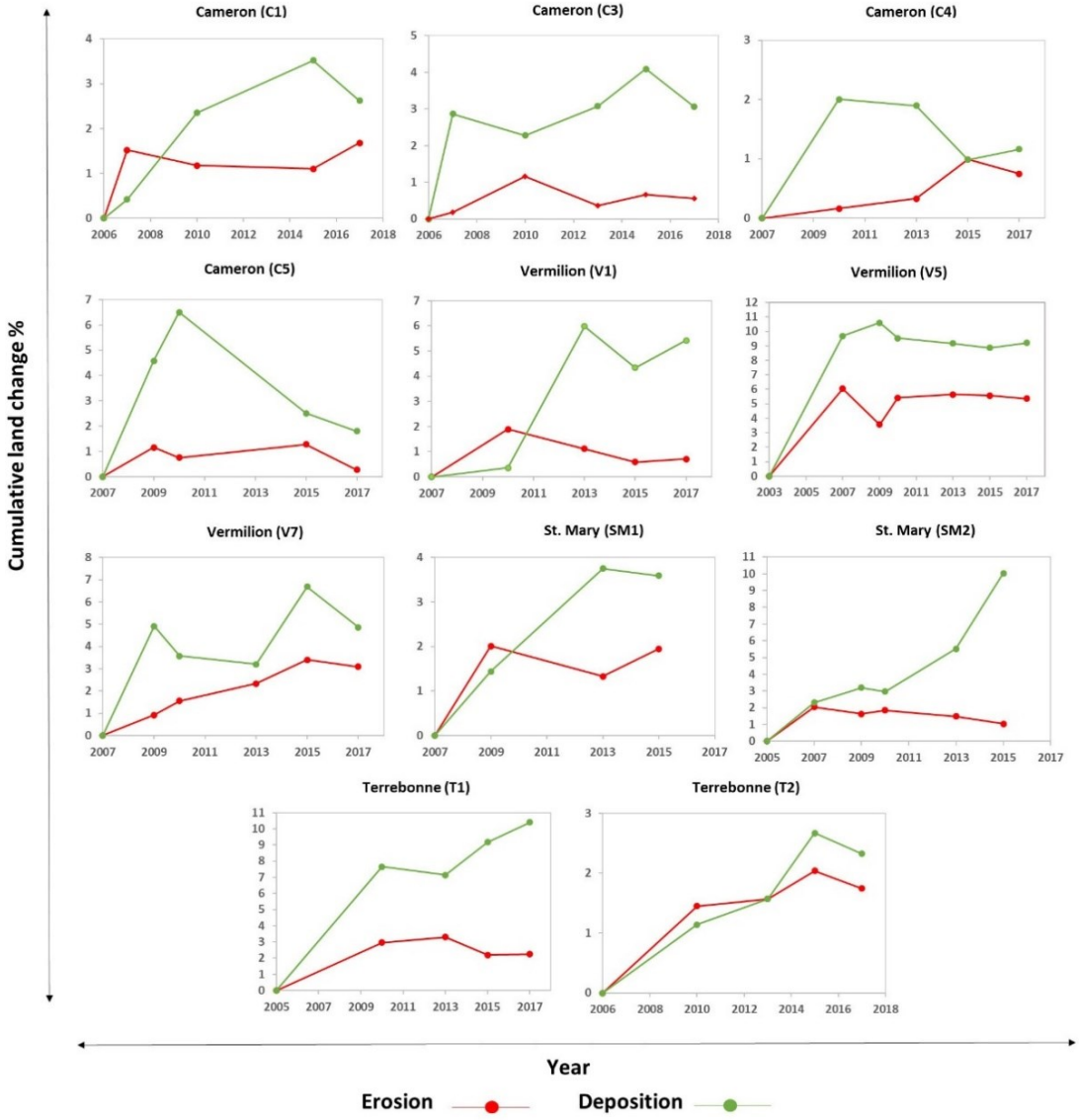

Figure 2.5 Land change trends of marsh terrace fields showing predominant deposition over time.

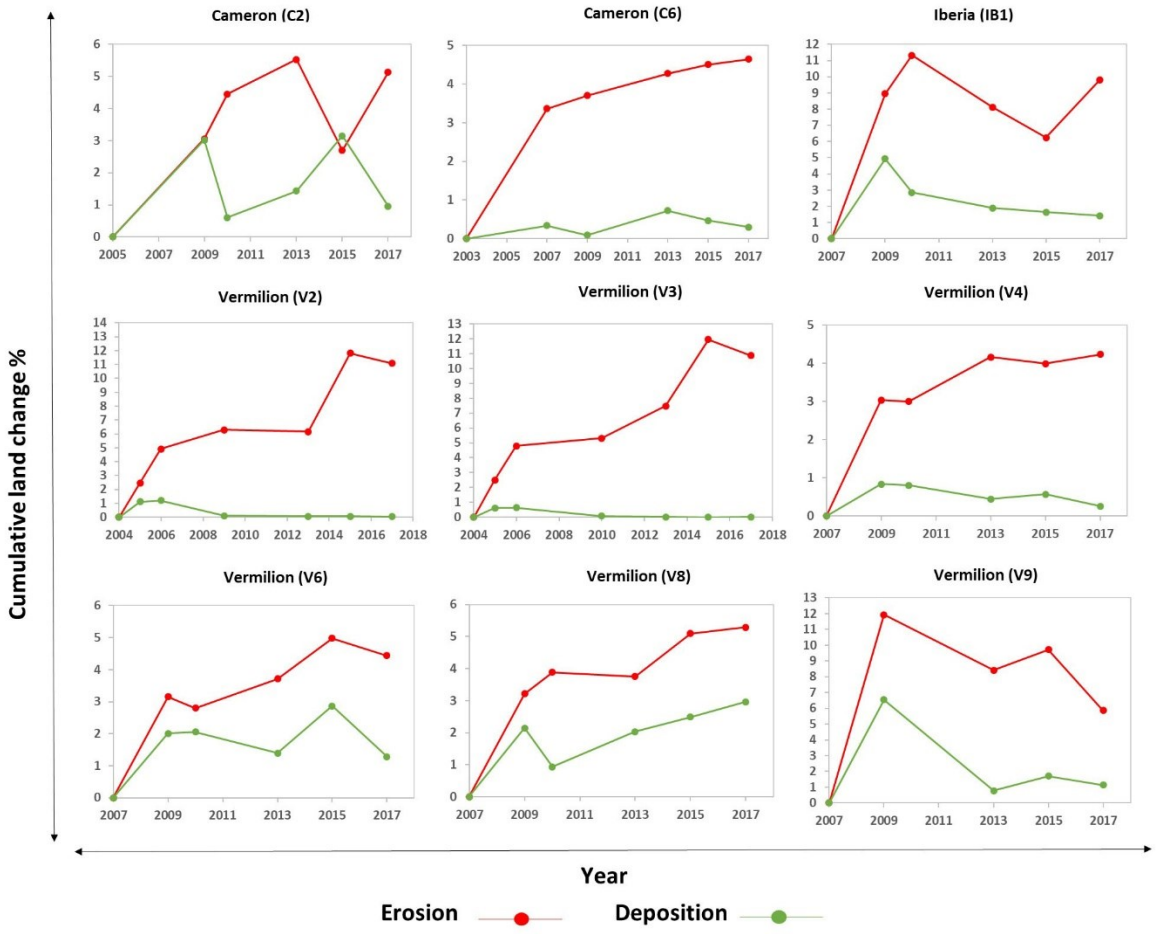

Figure 2.6 Land change trends of marsh terrace fields showing predominant erosion over time.

The analyses from the average cumulative land change by year of marsh terraces (Figure 2.7) showed that the average highest peak of marsh terraces erosion occurred in 2006 (−5%), 2009 (4%) and 2017 (−4%). The highest peaks of deposition occurred in 2007 (3%), 2009 (3.5%), 2015 (3.7%) and 2017 (3%).

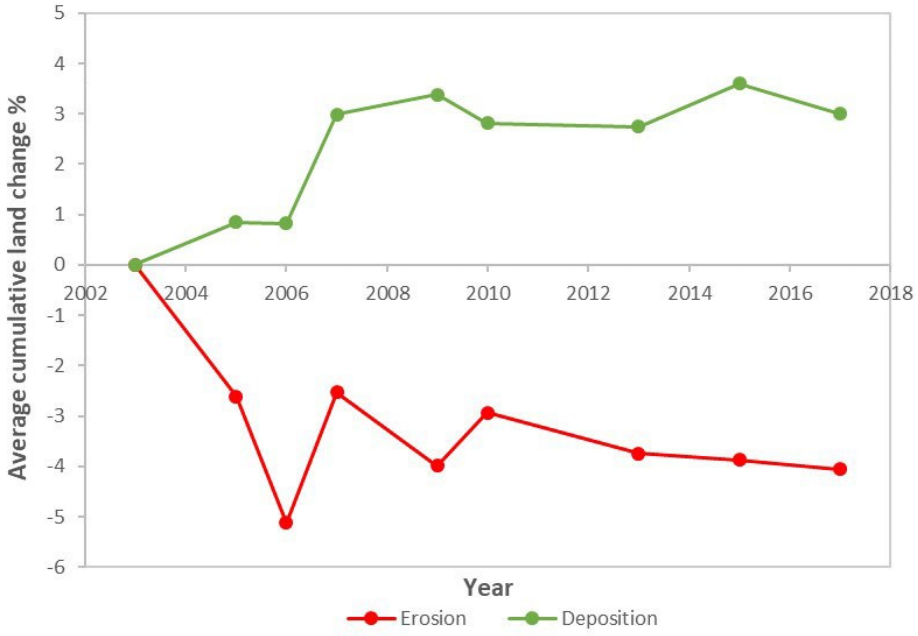

Figure 2.7 Average cumulative marsh terraces land change from all the sites by year.

Two tentative relationships were found between the terrace field performance (eroded and deposited) and independent terrace design factors (geomorphological location, shape, alignment, size, levees, adjacent to a channel): (1) terrace location (Chenier or Deltaic region) and (2) whether or not terrace fields were surrounded by channels and SMM (levees).

Discussion

Marsh Terrace Performance and Geomorphological Location

Findings from this study show that 11 out of 20 marsh terrace fields of study resulted in overall deposition. This success rate is particularly important within the context of local subsidence (5–10 mm per year) [41,59–61] and sea level rise (12 ± 8 mm per year) [41] in coastal Louisiana. The fact that there is over 50% deposition in the terrace fields of study under both sea-level rise and subsidence indicates a measure of success.

Previous studies have reported that the Geomorphic regions (Chenier and Deltaic) have an erosional and depositional trend based on their sediment supply and on the geological processes at work in those regions [41,62]. The Chenier Plain is newer and formational with its central part still erosional [62]. The erosional nature of the Chenier Plain could be related to mixed performance results showing predominant terrace erosion in nine out of 17 terrace fields of study located in the Chenier region. The Deltaic region is older [63] with vertical accretion and surface elevation (mean elevation of salt marshes surfaces) rates greater than that of the Chenier Plain. These rates show a decreasing trend from east (Deltaic region) to west (Chenier region) in coastal Louisiana [41]. The three terrace study fields showed predominant deposition in the Deltaic Plain. Although the number of study sites in the Deltaic region were limited and three study sites are not enough to make conclusions regarding success rates related to geomorphic processes, our findings follow the erosional and depositional trends of the geomorphic regions explained above. Greater deposition rates were found in the Deltaic than in the Chenier Plain.

On the other hand, sea level rise and subsidence rates in the Deltaic region are greater than that of the Chenier Plain [41,64]. Yet, all three sites in the Deltaic region are depositional, while there are mixed results in the Chenier region. However, all three sites in the Deltaic region were also connected to or surrounded by channels with external sediment supply, which may have potentially affected the interpretation of these results.

More research is needed to understand how marsh terraces perform relative to the geomorphologic region. Finding suitable sites for marsh terrace construction is difficult in the Deltaic region because the soils are less cohesive (organic soils) [65] than soils in the Chenier Plain which is composed of mudflats (organic, silty clay soils) [43,62]. Additionally, most

Louisiana marshes have thick organic soils with low shear strengths and low elevation which make marshes more vulnerable to wave and wind-driven erosion than other marshes in the world [66].

Marsh Terrace Performance Related to Channels and Levees

An important finding from the relationship between marsh terrace design factors and terrace longevity was related to whether or not the terraces were surrounded by channels. Fourteen of the 20 sites had a high density of channels connected or adjacent to the terrace fields of study. All 11 depositional sites had a high density of adjacent or connecting channels. This indicates that an external sediment source promotes predominant deposition in marsh terraces. Similarly, Good et al. (2005) [36] inferred that differences in marsh growth between terraced fields are related to amounts of sediment entering the ponds. Conversely, Day et al. (2000) [67] stated that wetlands with a high density of channels are generally related to high rates of land loss, among other factors.

Predominant erosion was found in nine terrace sites that were all located in the Chenier region. In the Chenier Plain there is a particularly high concentration of levees [46]. These levees are used as a structural marsh management (SMM) technique. SMM techniques alter sediments' biological and physical characteristics, decreasing sediment supply to the marsh fields [10,68] and reducing marsh deposition [69,70]. So, in this area, even if there are adjacent or channels with high channel density connected to the marsh fields, these channels may be sediment starved and not able to contribute sediment to the terrace fields [49] because levees restrict tidal flows. This anthropogenic factor could be a reason of predominant terrace erosion in the Chenier region.

Sometimes marsh terraces are combined with other restoration techniques such as river diversions [7]. Marsh terraces were included in the output embayment of a river crevasse project in Plaquemines Parish Louisiana. Terraces were incorporated with the purpose to capture and settle sediment carried by the Mississippi River. The results were promising with five years after terrace

construction emergent marsh increased by 3.2 ha (1%) within the terrace field boundaries [71]. Therefore, future sediment diversion plans in the Deltaic Plain [72] may considerably contribute to the amount of sediment entering the terrace fields, enhancing deposition and potentially reducing land erosion in the Chenier Plain [63]. Furthermore, sediment diversion plans should incorporate marsh terracing to encourage the deposition of sediments in strategic locations. The present study agrees with Day et al. (2000) [67] who mentioned that various restoration projects (e.g., marsh terracing) can be implemented to reduce land loss, but ultimately riverine input or an external source of sediment loading is necessary for creating new land.

Marsh Terrace Performance and Storm Events

Storm surge can inundate inland marshes, alter the sediment transport processes, and can act as an important agent of wetland loss [62]. Storms can either be land destructive (erosional) or constructive (depositional) [73]. The average cumulative highest peaks of erosion in the terrace fields of study were in 2005–2006 and 2007–2009. It has already been shown that in 2005 category 5 hurricanes Katrina and Rita and in 2008 category 4 hurricanes Gustav and Ike contributed to land loss [65,73]. Our results, showing increased terrace erosion during these time periods, corroborate findings that these storms were erosional. These results also agree with previous studies [18,74,75] that mentioned episodic events like strong storms (e.g., greater than category three hurricanes) contributed significantly to high rates of land loss in the northern coast of the Gulf of Mexico.

Tweel and Turner (2012) [76] reported that hurricanes are a potential driver for land loss but they also demonstrated that hurricanes Katrina, Rita, Gustav, and Ike deposited great amounts of sediment in the northern Gulf of Mexico. While overall erosion between all terrace fields of study peaked during the periods including storm events, deposition was also observed within the

marsh terraces fields of study in the same time periods. Possibly the sediment source for terrace deposition was from the sediment removed from other land features surrounding the marsh terrace field or from sediment supplied by the storm surge. In fact, according to Draut et al. (2005) [77] and Jankowski et al. (2017) [41], energetic events like storms and cold fronts are factors that contribute to wetland deposition in coastal Louisiana. However, the average cumulative marsh terrace deposition observed in this study was not enough to offset the average cumulative marsh terrace erosion in 2006 and 2009.

Conclusions

This study assessed marsh terrace performance of 20 terrace fields in coastal Louisiana using a remote sensing approach. The change in marsh terrace areas was measured over time using NAIP imagery from 2003 until 2017 from five Louisiana coastal parishes. Marsh terrace performance over time shows more predominant deposition than erosion in the 20 terrace fields of study, even in the face of subsidence and sea level rise. Their longevity within a 10–14-year time period effectively achieved one of the terrace restoration goals, which is marsh creation. A relationship was found between geomorphological area, sediment supply, and adjacent or connecting channels with terrace fields of study performance. High density of channels surrounding or adjacent to the terrace fields, and external source of sediment loading are likely important drivers encouraging terrace deposition. However, further analysis is necessary to understand the reasons for differences in performance of these terraces. In the future, these results will be related to environmental factors (sediment type, sediment load, soil strength, salinity, terrace location in relation to wave energy, etc.) and other drivers (wind and wave energy) that might play an important role for the success of this restoration technique. This will help restoration planners select optimal sites and designs for marsh terrace implementation.

This study is particularly important given the lack of previous research on marsh terrace effectiveness and longevity over time in multiple sites and over multiple years. We expect that this study will encourage new research assessing this technique's effectiveness and identifying the most effective terrace designs. This will allow restoration agencies to address one of the biggest challenges in wetlands restoration projects, which is applying lessons learned in previous projects by assessing the results of previously implemented techniques.

REFERENCES

1. Underwood, S.G.; Steyer, G.D.; Good, B.; Chambers, D. Bay Bottom Terracing and Vegetative Planting: An Innovative Approach for Habitat and Water Quality Enhancement. In *Annual Conference on Wetlands Restoration and Creation. Hillsborough Community College*. F.J. Webb, Jr. (ed): Tampa, FL, USA, 1991; pp. 164–173.

2. Rozas, L.P.; Minello, T.J. Marsh Terracing as a Wetland Restoration Tool for Creating Fishery Habitat. *Wetlands* **2001**, *21*, 327–341.

3. Turner, R.E.; Streever, B. *Approaches to Coastal Wetland Restoration: Northern Gulf of Mexico*; Kugler Publications: Hague, Netherlands, 2002.

4. U.S. Fish and Wildlife service (FWS). Available online: https://www.fws.gov/gisdownloads/R4/Louisiana ESO/ (accessed on 31 July 2019).

5. Coastal Wetlands Planning, Protection and Restoration Act (CWPPRA). Available online: https://lacoast.gov/new/Pubs/Reports/project.aspx (accessed on 31 July 2019).

6. O'Connell, J.L.; Nyman, J.A. Marsh Terraces in Coastal Louisiana Increase Marsh Edge and Densities of Waterbirds. *Wetlands* **2010**, *30*, 125–135.

7. Brasher, M.G. *Review of the Benefits of Marsh Terraces in the Northern Gulf of Mexico*; Ducks Unlimited, Inc., Gulf Coast Joint Venture: Lafayette, LA, USA, 2015.

8. Steyer, G.D. Sabine Terracing Project Final Report. **1993,** *La. Dep. Nat. Resour. Coast. Resour. Div. DNR Project number* 4351089: Baton Rouge, LA, USA.

9. Wang, W.; Liu, H.; Li, Y.; Su, J. Development and Management of Land Reclamation in China. *Ocean Coast. Manag.* **2014**, *102*, 415–425.

10. Kennish, M.J. Coastal Salt Marsh Systems in the US: A Review of Anthropogenic Impacts. *J. Coast. Res.* **2001**, *17*, 731–748.

11. Nyman, J.A.; Chabreck, R.H. Managing Coastal Wetlands for Wildlife. *Wildl. Tech. Man. Manag.* **2012**, *2*, 133–156.

12. Kentula, M.E. Perspectives on Setting Success Criteria for Wetland Restoration. *Ecol. Eng.* **2000**, *15*, 199–209.

13. La Peyre, M.K.; Reams, M.A.; Mendelssohn, I.A. Linking Actions to Outcomes in Wetland Management: An Overview of US State Wetland Management. *Wetlands* **2001**, *21*, 66.

14. Guo, M.; Li, J.; Sheng, C.; Xu, J.; Wu, L. A Review of Wetland Remote Sensing. *Sensors* **2017**, *17*, 777.

15. FGDC. *Application of Satellite Data for Mapping and Monitoring Wetlands*; Technical Report 1,Wetlands Subcomittee. Federal Geographic Data Committee (FGDC): Washington, DC, USA, 1992.

16. Penland, S.; Beall, A.D.; Britsch III, L.D. Geologic Classification of Coastal Land Loss between 1932 and 1990 in the Mississippi River Delta Plain, Southeastern Louisiana. *Gulf Coast Assoc. Geol. Soc. Trans.* **2002**, 52, 799-807.

17. Barras, J.A.; Beville, S.; Britsch, D.; Hartley, S.; Hawes, S.; Johnston, J.; Kemp, P.; Kinler, Q.; Martucci, A.; Porthouse, J. *Historical and Projected Coastal Louisiana Land Changes: 1978–2050*; *USGS Open-file report 03-334. United States Geological Survey,* Lafayette,Louisisana, *USA.* 2003.

18. Couvillion, B.R.; Barras, J.A.; Steyer, G.D.; Sleavin, W.; Fischer, M.; Beck, H.; Trahan, N.; Griffin, B.; Heckman, D. *Land Area Change in Coastal Louisiana from 1932 to 2010*; *U.S.Geol. Surv.Sci. Invest Map 3164:* Reston,VA, USA, 2011.

19. Oliver-Cabrera, T.; Wdowinski, S. InSAR-Based Mapping of Tidal Inundation Extent and Amplitude in Louisiana Coastal Wetlands. *Remote Sens.* **2016**, *8*, 393.

20. McCarthy, J.; Gumbricht, T.; McCarthy, T.S. Ecoregion Classification in the Okavango Delta, Botswana from Multitemporal Remote Sensing. *Int. J. Remote Sens.* **2005**, *26*, 4339–4357.

21. Adam, E.; Mutanga, O.; Rugege, D. Multispectral and Hyperspectral Remote Sensing for Identification and Mapping of Wetland Vegetation: A Review. *Wetl. Ecol. Manag.* **2010**, *18*, 281–296.

22. Wu, Q. *GIS and Remote Sensing Applications in Wetland Mapping and Monitoring*; *Comprehensive Geographic Systems; Huang, B., Ed.; Elsevier:* Oxford, UK, 2018; pp140-157.

23. Jensen, J.R. *Introductory Digital Image Processing: A Remote Sensing Perspective*; Prentice Hall: Englewood Cliffs, NJ, USA, 1996.

24. Klemas, V. Remote Sensing Techniques for Studying Coastal Ecosystems: An Overview. *J. Coast. Res.* **2010**, *27*, 2–17.

25. Ozesmi, S.L.; Bauer, M.E. Satellite Remote Sensing of Wetlands. *Wetl. Ecol. Manag.* **2002**, *10*, 381–402.

26. Lu, D.; Mausel, P.; Brondizio, E.; Moran, E. Change Detection Techniques. *Int. J. Remote Sens.* **2004**, *25*, 2365–2401.

27. Seif, A.; Mokarram, M. Change Detection of Gil Playa in the Northeast of Fars Province, Iran. *Am. J. Sci. Res.* **2012**, *86*, 122–130.

28. Butt, A.; Shabbir, R.; Ahmad, S.S.; Aziz, N. Land Use Change Mapping and Analysis Using Remote Sensing and GIS: A Case Study of Simly Watershed, Islamabad, Pakistan. *Egypt. J. Remote Sens. Sp. Sci.* **2015**, *18*, 251–259.

29. Zoran, M.; Anderson, E. The Use of Multi-Temporal and Multispectral Satellite Data for Change Detection Analysis of the Romanian Black Sea Coastal Zone. *J. Optoelectron. Adv. Mater.* **2006**, *8*, 252.

30. Ahmad, F. Detection of Change in Vegetation Cover Using Multi-Spectral and Multi-Temporal Information for District Sargodha, Pakistan. *Soc. Nat.* **2012**, *24*, 557–571.

31. Jensen, J.R. Digital Image Processing: A Remote Sensing Perspective. 3rd ed.; *PearsonPrentice Hall*: Upper Saddle River, NJ, USA, 2005.

32. Feagin, R.A.; Wu, X. Ben. Spatial Pattern and Edge Characteristics in Restored Terrace versus Reference Salt Marshes in Galveston Bay. *Wetlands* **2006**, *26*, 1004–1011.

33. Rozas, L.P.; Minello, T.J. Using Nekton Growth as a Metric for Assessing Habitat Restoration by Marsh Terracing. *Mar. Ecol. Prog. Ser.*, **2009**, *394*, 179–193.

34. Loveless, J.B.; Smee, D.L. Assessing the Efficacy of Marsh Restoration via Terracing by Comparing Vegetation Density and Nekton Abundance Before and After Restoration. *Gulf Mex. Sci.* **2018**, *34*, 5.

35. Ducks Unlimited. Geodatabase of Existing Marsh Terraces.Unpublished material. Lafayette, Louisiana, USA, 2015.

36. Good, B.; Peele, H.; Bourgeois, R. Aerial Growth of the Sabine Marsh Terracing Project over a Ten-Year Period. *Rep. Louisiana Dep. Nat. Resour. Interag. Agreement* 05–2512. Baton Rouge, LA, USA, **2005**.

37. Castellanos, D.; Aucoin, S. *Operations, Maintenance, and Monitoring Report for Little Vermilion Bay Sediment Trapping (TV-12)*; *Louisiana Department of Natural Resources, Coastal Restoration Division*: Lafayette, LA, USA, 2004.

38. Thibodeaux, C.; Guidry, M. *2009 Operations*, *Maintenance*, *and Monitoring Report for Pecan Island Terracing (ME-14)*; *Lousiana Department of Natural Resources, Coastal Restoration Division*: Lafayette, LA, USA, 2009.

39. Miller, M.; Aucoin, S. *Operations, Maintenance, and Monitoring Report for the Four-Mile Canal Terracing and Sediment Trapping (TV-18); Coastal Protection and Restoration Authority of Louisiana.* Lafayette, LA, USA, 2011.

40. USDA. National Agricultural Imagery Program (NAIP).Geospatial Data Gateway. Available online: https://datagateway.nrcs.usda.gov/. (accesed on 01 June 2018).

41. Jankowski, K.L.; Törnqvist, T.E.; Fernandes, A.M. Vulnerability of Louisiana's Coastal Wetlands to Present-Day Rates of Relative Sea-Level Rise. *Nat. Commun.* **2017**, *8*, 14792.

42. USDA. Farm Service Agency. NAIP Imagery. Available online: https://www.fsa.usda.gov/programs-and-services/aerial-photography/imagery-programs/naip-imagery/ (accessed on 1 June 2018).

43. Brasher, M.G. *Ducks Unlimited, Inc., Gulf Coast Joint Venture: Lafayette*, LA, USA. Personal communication, 2018.

44. Simons, K.L. *A Comparison of Two Common Classification Procedures for Economical Urban Land Cover Mapping Using NAIP Imagery*; M.S. Brigham Young University. UT, USA. 2009.

45. (CPRA) Coastal Protection and Restoration Authority of Louisiana. *Coastwide Reference Monitoring System-Wetlands Monitoring Data*. Available online: http://cims.coastal.louisiana.gov. (Accesed on 16 June 2018).

46. Day, R.H.; Holz, R.K.; Day, J.W. An Inventory of Wetland Impoundments in the Coastal Zone of Louisiana, USA: Historical Trends. *Environ. Manag.* **1990**, *14*, 229–240.

47. Wicker, K.M.; Roberts, D.; Davis, D. *Rockefeller State Wildlife Refuge and Game Preserve: Evaluation of Wetland Management Techniques*; *Louisiana Department of Natural Resources, Coastal Management Section:* Baton Rouge, LA, USA. 1983.

48. Cowan, J.H.; Turner, R.E.; Cahoon, D.R. Marsh Management Plans in Practice: Do They Work in Coastal Louisiana, USA? *Environ. Manag.* **1988**, *12*, 37–53.

49. Bolduc, F.; Afton, A.D. Sediments in Marsh Ponds of the Gulf Coast Chenier Plain: Effects of Structural Marsh Management and Salinity. *Wetl. Ecol. Manag.* **2005**, *13*, 395–404.

50. ESRI. *ArcGIS Desktop*; Environmental Systems Research Institute: Redlands, CA, USA, 2011.

51. Hexagon Geospatial. *ERDAS IMAGINE*. Erdas Inc: Inc. Madison, AL, 2016.

52. Hammond, M. *PythonWin IDE amd GUI*; 2010 Python Software Foundation. Retrieved from: https://www.python.org/

53. Congalton, R.G. A Review of Assessing the Accuracy of Classifications of Remotely Sensed Data. *Remote Sens. Environ.* **1991**, *37*, 35–46.

54. Congalton, R.G.; Green, K. *Assessing the Accuracy of Remotely Sensed Data: Principles and Practices*; CRC Press: Boca Raton, FL, USA, 2002.

55. Google Earth. Available online: https://www.google.com/earth/ (accesed on 1 December 2019).

56. Mohammed, J. Land Use and Cover Change Assessment Using Remote Sensing and GIS: Dohuk City, Kurdistan, Iraq (1998–2011). *Int. J. Geomat. Geosci.* **2013**, *3*, 552–569.

57. Ratnaparkhi, N.S.; Nagne, A.D.; Gawali, B. A Land Use Land Cover Classification System Using Remote Sensing Data. *Changes* **2014**, *7*, 8.

58. Hurlbert, S.H. Pseudoreplication and the Design of Ecological Field Experiments. *Ecol. Monogr.* **1984**, *54*, 187–211.

59. González, J.L.; Tornqvist, T.E. Coastal Louisiana in Crisis: Subsidence or Sea Level Rise? *Eos. Trans. Am. Geophys. Union* **2006**, *87*, 493–498.

60. Yuill, B.; Lavoie, D.; Reed, D.J. Understanding Subsidence Processes in Coastal Louisiana. *J. Coast. Res.* **2009**, 23–36. doi:10.2112/SI54-012.1.

61. Morton, R.A.; Bernier, J.C. Recent Subsidence-Rate Reductions in the Mississippi Delta and Their Geological Implications. *J. Coast. Res.* **2010**, *26*, 555–561.

62. Owen, D.E. Geology of the Chenier Plain of Cameron Parish, Southwestern Louisiana. *Geol. Soc. Am. Field Guide* **2008**, *14*, 27–38.

63. Hijma, M.P.; Shen, Z.; Törnqvist, T.E.; Mauz, B. Late Holocene Evolution of a Coupled, Mud-Dominated Delta Plain–Chenier Plain System, Coastal Louisiana, USA. *Earth Surf. Dyn.* **2017**, *5*, 689.

64. Penland, S.; Ramsey, K.E. Relative Sea-Level Rise in Louisiana, and the Gulf of Mexico: 1908–1988. *J. Coast. Res.* **1990**, *6*, 323–342.

65. Day, J.W.; Boesch, D.F.; Clairain, E.J.; Kemp, G.P.; Laska, S.B.; Mitsch, W.J.; Orth, K.; Mashriqui, H.; Reed, D.J.; Shabman, L. Restoration of the Mississippi Delta: Lessons from Hurricanes Katrina and Rita. *Science* **2007**, *315*, 1679–1684.

66. Howes, N.C.; FitzGerald, D.M.; Hughes, Z.J.; Georgiou, I.Y.; Kulp, M.A.; Miner, M.D.; Smith, J.M.; Barras, J.A. Hurricane-Induced Failure of Low Salinity Wetlands. *Proc. Natl. Acad. Sci. USA* **2010**, *107*, 14014–14019.

67. Day, J.W.; Britsch, L.D.; Hawes, S.R.; Shaffer, G.P.; Reed, D.J.; Cahoon, D. Pattern and Process of Land Loss in the Mississippi Delta: A Spatial and Temporal Analysis of Wetland Habitat Change. *Estuaries* **2000**, *23*, 425–438.

68. Reed, D.J.; De Luca, N.; Foote, A.L. Effect of Hydrologic Management on Marsh Surface Sediment Deposition in Coastal Louisiana. *Estuaries* **1997**, *20*, 301–311.

69. Cahoon, D.R. Recent Accretion in Two Managed Marsh Impoundments in Coastal Louisiana. *Ecol. Appl.* **1994**, *4*, 166–176.

70. Bryant, J.C.; Chabreck, R.H. Effects of Impoundment on Vertical Accretion of Coastal Marsh. *Estuaries* **1998**, *21*, 416–422.

71. Hymel, M.K.; Breaux, K.A. *2012 Operations, Maintenance, and Monitoring Report for Delta Management at Fort St. Philip*; *Coastal Protection and Restoration Authority of Louisiana*: New Orleans, LA, USA, 2012.

72. (CPRA) Coastal Protection and Restoration. *Louisiana's Comprehensive Master Plan. for a Sustainable Coast*; Coastal Protection Restoration Authority, Integrated Planning Team: Baton Rouge, LA, USA, 2017.

73. Morton, R.A.; Barras, J.A. Hurricane Impacts on Coastal Wetlands: A Half-Century Record of Storm-Generated Features from Southern Louisiana. *J. Coast. Res.* **2011**, *27*, 27–43.

74. Barras, J.A.; Bernier, J.C.; Morton, R.A. *Land Area Change in Coastal Louisiana, a Multidecadal Perspective (from 1956 to 2006)*; US Department of the Interior, US Geological Survey Scientific Investigations, 2008. Available online: https://pubs.usgs.gov/sim/3019/ (accesed on 4 June 2019).

75. Steyer, G.D.; Cretini, K.F.; Piazza, S.C.; Sharp, L.A.; Snedden, G.A.; Sapkota, S. *Hurricane Influences on Vegetation Community Change in Coastal Louisiana*; US Geological Survey: Reston, VA,USA, 2010.

76. Tweel, A.W.; Turner, R.E. Landscape-Scale Analysis of Wetland Sediment Deposition from Four Tropical Cyclone Events. *PLoS ONE* **2012**, *7*, e50528.

77. Draut, A.E.; Kineke, G.C.; Huh, O.K.; Grymes III, J.M.; Westphal, K.A.; Moeller, C.C. Coastal Mudflat Accretion under Energetic Conditions, Louisiana Chenier-Plain Coast, USA. *Mar. Geol.* **2005**, *214*, 27–47

CHAPTER III

MODELING WAVE CLIMATES AND WAVE REDUCTION IN MARSH TERRACE ENVIRONMENTS

Introduction

Marsh loss in the northern Gulf of Mexico is attributed to sea level rise, geomorphological processes, and wave erosion [2, 3]. In coastal Louisiana, coastal wetland erosion from wave energy results in marsh platform fragmentation and conversion from marsh to shallow water ponds [4–7]. In an attempt to slow wetland loss, restoration techniques have been implemented, such as living shorelines, sediment retention structures, sediment diversions, and marsh terraces, among others [8, 9]. Marsh terracing has been a common restoration technique in Texas and Louisiana since the beginning of the 1990s, and approximately 116 terrace projects have been built since then [10, 11]. This restoration technique consists of linear berms of soil constructed in inland shallow water bodies using on–site bottom substrate material. These terraces are generally populated by marsh vegetation subsequent to construction. Constructed marsh terraces have different designs with varying orientation, shapes, and spacing [8, 12]. The primary goal of marsh terracing is to reduce wave energy by minimizing fetch, thereby enhancing marsh creation inside the terrace footprint and reducing wind driven erosion of the surrounding marsh platform [13, 14]. Due to a lack of research using numerical modeling to study marsh terraces performance at reducing wave energy [1] , there is an increased need to understand the effect of terraces on wave climate in marsh environments using a wave model.

Inland shallow ponds in coastal Louisiana, where marsh terraces are constructed, are typically fetch limited environments that experience predominantly low energy wave conditions. Marsh terraces are not highly influenced by currents and are mostly isolated from tides. Therefore, wave energy is one of the main factors responsible for marsh erosion in these wetlands environments [1, 5, 15, 16]. However, there is uncertainty regarding the wind conditions that are most responsible for erosion. Research has shown that marsh losses in coastal Louisiana can be accelerated by extreme storm events such as hurricanes [17, 18]. Other studies show that more frequent and lower intensity storm events, such as cold front passage had a similar or even greater erosive effect than hurricanes in terraced marshes [19, 20]. It has also been demonstrated that long term erosion in marshes mainly occurs during low wave energy conditions from frequent weak (0–3 m/s) and intermediate(3–6 m/s) winds [20, 21]. Because of the uncertainty regarding what wind conditions are responsible for most erosion in terraces, it is important to understand marsh terrace performance under all wind conditions.

Numerical models play an important role in understanding wave climates in coastal areas and inland lakes. Numerical models enable large scale experiments with fine scale spatial and temporal resolution. The outputs of these models can help inform and support decision making processes in environmental engineering projects [22]. Hydrodynamic models are numerical models representing many hydrological systems (river, estuaries, coasts, basins, etc.) and their spatial and temporal dynamics (currents, water levels, waves, sediment transport and salinity). Wave models can assess conditions in a variety of coastal water bodies (deep, shallow, ocean, estuary, inland, fetch/depth limited, etc.) [23–29]. In wetland environments the dynamics of waves, water level, and sediment suspension has been widely assessed using hydrodynamic and wave models particularly relating these processes with the impact of hurricanes such as storm surge and

flooding [21, 30–37]. Few studies have addressed wave behavior related to marsh erosion in wetlands and shallow water environments during frequent winds using hydrodynamic models. Tonelli et al., (2010) simulated the impact of wave action on salt marsh boundaries as a function of tidal elevation and wave height for three different edge shapes using a numerical Boussinesq–type wave model. One of their findings was that wave energy dissipation is maximized just above of the marsh platform elevation when wave reflection is minimized and wave breaking happens at the marsh edge [38]. Marani et al., (2011) using a parametrical wave model and long–term observations of a lagoon in Italy, found that the rate of marsh lateral erosion and incident wave power density has a linear relationship. Mcloughlin et al., (2015) analyzed marsh edge erosion at four salt marshes in Virginia over a 50–year period using aerial imagery and numerical wave models. They used a parametric model [39] and SWAN to calculate incident wave energy flux in relation to volumetric erosion rates. They confirmed the important role of waves driving marsh edge erosion in shallow coastal bays [24]. Leonardi et al., (2016) also found a linear relationship between erosion rates of marsh boundaries and incoming wave energy, concluding that salt marsh fragmentation is due to everyday frequent wind and wave conditions and therefore is predictable. Valentine and Mariotti (2019) used a simple 2D model to assess marsh retreat due to wind waves in Barataria Bay, LA. Their model accurately predicted marsh erosion in microtidal coastal bays, and identified three erosive processes based on wind direction causing water level fluctuations that enhance edge erosion [40].

Research evaluating hydrodynamic processes in terraced marshes is limited. Mathews (2020) developed a hypothetical model using Delft3D in a synthetic basin to test different terrace designs. The Delft3D–Flow module was used to simulate sediment dynamics and circulation patterns under hypothetical wind scenarios, including a constant wind velocity (15 m/s) and three

wind direction scenarios (0, 45 or 90º). However, their study did not simulate the effect of wind driven waves on terraces. Mathews (2020) and French et al., (2020) concluded that the chevron design effectively reduced total shear stress and water velocities, mainly if constructed perpendicular to wind directions associated with erosive wave conditions. To our knowledge, there are no publications that numerically model wave climates in real marsh terrace field scenarios, thus demonstrating the need for the present study.

The main objective of this research is to simulate wave climates in marsh terrace fields during frequent wind conditions using a numerical model. The objectives of this study would be to: 1) quantify how well the model represents observed wave conditions in marsh terraces; 2) describe the wave climate in terraced and unterraced fields; and 3) quantify the effect of marsh terraces on wave height and therefore wave energy dynamics. This new knowledge will provide great improvement in the design optimization and implementation of restoration techniques such as marsh terraces.

Materials and Methods

Study Area

Wave climate characteristics were measured and modeled in two marsh terrace fields in coastal Louisiana (Figure 3.1). Both terrace fields were located in the Chenier Plain of southwestern Louisiana. Most of the terrace fields built in Louisiana are located in the Chenier Plain due to optimal construction conditions such as density of inland ponds and presence of cohesive sediments [42]. The two study sites have different terrace design features, as described in the subsequent paragraphs.

The chevron terrace field study site shown in figure (3.1c) has a v–shaped chevron design aligned N to S with a 150–degree angle. Individual terraces are 300 meters long and five to ten

meters wide. The open water area where this chevron terrace field was built has an area of 1.75 square kilometers. This chevron terrace field of study was characterized by cumulative depositional trends over time [14].

The rectangular terrace field study site shown in figure (3.1d) has a semi enclosed rectangular terrace design linearly aligned north (N) to south (S), with an average terrace length of 35 meters and widths ranging from five to ten meters. The pond area, where the rectangular terraces are located, has an area of 2.75 square kilometers. This rectangular terrace field of study was characterized by cumulative erosional trends over time [14].

Due to the distance to marine open water and hydrologic modifications, the effects of currents and tides are negligible in these study sites. The two terrace fields were selected based on the following criteria: 1) representative terrace designs that are commonly constructed in coastal Louisiana and different from each other [11]; 2) marsh terrace fields with sufficient water depth to deploy wave instruments; and 3) access permission by landowners to deploy wave instrumentation.

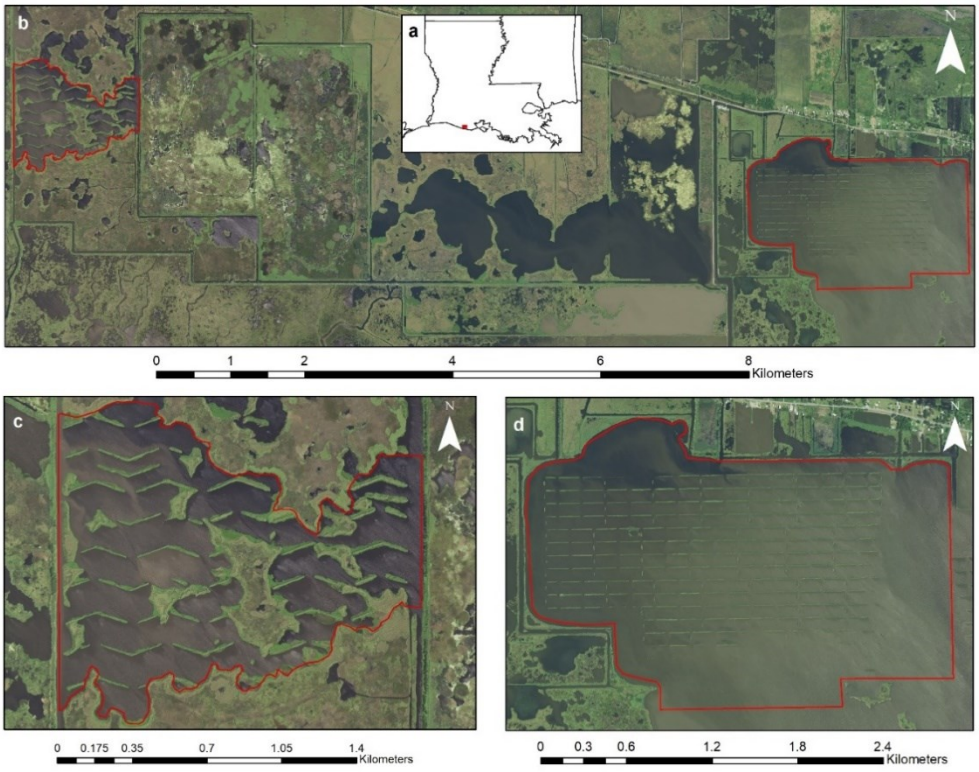

Figure 3.1 (a) Map of the state of Louisiana. Red point shows the general location of marsh terrace fields of study. (b) NAIP imagery of the two marsh terraces field of study in Vermilion Parish, Louisiana. (c) NAIP imagery of the chevron terrace field of study; (d) NAIP imagery of the rectangular terrace field study. Red polygons enclose marsh terrace fields of study.

Wave Data

Wave measurements were collected at each marsh terrace study site. In the rectangular terrace field of study wave data were collected during 159 days from November 1st, 2018, to April 9th, 2019. In the chevron terrace field of study wave data was collected during 146 days from April 10th, 2019, to September 3rd, 2019. Model validation indicated that the simulated wave data included two Nortek 1000 Signature series acoustic Doppler current profilers (ADCP) deployed on aluminum frames placed on the marsh floor at 1 m depth approximately (Figure 3.2 and 3.3).

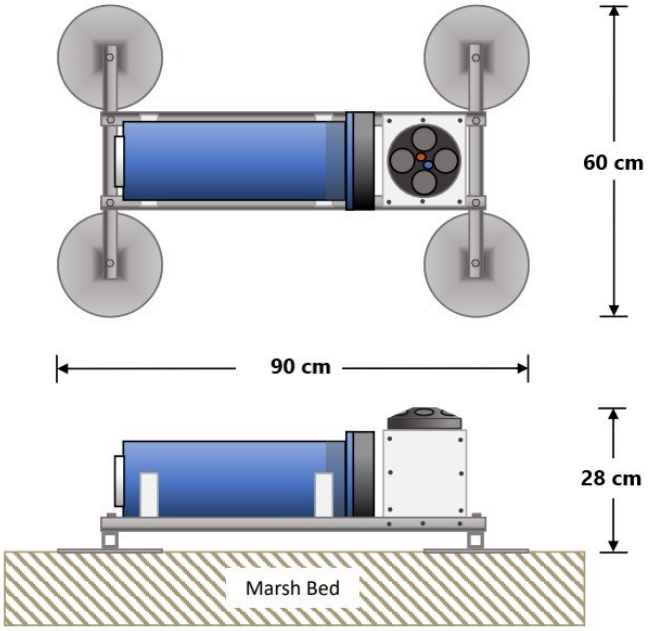

Figure 3.2 Conceptual schematic of a Nortek 1000 signature series ADCP deployed on an aluminum frame on a marsh bed.

Figure 3.3 Nortek 1000 signature series ADCP mounted in aluminum frame (left). ADCP retrieval at a marsh terrace site in coastal LA. (right).

ADCP's collected wave measurements once per hour during 17 minute ensemble bursts with a sampling rate frequency of 8 Hz, as is recommended in short fetch conditions [25]. The

wave instrumentation measured wave climates using five acoustic beams that record water surface elevation and velocity in 2 cm bins between the water surface and a section 10 cm above the instrument [19]. Wave statistics calculated from the measurements include: significant wave height (Hs), mean wave period (Tm), peak period (Tpeak), mean wave direction (Dir), wave peak direction (Dirpeak), directional spread (Dirspread), water column acoustic backscatter intensity, and water depth (h).

In the rectangular terrace field of study one ADCP (R1) was deployed at the eastern boundary in the unterraced area to collect data to input in the wave model as incident wave conditions. Another ADCP (R2) was deployed within the terraced area for model validation purposes in the rectangular computational domain (Figure 3.4).

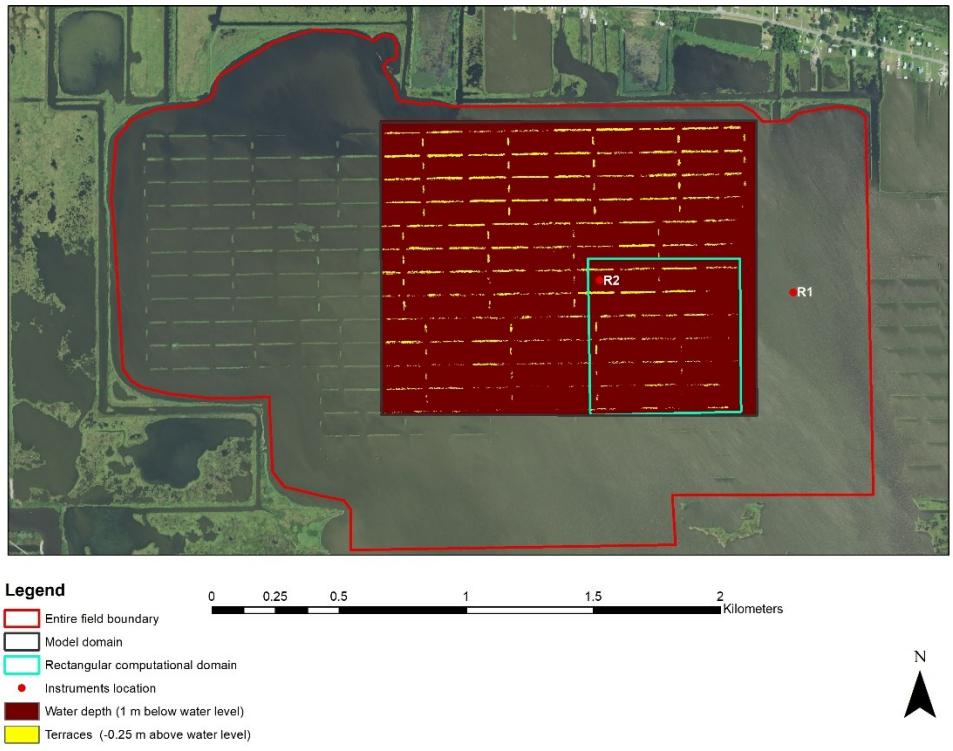

Figure 3.4 Rectangular terrace field of study showing the computational domain, bathymetry, and instruments location.

In the chevron terrace field of study, two ADCPs (C1 and C2) were deployed within the area between terraces due to lack of open boundaries in the field of study (Figure 3.5). Wave measurements from C1 and C2 were used as incident conditions and model validation points depending on the direction of the incident wind–wave used to force the model. The chevron 1 computational domain (Figure 3.5b) was used when the wave direction was coming from the northeast (NE). Therefore, C1 measurements were used as incident wave conditions and C2 measurements as the model validation point. The chevron 2 computational domain (Figure 3.5c) was used when the wave direction was coming from the southeast (SE). Therefore, C2 measurements were used as incident wave conditions and C1 measurements as the model validation point.

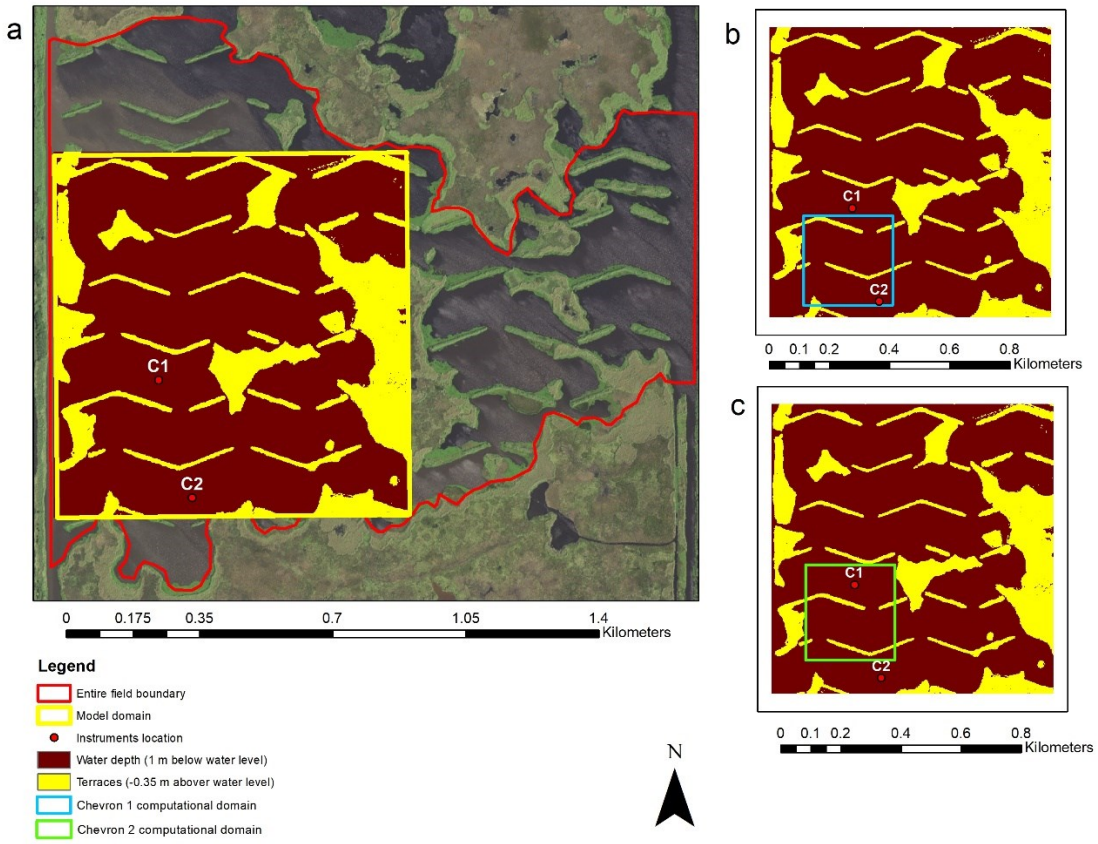

Figure 3.5 (a) Chevron terrace field of study showing the model domain, bathymetry, and instruments location. (b) Chevron 1 computational domain. (c) Chevron 2 computational domain.

Wind Data

Wind data were collected near the study sites during the periods when wave data were collected (159 days). For both terrace fields of study, wind data was downloaded from the nearest National Oceanic and Atmospheric Administration (NOAA) weather station. For the rectangular terrace field of study, wind data was obtained from NOAA station FRWL1–8766072 located at the Freshwater Canal Locks, approximately 25 km to the east of the study site. The most frequent recorded wind direction during this period was NNE and ESE (Figure 3.6a).

Although NOAA station FRWL1 was also the closest available weather station to the chevron terrace field, it lacked wind data for the period when wave instruments were deployed at that study site. Thus, wind data for the chevron terraced field of study was obtained from the next closest NOAA weather station WBAN:00184, located at the Abbeville Municipal Airport, approximately 62 km to the northeast of the study site. The most frequent recorded wind direction during this period was SE (Figure 3.6b). Wind direction variability between the two sites was likely influenced by the different seasons in which the instruments were deployed [19].

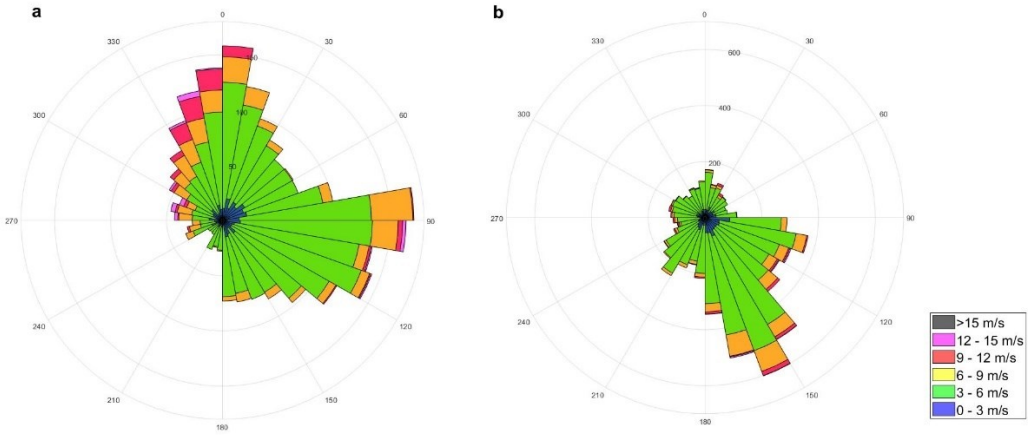

Figure 3.6 Wind roses showing average winds recorded by NOAA stations during the wave data collection time. (a) NOAA station FRWL1–8766072 (November 1st, 2018–April 9th, 2019). (b) NOAA station WBAN:00184 (April 10th–September 3rd,2019).

Wave Model

This study used the Simulating WAves Nearshore (SWAN) model version 40.85 [43] to simulate wave climates and quantify wave parameters such as significant wave height (Hs), mean wave period (Tm), and mean wave direction (Dir). SWAN is a numerical third–generation phase–

averaged model based on the spectrum concept that solves the energy balanced equation to simulate wave conditions in coastal and inland shallow water environments. SWAN simulates wind wave generation in time and space accounting for the following shallow water environment physics: refraction, shoaling, bottom friction, depth–induced wave breaking, white capping and nonlinear wave–wave interactions such as triads and quadruplets [43]. SWAN formulations, theories, equations, model validation, and verification have been well described in previous studies [26, 43–47]. Because this model is primarily based on first principles of physics, the model was not calibrated. Major limitations of SWAN include: 1) reflection is not simulated and diffraction is not specifically modeled, only approximated [46] 2) the model does not consider Bragg–scattering and wave tunneling [48].

Model simulations for each terrace site were performed using the following input parameters and conditions:

- Most frequent and spatially uniform wind fields through the model domain.
- Incident wind and wave parameters for each simulation (Table 2.1).
- Spatially uniform water level.
- A 1 m resolution grid.
- One computational domain (rectangular domain) of 600 x 600 m spatial resolution in the rectangular terrace field of study (Figure 3.4). Two computational domains (chevron 1 and chevron 2) of 300 x 300 m spatial resolution in the chevron terrace field of study (Figure 3.5).
- Spatially uniform water depth of 1 m and terrace height of 0.25 m above zero crossing for the rectangular terrace field of study and 0.35 m above zero crossing for the chevron terrace field. Terrace slope 3:1 was set by default by the SWAN

version 40.85. To our knowledge, bathymetry data are not widely available for inland marsh ponds in costal Louisiana. Field surveys of bathymetry conducted at our study sites revealed uniform depth and terrace features.

- Terrace shape, spacing, length and width was extracted from the most recent (2019) National Agricultural Imagery Program (NAIP) imagery. The imagery was segmented into land and water classes. The resultant raster was transformed to a text file and imported to SWAN. Terraces were included in the computational domains as structures that were one grid cell wide via the bathymetry file. Terraces as part of the bathymetry file allowed high horizontal resolution.
- All runs were performed in stationary mode. Stationary mode is used for waves with short travel time through the computational domain of study such as fetch limited environments (lakes, ponds, and breakwater environments) [49].
- A computational domain direction resolution of 0 degrees was used.
- SWAN default shallow water physics for lake environments were activated [50] except for bottom friction. Previous studies have shown that the effects of bottom friction (bottom dissipation) are minor in these reduced fetch limited conditions independent of bed material; therefore, these factors had minor influence in wave growth [26, 39].

Scenario Selection

Stationary computational scenarios (Table 3.1) were selected from the period of instrument deployment. For the current study, a stationary computational scenario is defined as a single wind event (wind speed and direction) with unique wave conditions (Hs, Tm and Dirpeak) occurring in

a specific day and time (Table 3.1). The stationary computational scenario is selected after 40–60 minutes of constant wind conditions. A stratified random sampling method was used to select stationary computational scenarios. This method has been previously used in a variety of studies with different objectives, for example, to forecast precipitation in a basin in China [51], validate satellite imagery in global forest burned areas [52], characterize soil samples in microbiological studies [53], monitor regional riparian forests using remote sensing [54], and others. In the current study, wind data was classified selecting the most frequent and uniform winds (during 40–60 minutes) in each terrace field of study. The first and second strata (subgroup) were based on wind direction, including winds coming from the NE and SE, respectively. The third and fourth strata (subgroup) were selected under each wind direction based on wind speed, including weak (0–3 m/s), intermediate (3–6 m/s) and high (>6 m/s) winds. It is important to note that random sampling was conducted within each stratum (subgroup) to select the computational scenarios. Therefore, in both terrace fields of study, two wind directions (NE, SE) and one wind speed for each wind condition (weak, intermediate, high) were used individually as a computational scenario to run SWAN in three different computational domains (Figure 3.4 and 3.5).

For model validation, 12 stationary computational scenarios were conducted per instrument, with a total of 36 simulations between the two sites. For the comparison of terraced versus unterraced scenarios, 36 additional simulations were run in the hypothetical scenarios without terraces, using the same model validation conditions described in table 1. The parameters used to compare SWAN simulations and measured data included: significant wave height (Hs), mean period (Tm), and mean wave direction (Dir). Statistical parameters used to quantitatively assess model performance included: Root Mean Square Error (RMSE), Scatter Index (SI), Bias and Correlation Coefficient (R) which are defined by the following expressions:

$$RMSE = \sqrt{\frac{1}{N}\sum_{j=1}^{N}(0_j - P_j)^2} \tag{3.1}$$

$$SI = \frac{\sqrt{\frac{1}{N}\sum_{j=1}^{N}(0_j - P_j)^2}}{\frac{1}{N}\sum_{j=1}^{N} O_j} \tag{3.2}$$

$$BIAS = \frac{1}{N}\sum_{j=1}^{N}(O_j - P_j) \tag{3.3}$$

$$R = \frac{\sum_{j=1}^{N}(O_j - \bar{O})(P_j - \bar{P})}{\sqrt{\sum_{j=1}^{N}(O_j - \bar{O})^2(P_j - \bar{P})^2}} \tag{3.4}$$

Where N is the number of observations, O is the measure value, P is the predicted value and $\bar{O}, \bar{P}$ represent the mean values.

Table 3.1 SWAN simulation inputs for incident wind and wave parameters for both terrace fields of study.

Terrace field of study	Incident waves instrument	Date / Time	Wind speed (m/s)	Wind direction (°)	Hs (m)	Tm (s)	Dirpeak (°)
		11/11/2018 10 00	2.91	25	0.11	1.00	64
		11/16/2018 22 00	2.72	122	0.12	0.92	152
		12/25/2018 9 00	2.90	98	0.14	0.89	98
		1/3/2019 16 00	5.89	87	0.24	0.98	93
		1/6/2019 14 00	2.42	88	0.14	0.96	121
Rectangular	R1	1/21/2019 18 00	7.05	87	0.44	0.94	113
		1/30/2019 10 00	2.11	30	0.11	0.92	74
		1/31/2019 6 00	3.94	76	0.19	0.92	96
		2/1/2019 3 00	4.48	69	0.20	0.93	97
		2/1/2019 6 00	8.15	98	0.39	1.09	120
		3/11/2019 0 00	2.88	80	0.17	0.93	111
		3/7/2019 12 00	4.78	82	0.16	0.90	97
		4/12/2019 7 00	2.24	20	0.13	0.93	82
		4/15/2019 12 00	2.24	100	0.12	0.94	89
		4/16/19 19	4.02	110	0.09	0.93	45
		4/27/2019 18 00	4.02	130	0.15	0.92	46
		5/1/2019 19 00	4.47	110	0.08	0.96	33
Chevron	C1	5/3/2019 14 00	4.02	100	0.12	0.93	42
		6/11/2019 7 00	3.13	10	0.13	1.05	59
		6/21/2019 10 00	6.26	160	0.13	1.08	92
		7/12/2019 18 00	8.05	40	0.10	0.89	77
		7/12/2019 23 00	9.83	20	0.10	0.88	48
		9/2/2019 16 00	2.68	30	0.14	0.97	37
		8/29/2019 9 00	2.24	20	0.07	0.97	31
		4/16/2019 12 00	6.26	110	0.06	0.89	113
		4/22/2019 13 00	4.92	120	0.11	0.95	120
		4/27/2019 9 00	4.47	100	0.12	0.98	124
		4/29/2019 14 00	7.15	120	0.08	0.90	148
		5/7/2019 7 00	2.68	110	0.09	0.89	129
Chevron	C2	5/8/2019 17 00	7.60	130	0.10	0.88	140
		5/8/2019 23 00	5.81	130	0.07	0.87	138
		5/16/2019 15 00	4.02	150	0.14	0.95	162
		5/20/2019 9 00	4.02	140	0.12	0.98	119
		6/4/2019 8 00	2.24	160	0.12	0.93	122
		7/4/2019 20 00	1.34	140	0.14	0.90	99
		7/14/2019 13 00	4.47	150	0.10	0.94	172

Results and Discussion

Model Validation

Model validation results for the 36 stationary runs for both terrace fields of study are shown in 1:1 scatter plots (Figure 3.7) comparing model simulations to the measured data. Table (3.2) shows the model error statistics performed for all model validation instruments (R2, C1, C2) in both terrace fields of study.

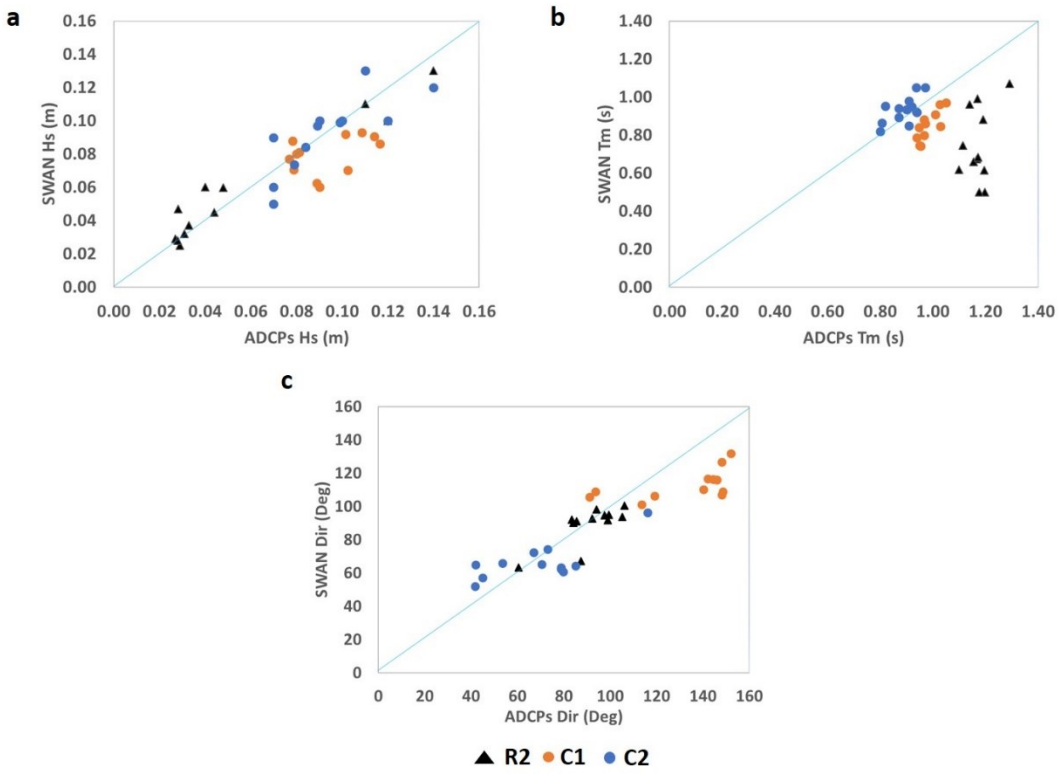

Figure 3.7 Model validation scatter plots comparing model simulations vs measured data for (a) Significant wave height (Hs), (b) Mean wave period (Tm), and (c) Mean wave Direction (Dir) for model validation instruments (R2, C1, C2).

Table 3.2 Model error statistics for both terrace fields of study. Wave instruments (R2, C1, C2) correspond to model validation points. Note that figure 3.4 and 3.5 maps these sites, instruments, and spatial model domains.

Terrace field of study	Instrument for model validation	Parameters	RMSE	BIAS	SI	R
Rectangular	R2	Hs (m)	0.01	0.00	0.19	0.97
		Tm (s)	0.46	-0.58	0.40	0.34
		Dir (dg)	8.29	-2.70	0.09	0.76
Chevron	C1	Hs (m)	0.02	-0.02	0.21	0.41
		Tm (s)	0.14	-0.16	0.14	0.64
		Dir (dg)	26.03	-25.66	0.20	0.59
Chevron	C2	Hs (m)	0.01	0.00	0.15	0.79
		Tm (s)	0.07	0.06	0.08	0.67
		Dir (dg)	15.02	-3.48	0.22	0.73

Significant Wave Height (Hs)

The range of significant wave height (Hs) measured by all instruments was between 0.03–0.14 m (Figure 3.7a). The range of Hs simulated by the model in all sites was between 0.03–0.13 m (Figure 3.7a). The measured range of Hs for R2 was from 0.03–0.14 m, for C1 from 0.08–0.12 m, and for C2 from 0.07–0.14 m (Figure 3.7a). The simulated ranges of Hs for R2 (0.03–0.13 m) and C2 (0.05–0.13 m) were similar compared to the measured range of Hs for both instruments (Figure 3.7a). However, for C1 the simulated range of Hs was lower (0.06–0.09 m), compared to the measured range of Hs (0.08–0.12 m, Figure 3.7a). For Hs, root mean square errors (RMSE) ranged from 0.01–0.02 m. The scatter index (SI) ranged between 0.15–0.21 for all wave instruments. A 0 bias was obtained for instruments R2 and C2, and a negative bias (–0.02) was found for C1. The correlation coefficients (R) for Hs were closer to 1 for R2 at 0.97 and C2 at 0.79, compared to a lower R for C1 at 0.42 (Table 3.2).

The range of measured and modeled Hs at R2 was greater than the ranges at either C1 or C2 (Figure 3.7a). This may be due to less variable wind and wave conditions occurring during the summer deployment for C1 and C2 compared to more variable winter conditions during the R2 deployment (Figure 3.7) [19]. The wider range of Hs observed at R2 could be due to greater wave events measured in the open water boundary at R1 which was used as incident wave conditions. Higher Hs was measured in the open water boundary at R1 (Figure 3.4) due to its longer fetch exposure compared with C1 or C2 that were exposed to smaller fetch (Figure 3.5).

The overall range of measured and simulated Hs (0.03–0.14 m) in the current study are commonly found in fetch limited environments [25]. The measured ranges of Hs agree with other studies conducted in similar conditions. Bottema et al., (2009) simulated and measured Hs smaller than 0.15 m for waves in lakes with fetch and depth limited conditions using SWAN [25]. Wiberg et al., (2019) found Hs ranging between 0.03–0.10 m in shallow (0.5–1.0 m) estuaries with the presence of oyster reefs. Their study compared wave measurements in protected and un–protected areas of the reefs to assess their effectiveness at reducing wave energy [55]. Also, Siemes et al., (2020) found small Hs (0.03 m) measured under weak and intermediate wind conditions in marshes protected by artificial structures. Their study utilized SWAN coupled to Delft 3D to analyze how different artificial structures affected the morphological development of salt marshes [56].

The SWAN default version 40.51 tends to underestimate wave parameters when simulating waves in fetch and depth limited shallow conditions [25, 27, 57–59]. In the current study, the negative bias (–0.02) for C1, shows a slight underestimation (1–33%) of measured Hs in most of the scenarios for C1. Previous studies found that SWAN underestimations of Hs and Tm in shallow water are attributed to an underestimation of the dimensionless ratio of Hs and the local water depth of the locally generated winds computed by SWAN [60, 61]. Similar to the current study,

Siemes et al., (2020) found that Hs values were underestimated by SWAN in marshes with artificial structures, possibly due to differences in bed level or to a default wave breaking parameter hypothesized to be too low. Due to the lack of bathymetry data, the current study assumed a uniform water depth and bed morphology according to field surveys conducted in the study sites. This assumption could also be a potential cause of disagreement between observed and modeled wave conditions. Elkut et al., (2021) also found a Hs underestimation by SWAN in <1 m depth. In this study, the lower R value for C1 (0.42) may be due to its deployment location in a shadow area at the leeward side of a terrace. According to Ilic et al., (2007) diffraction limitation of SWAN could affect Hs simulation in the shadow zone of the terrace. Nevertheless, the Hs RMSE, bias and SI for C1 were similar to other modeling studies [63].

Mean Wave Period (Tm)

Mean wave period (Tm) measured by all instruments was 0.80–1.29 s (Figure 3.7b). The range of Tm simulated by the model at all instrument locations was 0.74–1.07 s (Figure 3.7b). The measured range of Tm for R2 was from 1.10–1.29 s, for C1 it was 0.94–1.05 s, and for C2 it was 0.80–0.97 s (Figure 3.7b). The simulated ranges of Tm for R2 (0.50–1.07 s) and C1 (0.74–0.97 s) were lower compared to the measured range of Tm for both instruments (Figure 3.7b). However, for C2 the simulated range of Tm (0.82–1.05 s) was similar compared to the measured range of Tm (0.80–0.97 s, Figure 3.7b). For Tm, root mean square errors (RMSE) ranged between 0.07–0.46 s. The scatter index (SI) ranged between, 0.08–0.40 s for all wave instruments. A negative bias was obtained for R2 (–0.58) and C1 (–0.16), and a positive bias (0.06) was found for C2. The correlation coefficients (R) obtained for Tm were 0.34 for R2, 0.64 for C1, and 0.67 for C2 (Table 3.2).

The range of Tm (0.80–1.29 s) measured in the current study was similar to a previous study conducted by Wiberg et al., (2019) evaluating wave attenuation in a shallow water environments [55]. In their study, Tm of less than 2 s were measured in a shallow bay where waves were reduced by the presence of oyster reefs. The small, measured Tm is common in very low energy and shallow water environments such as marsh terrace fields. However, the wave instrument's ability to measure Tm accurately in these complex environments should be assessed in future studies. Dally (2018) experienced poor signal to noise ratio in the velocity measurements recorded by an ADCP deployed in shallow water during a short period of deployment. Therefore, in future studies, increasing the sampling frequency of the ADCPs could improve the accuracy of Hs and Tm measure in these shallow water environments [65]. According to Ellis and Sherman (2005), 10 Hz is the suggested sampling frequency to reduce wave parameters noise and error from measurements recorded in shallow water.

As previously mentioned, SWAN default version has a tendency to underestimate wave parameters when simulating waves in fetch and depth limited shallow lakes [25, 27, 57–59]. In the current study, the negative bias obtained for R2 (–0.58) and C1 (–0.16) showed Tm underestimations in all the scenarios for both instruments. The underestimations for R2 and C1 were 15–58% and 2–22% lower compared to the measured data, respectively. These underestimations were similar to those found in a ten–year data study for fetch and depth limited wave growth [25]. Bottema et al., (2009) found Tm underestimations between 10–25% in stationary scenarios modeled by the default SWAN version 40.51 in very short fetches [25]. Amrutha et al., (2016) also found Tm underestimations (16–31.5%) when hindcasting waves in a nearshore area of the Arabian Sea using SWAN. Dally (2018) also found Tm underestimations in a study comparing SWAN simulations with ADCP measurements in a nearshore environment. The

author obtained a negative bias (–0.48) for Tm which is similar to the results found in the current study. Elkut et al., (2021) also found Tm underestimations by SWAN in <1 m depth attributing them to model error and an improper detection of high frequencies by the wave gauges. Unfortunately, the reasons for SWAN Tm underestimations in this shallow water environments are not fully understood and might vary depending on the study area [64] However, Rogers et al 2003 hypothesized that the consistent underestimation of Tm by SWAN may be due to underestimation in low frequency energy (0.04–0.19 Hz) [68].

Mean Wave Direction (Dir)

In the computational scenarios assessed in this study, the range of mean wave direction (Dir) measured by all instruments was 42–152º (Figure 3.7c). The range of Dir simulated by the model was between 52–132º (Figure 3.7c). The measured range of Dir for R2 was from 61–106º, for C1 from 91–152º, and for C2 from 42–116º (Figure 3.7c). The simulated range of Dir for R2 (63–100º) was similar compared to the measured range of Dir (61–106 º). However, the simulated ranges for C1 (101–132º) and C2 (52–96º) differed between 12–41º and 1–20º, respectively, compared to the measured ranges of Dir. Root mean square errors (RMSE) ranged from 8.29–26.03º. The scatter index (SI) ranged between 0.09–0.22 for all wave instruments. A negative bias was obtained for R2 (–2.70), C1 (–25.66), and C2 (–3.48). The correlation coefficients (R) obtained were 0.76 for R2, 0.59 for C1, and 0.73 for C2 (Table 3.2).

The range of measured and modeled Dir was between 42–152º (Figure 3.7c). This range was consistent with the frequent wind conditions (10–160º, Figure 3.6, Table 3.1) and their variability during the deployment season [19]. However, the distance between the NOAA weather stations from where the wind data was acquired and the terrace fields of study (25 km from the rectangular site and 62 km from the chevron site) could be a possible reason for the disagreement

between observations and model results. Model simulations and error statistics for R2 and C2 were better compared with C1. C1 was located (Figure 3.5) in a shadow zone at the leeward side of a terrace where diffraction could affect the accuracy of the simulations compared to the measured data [62].

The range of RMSE (8.29–26.03º, Table 3.2) obtained in this study for Dir were higher compared to a previous study conducted in a complex shallow water environment [69]. Gorrel et al., (2011) simulated Dir utilizing SWAN and obtained RMSE < 5º in shallow waters (1 m) without the presence of breakwaters. In the current study, the negative bias obtained for all instruments, showed an underestimation of simulated Dir between 4–27% lower compared to the measured data. The simulation of wave direction is important for studies related to the optimization of wave breaking structures given that wind wave attenuation was found to be directly related with breakwater orientation [19, 41, 70].

Overall, model validation results for all wave parameters (Hs, Tm and Dir) evaluated in the current study are promising given the complexity of the study areas. Wave parameter underestimations found in this study agree with previous studies using the standard SWAN version when simulating waves in fetch and depth limited shallow lakes [25, 27, 57–59] or when encountering complex systems such as inlets or estuaries [71]. The potential reasons of SWAN underestimations were explained in the sections above for each wave parameter assessed. It is also important to mention that the accuracy and sensitivity of model error statistics could be associated with the wave and wind data used to force the model [72], the instrument's ability to measure small waves in complex systems, and the nature of the data (small and short waves) in fetch limited and low wave energy environments. For this reason, the narrow range of values obtained made the statistics parameters very sensitive to change.

Terraced vs Unterraced

To understand how terraces reduce significant wave height (Hs), this study compared study site wave climates in terraced scenarios versus hypothetical unterraced scenarios. A total of 36 hypothetical unterraced scenarios were run using the same incident wave and wind conditions from the 36 simulations in terraced scenarios conducted in the model validation (Table 3.1). The Hs was averaged throughout the spatial domain separately for each scenario. In all simulations, the average Hs was smaller in terraced scenarios compared to the hypothetical unterraced scenarios (Figure 3.8). Overall, average Hs reduction throughout the spatial domain, ranged between 18–84% for all scenarios.

In the rectangular terrace domain (Figure 3.4), terraces reduced the average Hs by 18–84%. It was found that Hs reduction varied based on different wind and wave conditions that were input in the model. In the same field, during weak (0–3 m/s) and intermediate (3–6 m/s) wind scenarios, Hs was reduced between 0.02–0.06 m. However, in high wind scenarios (>6 m/s), Hs was reduced between 0.07–0.1 m. Therefore, Hs dissipation was higher during high wind conditions.

In the chevron domains (Figure 3.5b, 3.5c), terraces reduced the average Hs between 32–82%. Contrary to the rectangular terrace domain, it was found that Hs reduction in the chevron domain did not vary based on different wind and wave conditions that were input in the model. In the same field, during weak (0–3 m/s), intermediate (3–6 m/s), and high wind scenarios (>6 m/s), Hs was reduced by 0.02–0.06 m. Therefore, Hs dissipation was similar during all wind conditions. Overall, the range of Hs reduction was higher in the rectangular terrace compared to the chevron terrace field, most likely due to terrace design features in the rectangular site such as: terraces interrupting fetch from four directions and closer terrace spacing. Therefore, fetch was interrupted more effectively from east–west in the rectangular terrace field.

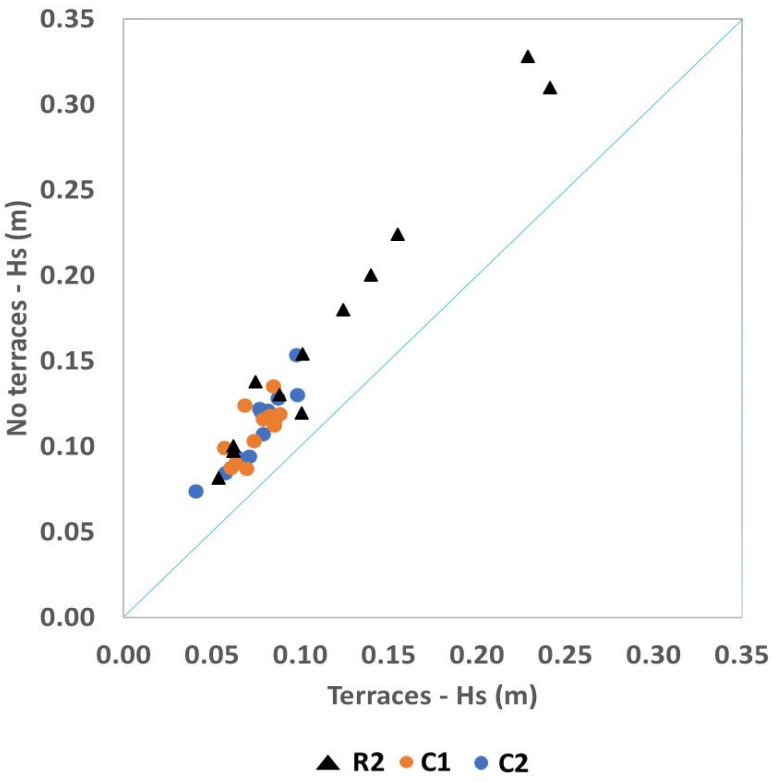

Figure 3.8 Average Hs (m) comparison of all scenarios with terraces vs no terraces.

For demonstrative purposes, we show two figures of Hs simulations in terraced vs unterraced scenarios for both fields of study (Figures 3.9 and 3.10). First, figure 3.9 shows an example of Hs simulated in the rectangular terrace field of study in a scenario with terraces (Figure 3.9a) and in a hypothetical pond without terraces (Figure 3.9b). In this example, the incident wave direction was approaching at 96° from the SE. The scenario with terraces clearly shows reduction of Hs due to the presence of terraces (Figure 3.9a). Hs gradually decreased to between 0.2–0.04 m when the wave travels away from the open boundaries and encounters the terraces. Hs was highly reduced in the shadow zone at the leeward side of the vertical terraces due to fetch interruption relative to the incident wave direction. In the hypothetical unterraced scenario (Figure 3.9b), Hs

ranged between 0.13–0.2 m, which was higher compared to the terraced scenario. In the same figure, Hs starts decreasing gradually possible due to depth limited conditions.

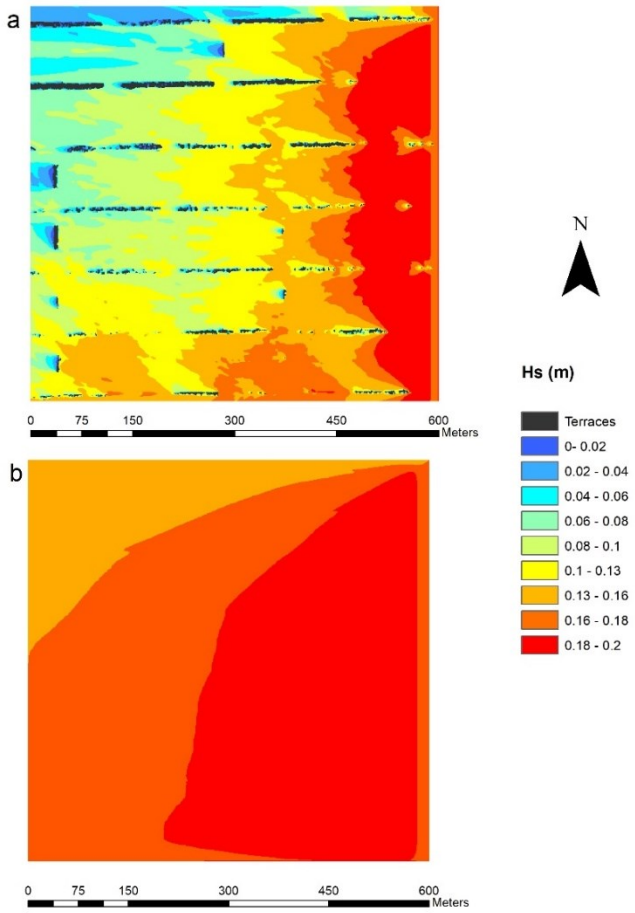

Figure 3.9 Hs simulations in the terraced (a) vs unterraced (b) scenario for the domain used in the rectangular terrace field of study.

Figure 3.10 shows an example of Hs simulated in the chevron terrace field of study in terraced vs unterraced scenarios when the incident wind and wave direction is coming at 77° from the NE (Figure 3.10 a, b) and at 113° SE (Figure 3.10 c, d), respectively. In both NE and SE scenarios with terraces (Figure 3.10 a, c), Hs was reduced to 0.02–0.08 m in the shadow zone at

the leeward side of the terraces. The Hs gradually increased when the wave traveled away from the leeward zone. Therefore, the chevron design dissipates waves similarly when the wind comes from either NE or SE. Hs was higher in the hypothetical unterraced ponds (Figure 3.10 b, d), compared to terraced scenarios, ranging between 0.09–0.15 m in the NE scenario and 0.08–0.10 m in the SE scenario.

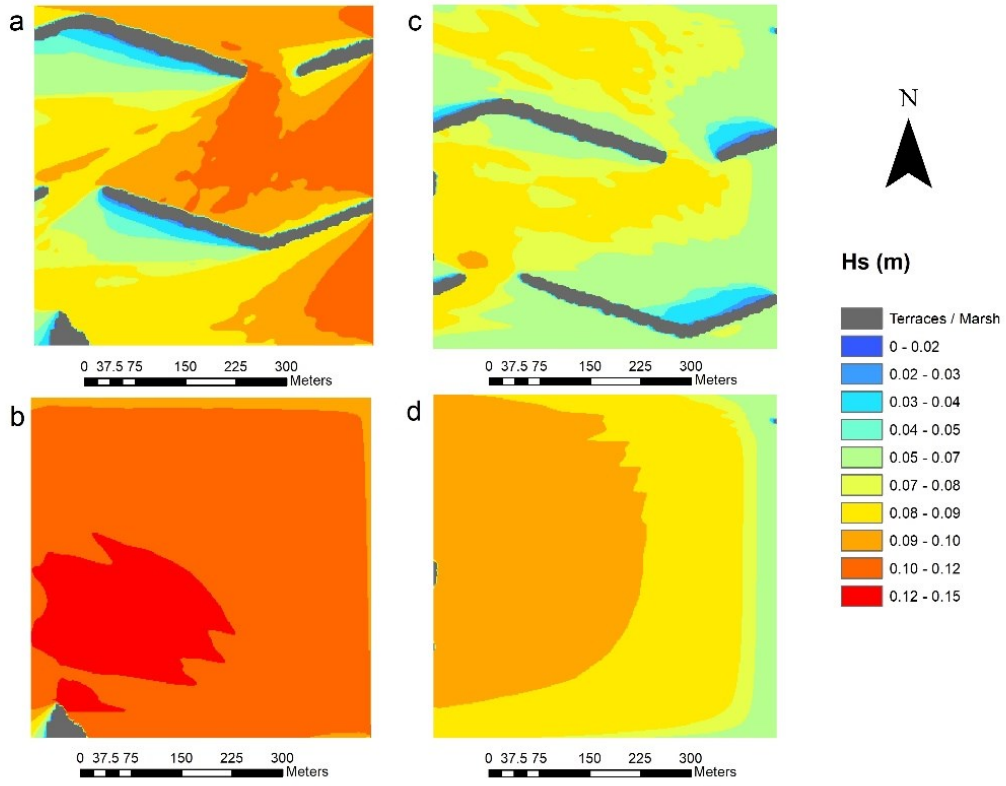

Figure 3.10 Hs simulations in terraced (a, c) versus unterraced (c, d) scenarios for both domains used in the chevron terrace field of study.

The results of the current study are consistent with Mathews (2020) who found that terraces reduced other hydrodynamic parameters such as total shear stress and water flow velocities in the leeward side of the terraces within the terrace field. Mathews (2020) also found that the same hydrodynamic parameters were higher in scenarios without terraces. However, their study did not

simulate wind driven waves. In the current study, the wave reduction obtained behind terraces (sheltered zone) was similar to a phenomenon known as island sheltering. According to Ti et al., (2018) island sheltering occurs when wave energy is attenuated behind islands. In accordance with this study, we confirmed that Hs and therefore wave energy, decreases in sheltering zones due to the presence of a structure.

The results obtained in this study, were similar to other studies assessing wave attenuation by natural or artificial breakwaters. Cooper and Mulligan (2016) found that breakwaters reduced Hs up to 63% compared to scenarios without breakwater. Wiberg et al., (2019) found an average Hs attenuation between 30–50% by oyster reefs in water depths similar to our study (0.5–1.0 m). The current study also supports the findings from Vona et al., (2020) showing that the average Hs reduction by a single breakwater ranged between 10–50% in all the simulated scenarios using Delf3D and SWAN. Also Vieria et al., (2020) found a substantial reduction of Hs due to the influence of an emerged detached breakwater protecting a coastal zone using SWAN and Xbeach. Future studies should include the marsh shoreline in the computational domain of terraced and unterraced scenarios in order to assess its effects on wave behavior. Marsh platform could potentially reduce mean Hs in the entire domain and affect the percentage of Hs reduction in the comparison between terraced and unterraced scenarios. Moreover, marsh platform could affect Dir within the computational domains.

Conclusions

This study utilized a numerical wave model to understand wave dynamics in two marsh terrace fields during frequent wind conditions in coastal Louisiana. Results from this study demonstrate SWAN's ability to simulate measured waves in marsh terrace fields, compare wave

climates in terraced and unterraced fields, and identify the role of marsh terraces at reducing significant wave height. The results also demonstrate the ability of marsh terraces to reduce wind driven waves. Results from the comparison of wave climates in terraced and unterraced fields showed that Hs was reduced by up to 84% in all the terraced scenarios proving the efficacy of this restoration technique.

Overall, the SWAN model was able to simulate wave conditions in marsh terrace fields even in the complex conditions of sheltered environments. The measured and modeled small (0.03–0.14 m) and high–frequency (0.80–1.29 s) waves found in this study are characteristic of other studies in low energy environments [25, 55, 56, 69]. Wave direction ranged between 42–152º in accordance with the most frequent wind directions during the deployment periods.

Model validation indicated that the simulated and observed data at both terrace fields of study were similar, particularly for significant wave height (RMSE: 0.01–0.02 m; R: 0.97 for R2, 0.79 for C2 and 0.42 for C1) and wave direction (RMSE: 8.29–26.03º; R: 0.76 for R2, 0.73 for C2, and 0.59 for C1,), demonstrating that SWAN was appropriate for use in marsh terrace systems. However, the accuracy of the simulations was likely affected by model limitations and the instruments' ability to measure small waves in complex systems. Also, model error statistics were very sensitive to change, possibly due to the nature of the narrow range of data measured in the marsh terrace fields. To improve the accuracy of the simulations, future studies may require the use of a phased decoupled refraction–diffraction approximation, particularly in the shadow zone of the terraces and around their tips. Future studies should also conduct model validation utilizing wind conditions (cold front passages, hurricanes) that are more likely to result in erosive waves based on previous studies. It is important to note that the most frequent wind conditions are not always necessarily the wind conditions that result in marsh erosion. Therefore, utilizing higher

wind conditions and greater Hs values as an input in SWAN could potentially strength and improve model validation results.

To our knowledge, this is the first study evaluating real wind wave climates in terrace fields utilizing a numerical wave model such as SWAN. Results indicate that 1) SWAN is appropriate for use in these low energy and geometrically complex marsh terrace systems and 2) marsh terraces are effective at reducing wave energy. Future studies assessing a variety of terrace configurations including different spacing, shape and orientation relative to wave height reduction, are recommended to optimize the use of this restoration technique. Also, more research assessing terrace designs relative to erosional forces are encouraged to determine the effectiveness of terraces at reducing marsh erosion in coastal Louisiana.

REFERENCES

[1] Brasher, M. G. Review of the Benefits of Marsh Terraces in the Northern Gulf of Mexico. **2015**, No. May.

[2] Smith, J. M.; Cialone, M. A.; Wamsley, T. V; McAlpin, T. O. Potential Impact of Sea Level Rise on Coastal Surges in Southeast Louisiana. *Ocean Eng.*, **2010**, *37* (1), 37–47.

[3] González, J. L.; Tornqvist, T. E. Coastal Louisiana in Crisis: Subsidence or Sea Level Rise? *Eos, Trans. Am. Geophys. Union*, **2006**, *87* (45), 493–498.

[4] Turner, R. E.; Rao, Y. S. Relationships between Wetland Fragmentation and Recent Hydrologic Changes in a Deltaic Coast. *Estuaries*, **1990**, *13* (3), 272–281.

[5] Wilson, C. A.; Allison, M. A. An Equilibrium Profile Model for Retreating Marsh Shorelines in Southeast Louisiana. *Estuar. Coast. Shelf Sci.*, **2008**, *80* (4), 483–494.

[6] Ortiz, A. C.; Roy, S.; Edmonds, D. A. Land Loss by Pond Expansion on the Mississippi River Delta Plain. *Geophys. Res. Lett.*, **2017**, *44* (8). https://doi.org/10.1002/2017GL073079.

[7] Vinent, O. D.; Herbert, E. R.; Coleman, D. J.; Himmelstein, J. D.; Kirwan, M. L. Onset of Runaway Fragmentation of Salt Marshes. *One Earth*, **2021**.

[8] Turner, R. E.; Streever, B. *Approaches to Coastal Wetland Restoration: Northern Gulf of Mexico*; Kugler Publications, 2002.

[9] Nyman, J. A.; Chabreck, R. H. Managing Coastal Wetlands for Wildlife. *Wildl. Tech. Manual. John Hopkins Univ. Press. Balt. Maryland, USA*, **2012**, 133–156.

[10] Underwood, S. G.; Steyer, G. D.; Good, B.; Chambers, D. Bay Bottom Terracing and Vegetative Planting: An Innovative Approach for Habitat and Water Quality Enhancement. In *Annual Conference on Wetlands Restoration and Creation. Hillsborough Community College, Tampa, FL, USA*; 1991; pp 164–173.

[11] Brasher, M. G.; Hetherwick, J.; Cenac, W. Personal Communication, 2021.

[12] Rozas, L. P.; Minello, T. J. Marsh Terracing as a Wetland Restoration Tool for Creating Fishery Habitat. *Wetlands*, **2001**, *21* (3), 327–341.

[13] O'Connell, J. L.; Nyman, J. A. Marsh Terraces in Coastal Louisiana Increase Marsh Edge and Densities of Waterbirds. *Wetlands*, **2010**, *30* (1), 125–135.

[14] Osorio, R. J.; Linhoss, A. Evaluation of Marsh Terraces for Wetland Restoration: A Remote Sensing Approach. *Water*, **2020**, *12* (2), 336.

[15] Marani, M.; D'Alpaos, A.; Lanzoni, S.; Santalucia, M. Understanding and Predicting Wave Erosion of Ma[1] Marani, M.; D'Alpaos, A.; Lanzoni, S.; Santalucia, M. Understanding and Predicting Wave Erosion of Marsh Edges. Geophys. Res. Lett., 2011, 38 (21).Rsh Edges. *Geophys. Res. Lett.*, **2011**, *38* (21).

[16] Schwimmer, R. A. Rates and Processes of Marsh Shoreline Erosion in Rehoboth Bay, Delaware, USA. *J. Coast. Res.*, **2001**, 672–683.

[17] Steyer, G. D.; Cretini, K. F.; Piazza, S. C.; Sharp, L. A.; Snedden, G. A.; Sapkota, S. *Hurricane Influences on Vegetation Community Change in Coastal Louisiana*; US Geological Survey, 2010.

[18] Couvillion, B. R.; Barras, J. A.; Steyer, G. D.; Sleavin, W.; Fischer, M.; Beck, H.; Trahan, N.; Griffin, B.; Heckman, D. Land Area Change in Coastal Louisiana from 1932 to 2010. **2011**.

[19] French, J.; Skarke, A. Optimization of Marsh Terracing as a Wetland Restoration Technique: Mitigation of Cohesive Sediment Erosion by Waves Associated with Frontal Passage, Mississippi State University, 2020.

[20] Leonardi, N.; Ganju, N. K.; Fagherazzi, S. A Linear Relationship between Wave Power and Erosion Determines Salt-Marsh Resilience to Violent Storms and Hurricanes. *Proc. Natl. Acad. Sci.*, **2016**, *113* (1), 64–68.

[21] Leonardi, N.; Carnacina, I.; Donatelli, C.; Ganju, N. K.; Plater, A. J.; Schuerch, M.; Temmerman, S. Dynamic Interactions between Coastal Storms and Salt Marshes: A Review. *Geomorphology*, **2018**, *301*, 92–107.

[22] Campolongo, F.; Cariboni, J.; Saltelli, A. An Effective Screening Design for Sensitivity Analysis of Large Models. *Environ. Model. Softw.*, **2007**, *22* (10), 1509–1518.

[23] Hughes, S. A. *Physical Models and Laboratory Techniques in Coastal Engineering*; World Scientific, 1993; Vol. 7.

[24] McLoughlin, S. M.; Wiberg, P. L.; Safak, I.; McGlathery, K. J. Rates and Forcing of Marsh Edge Erosion in a Shallow Coastal Bay. *Estuaries and Coasts*, **2015**, *38* (2), 620–638.

[25] Bottema, M.; van Vledder, G. P. A Ten-Year Data Set for Fetch-and Depth-Limited Wave Growth. *Coast. Eng.*, **2009**, *56* (7), 703–725.

[26] Breugem, W. A.; Holthuijsen, L. H. Generalized Shallow Water Wave Growth from Lake George. *J. Waterw. port, coastal, Ocean Eng.*, **2007**, *133* (3), 173–182.

[27] van der Westhuysen, A. J. Modeling of Depth-induced Wave Breaking under Finite Depth Wave Growth Conditions. *J. Geophys. Res. Ocean.*, **2010**, *115* (C1).

[28] Salmon, J. E.; Holthuijsen, L. H.; Zijlema, M.; van Vledder, G. P.; Pietrzak, J. D. Scaling Depth-Induced Wave-Breaking in Two-Dimensional Spectral Wave Models. *Ocean Model.*, **2015**, *87*, 30–47.

[29] Cavaleri, L.; Abdalla, S.; Benetazzo, A.; Bertotti, L.; Bidlot, J.-R.; Breivik, Ø.; Carniel, S.; Jensen, R. E.; Portilla-Yandun, J.; Rogers, W. E. Wave Modelling in Coastal and Inner Seas. *Prog. Oceanogr.*, **2018**, *167*, 164–233.

[30] Möller, I.; Kudella, M.; Rupprecht, F.; Spencer, T.; Paul, M.; Van Wesenbeeck, B. K.; Wolters, G.; Jensen, K.; Bouma, T. J.; Miranda-Lange, M. Wave Attenuation over Coastal Salt Marshes under Storm Surge Conditions. *Nat. Geosci.*, **2014**, *7* (10), 727–731.

[31] Sheng, Y. P.; Lapetina, A.; Ma, G. The Reduction of Storm Surge by Vegetation Canopies: Three-dimensional Simulations. *Geophys. Res. Lett.*, **2012**, *39* (20).

[32] Smolders, S.; Plancke, Y.; Ides, S.; Meire, P.; Temmerman, S. Role of Intertidal Wetlands for Tidal and Storm Tide Attenuation along a Confined Estuary: A Model Study. *Nat. hazards earth Syst. Sci.*, **2015**, *15* (7), 1659–1675.

[33] Temmerman, S.; De Vries, M. B.; Bouma, T. J. Coastal Marsh Die-off and Reduced Attenuation of Coastal Floods: A Model Analysis. *Glob. Planet. Change*, **2012**, *92*, 267–274.

[34] Wamsley, T. V; Cialone, M. A.; Smith, J. M.; Ebersole, B. A.; Grzegorzewski, A. S. Influence of Landscape Restoration and Degradation on Storm Surge and Waves in Southern Louisiana. *Nat. Hazards*, **2009**, *51* (1), 207–224.

[35] Mariotti, G.; Fagherazzi, S.; Wiberg, P. L.; McGlathery, K. J.; Carniello, L.; Defina, A. Influence of Storm Surges and Sea Level on Shallow Tidal Basin Erosive Processes. *J. Geophys. Res. Ocean.*, **2010**, *115* (C11).

[36] Barbier, E. B.; Georgiou, I. Y.; Enchelmeyer, B.; Reed, D. J. The Value of Wetlands in Protecting Southeast Louisiana from Hurricane Storm Surges. *PLoS One*, **2013**, *8* (3).

[37] Dietrich, J. C.; Tanaka, S.; Westerink, J. J.; Dawson, C. N.; Luettich, R. A.; Zijlema, M.; Holthuijsen, L. H.; Smith, J. M.; Westerink, L. G.; Westerink, H. J. Performance of the Unstructured-Mesh, SWAN+ ADCIRC Model in Computing Hurricane Waves and Surge. *J. Sci. Comput.*, **2012**, *52* (2), 468–497.

[38] Tonelli, M.; Fagherazzi, S.; Petti, M. Modeling Wave Impact on Salt Marsh Boundaries. *J. Geophys. Res. Ocean.*, **2010**, *115* (C9).

[39] Young, I. R.; Verhagen, L. A. The Growth of Fetch Limited Waves in Water of Finite Depth. Part 1. Total Energy and Peak Frequency. *Coast. Eng.*, **1996**, *29* (1–2), 47–78.

[40] Valentine, K.; Mariotti, G. Wind-Driven Water Level Fluctuations Drive Marsh Edge Erosion Variability in Microtidal Coastal Bays. *Cont. Shelf Res.*, **2019**, *176*, 76–89.

[41] Mathews, M. C. Geomorphic Effectiveness of Marsh Terracing as a Coastal Restoration Technique in Southern Louisiana. Tulane University School of Science and Engineering 2020.

[42] Ducks Unlimited. Geodatabase of Existing Marsh Terraces, 2015.

[43] Booij, N.; Ris, R. C.; Holthuijsen, L. H. A Third-generation Wave Model for Coastal Regions: 1. Model Description and Validation. *J. Geophys. Res. Ocean.*, **1999**, *104* (C4), 7649–7666.

[44] Booij, N.; Holthuijsen, L. H.; Ris, R. C. The" SWAN" Wave Model for Shallow Water. In *Coastal Engineering 1996*; 1997; pp 668–676.

[45] Ris, R. C.; Holthuijsen, L. H.; Booij, N. A Third-generation Wave Model for Coastal Regions: 2. Verification. *J. Geophys. Res. Ocean.*, **1999**, *104* (C4), 7667–7681.

[46] Gonçalves, M.; Rusu, E.; Soares, C. G. Evaluation of the Wave Models SWAN and STWAVE in Shallow Water Using Nested Schemes. *Marit. Eng. Technol.*, **2012**, *481*, 178–185.

[47] Ou, S.-H.; Liau, J.-M.; Hsu, T.-W.; Tzang, S.-Y. Simulating Typhoon Waves by SWAN Wave Model in Coastal Waters of Taiwan. *Ocean Eng.*, **2002**, *29* (8), 947–971.

[48] TUDelft. SWAN model features http://swanmodel.sourceforge.net/features/features.htm.

[49] SWAN team. SWAN User Manual. Delft University of Technology 2012, p 94.

[50] Team, S. Scientific and Technical Documentation, SWAN Cycle III Version 41.01. *Delft Univ. Technol. Dep. Civ. Eng. Delft, Netherlands*, **2015**.

[51] Hu, Y.; Schmeits, M. J.; Jan van Andel, S.; Verkade, J. S.; Xu, M.; Solomatine, D. P.; Liang, Z. A Stratified Sampling Approach for Improved Sampling from a Calibrated Ensemble Forecast Distribution. *J. Hydrometeorol.*, **2016**, *17* (9), 2405–2417.

[52] Padilla, M.; Stehman, S. V; Chuvieco, E. Validation of the 2008 MODIS-MCD45 Global Burned Area Product Using Stratified Random Sampling. *Remote Sens. Environ.*, **2014**, *144*, 187–196.

[53] Wallenius, K.; Niemi, R. M.; Rita, H. Using Stratified Sampling Based on Pre-Characterisation of Samples in Soil Microbiological Studies. *Appl. soil Ecol.*, **2011**, *51*, 111–113.

[54] Claggett, P. R.; Okay, J. A.; Stehman, S. V. Monitoring Regional Riparian Forest Cover Change Using Stratified Sampling and Multiresolution Imagery 1. *JAWRA J. Am. Water Resour. Assoc.*, **2010**, *46* (2), 334–343.

[55] Wiberg, P. L.; Taube, S. R.; Ferguson, A. E.; Kremer, M. R.; Reidenbach, M. A. Wave Attenuation by Oyster Reefs in Shallow Coastal Bays. *Estuaries and Coasts*, **2019**, *42* (2), 331–347.

[56] Siemes, R. W. A.; Borsje, B. W.; Daggenvoorde, R. J.; Hulscher, S. J. M. H. Artificial Structures Steer Morphological Development of Salt Marshes: A Model Study. *J. Mar. Sci. Eng.*, **2020**, *8* (5), 326.

[57] de Waal, J. P. Wave Growth Limit in Shallow Water. In *Ocean Wave Measurement and Analysis (2001)*; 2002; pp 560–569.

[58] Bottema, M.; Beyer, D. Evaluation of the SWAN Wave Model for the Dutch IJsselmeer Area. In *Ocean Wave Measurement and Analysis (2001)*; 2002; pp 580–609.

[59] Elkut, A. E.; Taha, M. T.; Zed, A. B. E. A.; Eid, F. M.; Abdallah, A. M. Wind-Wave Hindcast Using Modified ECMWF ERA-Interim Wind Field in the Mediterranean Sea. *Estuar. Coast. Shelf Sci.*, **2021**, *252*, 107267.

[60] van Vledder, G.; Groeneweg, J.; van der Westhuysen, A. Numerical and Physical Aspects of Wave Modelling in a Tidal Inlet. In *Coastal Engineering 2008: (In 5 Volumes)*; World Scientific, 2009; pp 424–436.

[61] Groeneweg, J.; van der Westhuysen, A.; van Vledder, G.; Jacobse, S.; Lansen, J.; van Dongeren, A. Wave Modelling in a Tidal Inlet: Performance of SWAN in the Wadden Sea. In *Coastal Engineering 2008: (In 5 Volumes)*; World Scientific, 2009; pp 411–423.

[62] Ilic, S.; Van Der WESTHUYSEN, A. J.; Roelvink, J. A.; Chadwick, A. J. Multidirectional Wave Transformation around Detached Breakwaters. *Coast. Eng.*, **2007**, *54* (10), 775–789.

[63] Ti, Z.; Wei, K.; Qin, S.; Li, Y.; Mei, D. Numerical Simulation of Wave Conditions in Nearshore Island Area for Sea-Crossing Bridge Using Spectral Wave Model. *Adv. Struct. Eng.*, **2018**, *21* (5), 756–768.

[64] Dally, W. R. Comparison of a Mid-Shelf Wave Hindcast to ADCP-Measured Directional Spectra and Their Transformation to Shallow Water. *Coast. Eng.*, **2018**, *131*, 12–30.

[65] Brumley, B. H.; Cabrera, R. G.; Deines, K. L.; Terray, E. A. Performance of a Broad-Band Acoustic Doppler Current Profiler. *IEEE J. Ocean. Eng.*, **1991**, *16* (4), 402–407.

[66] Ellis, J. T.; Sherman, D. J. Effects of Sampling Frequency on Wave Characterization. *Zeitschrift fur Geomorphol. Suppl. Coasts Under Stress II*, **2005**, 183.

[67] Amrutha, M. M.; Kumar, V. S.; Sandhya, K. G.; Nair, T. M. B.; Rathod, J. L. Wave Hindcast Studies Using SWAN Nested in WAVEWATCH III-Comparison with Measured Nearshore Buoy Data off Karwar, Eastern Arabian Sea. *Ocean Eng.*, **2016**, *119*, 114–124.

[68] Rogers, W. E.; Hwang, P. A.; Wang, D. W. Investigation of Wave Growth and Decay in the SWAN Model: Three Regional-Scale Applications. *J. Phys. Oceanogr.*, **2003**, *33* (2), 366–389.

[69] Gorrell, L.; Raubenheimer, B.; Elgar, S.; Guza, R. T. SWAN Predictions of Waves Observed in Shallow Water Onshore of Complex Bathymetry. *Coast. Eng.*, **2011**, *58* (6), 510–516. https://doi.org/https://doi.org/10.1016/j.coastaleng.2011.01.013.

[70] Cooper, A. H.; Mulligan, R. P. Application of a Spectral Wave Model to Assess Breakwater Configurations at a Small Craft Harbour on Lake Ontario. *J. Mar. Sci. Eng.*, **2016**, *4* (3), 46.

[71] Groeneweg, J.; Van Nieuwkoop, J. SWAN's Underestimation of Long Wav e Penetration into Coastal Systems. **2015**.

[72] Rogers, W. E.; Kaihatu, J. M.; Hsu, L.; Jensen, R. E.; Dykes, J. D.; Holland, K. T. Forecasting and Hindcasting Waves with the SWAN Model in the Southern California Bight. *Coast. Eng.*, **2007**, *54* (1), 1–15. https://doi.org/https://doi.org/10.1016/j.coastaleng.2006.06.011.

[73] Vona, I.; Gray, M. W.; Nardin, W. The Impact of Submerged Breakwaters on Sediment Distribution along Marsh Boundaries. *Water*, **2020**, *12* (4), 1016.

[74] Vieira, B. F. V; Pinho, J. L. S.; Barros, J. A. O.; Antunes do Carmo, J. S. Hydrodynamics and Morphodynamics Performance Assessment of Three Coastal Protection Structures. *J. Mar. Sci. Eng.*, **2020**, *8* (3), 175.

CHAPTER IV

ASSESMENT OF MARSH TERRACE DESIGNS FOR WAVE REDUCTION UTILIZING A WAVE MODEL

Introduction

Marsh Terracing

Marsh terraces are linear, narrow, and discontinuous berms of sediment constructed from *in situ* sediment in inland shallow coastal ponds in the Northern Gulf of Mexico [1, 2]. Marsh terracing is a wetland restoration technique that has been implemented for more than 30 years in Texas and Louisiana in response to marsh loss due to wave erosion, subsidence, and sea level rise [3, 4]. Since the beginning of the 1990's until 2018, approximately 116 restoration projects with terraces arranged in a variety of designs have been built [5, 6]. Based on the most recent Louisiana terrace inventory database created by the National Audubon Society [7] the most common terrace designs include chevron (31%), linear (32%) and square (grid, 6%) with different spacings and orientations depending on the location [6, 8]. The construction of the most common terrace designs could be due to space optimization in the ponds, or because common designs are easier to construct as they follow a pattern within the terrace site. Other terrace designs built in coastal Louisiana have a variety of geometric patterns such as rectangular (4%), and arbitrary (without a pattern, 27 %) designs [7]. The variability of designs could be due to marsh terracing projects are usually implemented for specific purposes as necessary, such as the protection of a pipeline, a shoreline, or a levee [6]. Marsh terraces are built to attenuate the

energy of wind driven waves, create new marsh and reduce marsh erosion [9]. The objectives of this restoration technique are to by minimize fetch and therefore reducing significant wave height (Hs) [1, 10].

Study Definitions

For the current study, several terms will be defined. **Terrace design**: A computational marsh terrace grid having a specified terrace shape and spacing between terraces. **Representative terrace**: a real terrace designed with the most common terrace shape and spacing between terraces built in the northern Gulf of Mexico. **Hypothetical terrace design:** a hypothetical terrace designed with a terrace spacing that was modified from a representative terrace. **Stationary wind conditions:** constant wind event (wind speed and direction) for 40-60 minutes. **Wind/wave scenario:** a model run that is based on a single wind event with unique wave conditions measured on a specific day and time. The Wind/wave scenarios are selected from stationary wind conditions. **Wind event:** low, prefrontal, or postfrontal wind conditions. **Low wind event:** a wind event with speeds ranging from of 3–6 m/s and a wind direction coming from the NNE and ESE according to the wind data observed in the current study. **Prefrontal wind event:** winds occurring before a cold front passage [11] with wind speeds ranging 6–12 m/s coming from the SE. **Postfrontal wind event:** winds occurring after a cold front passage [11] with wind speeds ranging 6–12 m/s coming from the NNW. **Significant wave height (Hs) reduction:** Hs reduction is calculated based on comparing the incident Hs to the Hs behind the terrace features.

Previous Research Assessing Marsh Terrace Performance

Recent research quantified the efficacy of terraces at reducing Hs and therefore wave energy in real marsh terrace fields compared with hypothetical ponds without terraces [10]. Another study evaluated the performance of multiple marsh terrace projects over time demonstrating higher deposition than erosion in terraced locations. [12, 13]. Other studies suggest that the optimal terrace orientation, for reducing the occurrence of erosive forces, is perpendicular to the wind directions associated with cold front passages [13, 14]. Previous research [1, 10, 12–14] encouraged the assessment of different terrace design features such as shape, length and spacing between terraces to determine an optimal terrace design. However, to our knowledge, no studies have assessed the effectiveness of marsh terrace designs (different shape, terrace length and spacings) at reducing Hs utilizing a numerical wave model.

Wave Model Studies in Environments Protected by Structures

Numerical models such as the Simulating WAves Nearshore (SWAN), Delft 3D, STWAVE, Xbeach, and REFDIF have been used to assess wave conditions in shallow water environments that are semi-protected by an artificial or a natural marine structure. Cooper and Mulligan (2016) utilized SWAN and Delft 3D to assess breakwater designs in Lake Ontario. Their study demonstrated that breakwaters attenuated wave heights up to 63% compared to no breakwater scenario and that a breakwater extension attenuated wave heights 54% more [15]. Vona et al., (2020) utilized SWAN and Delft 3D to quantify the effects of breakwaters on wave reduction, sediment distribution, and marsh evolution to assess the impact of waves and currents on marsh shorelines. Their results showed an average Hs reduction between 10-50% in all the simulations, concluding that breakwaters are effective at protecting marsh boundaries from erosion due to wave energy. Vieira et al., (2020) assessed hydrodynamical and morphodynamical

aspects of three coastal protection structures, including submerged and subaerial breakwaters using SWAN and Xbeach. Their study found that the emerged breakwater was the most effective at reducing Hs; however, the submerged breakwater performed better in the morphodynamics processes.

Numerical Modeling Studies in Marsh Terrace Environments

Few studies have used numerical modeling to assess wave conditions and hydrodynamics in marsh terrace environments. A recent study showed that SWAN effectively simulates wave climates in real marsh terrace fields [10]. Osorio et al., 2021 demonstrated that wave climates in marsh terrace fields are characterized by wind driven waves with Hs ranging from 0.03-0.14 m during low wind conditions, and wind speeds ranging from 0-6 m/s coming from the SE and NE depending on the season. The same study demonstrated an 84% reduction in Hs in simulations with terraces compared to unterraced simulations. Mathews (2020) conducted a study using Delft3D to simulate hydrodynamic conditions in hypothetical designs (linear, chevron, square). Their study found an overall reduction of water velocities and bed shear stresses within terraces and at the leeward side of the terraces. However, Mathews (2020) did not simulated waves climates in their studies, which supports the need of the current study.

Objectives

Based on the results and recommendations of previous research [1, 10, 12–14], the main objective of this study is to assess the effectiveness of the most common terrace shapes (linear, chevron, square), constructed perpendicular to wind directions, at reducing Hs during the most frequent low winds and cold front passages in the Northern Gulf of Mexico. The current study assessed low wind events and cold front passages based on previous research [13, 14, 18]

demonstrating that the most erosive forces in marshes occur during those two wind events. For this study, SWAN was utilized to simulate wind driven waves in representative and hypothetical terrace designs by using real wind and wave data measured in a real marsh terrace site and validated in a previous study [10]. The results of this study will 1) Identify the most optimal terrace shape at reducing Hs. 2) Find an optimal terrace spacing between terraces for reducing Hs 3) Assess terrace design effectiveness at reducing Hs during frequent low wind events and cold front passages, and 4) Estimate the construction costs of various terrace shape and spacing for design consideration.

Materials and Methods

Terrace Designs

This study visually identified the most common terrace shapes constructed in the Northern Gulf of Mexico using a marsh terrace geodatabase created by Ducks Unlimited (DU) [8], a Louisiana terrace inventory database (LTIGAR) created by the National Audubon Society [7], and Google Earth Pro [19]. The most common terrace shapes constructed include linear, chevron, and square (Figure 4.1). This information was corroborated through personal communications with DU engineers and scientists [6]. Also, DU staff mentioned that terrace shape and spacing varies among projects relative to the project goal and the pond area where the project will be constructed. According to a database of marsh terracing projects constructed by DU from 2009 until 2020 [6, 20], terrace spacing ranges between 90–152 m. However, the most common terrace spacing implemented within the same project is approximately 110 m between terraces [6].

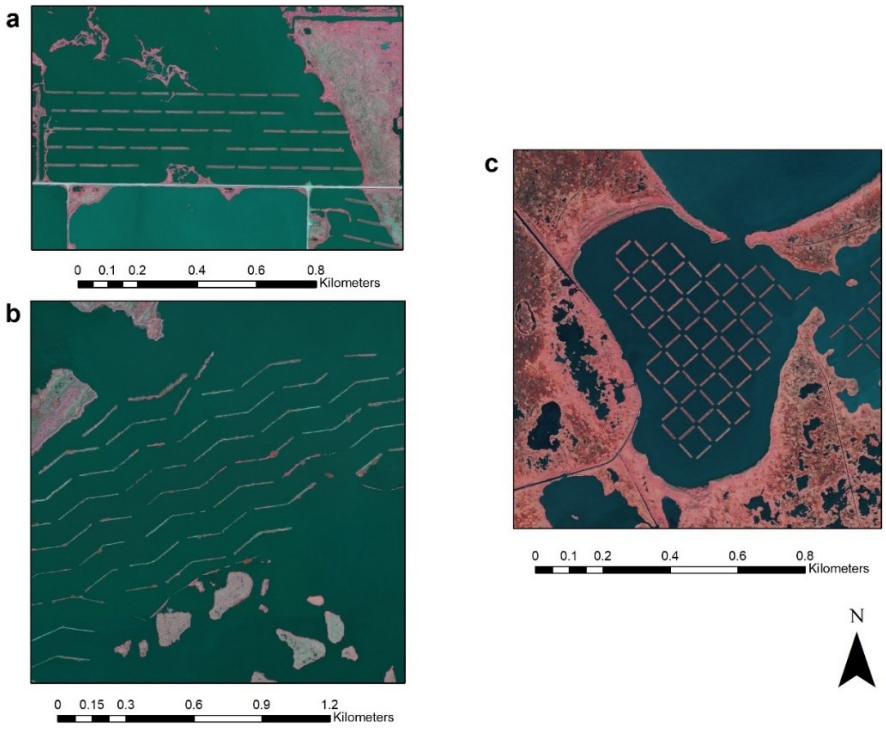

Figure 4.1 Examples of the most common terrace designs constructed in the Northern Gulf of Mexico. (a) Linear design at Cameron Parish, LA. (b) Chevron design at Cameron Parish, LA. (c) Square design at Jefferson County, TX.

Wave Data

The current study used wave data measured in a real marsh terrace site in Vermilion Parish, LA (Figure 4.2). Wave data collected was used as incident wave conditions for the terrace designs evaluated through the model. Wave observations were recorded by a Nortek Signature1000 acoustic doppler profiler (ADCP). The ADCP (R1) was deployed outside of a terrace field at the eastern boundary in the unterraced area (Figure 4.2). It is important to mention that the same wave data from this instrument was used successfully in a recent study that simulated and validated wave climates in marsh terraces using SWAN [10].

Figure 4.2 Wave instrument location in a real marsh terrace site at Vermilion Parish, LA. The wave data used to force the model in the current study was recorded by the depicted ADCP (R1).

Wave data was collected for five months (159 days) from November 1st, 2018, to April 9th, 2019. The ADCP was deployed on an aluminum frame placed on the marsh floor approximately in water depth of 1 m. The ADCP recorded wave measurements at 8 Hz, and it was programmed to sample ensemble wave bursts for 17 min every hour. Wave data was processed, and wave statistics were calculated using the Ocean Contour ADCP data processing software [21] . Wave statistics include significant wave height (Hs), mean wave period (Tm), peak period (Tpeak), wave mean direction (Dir), wave peak direction (Dirpeak), directional spread (Dirspread), water column acoustic backscatter intensity, water depth (h).

Wind Data

The current study used wind data obtained from the nearest weather station to the terrace site where wave data was collected (Figure 4.2). Wind data was used as model input wind

conditions for the terrace designs. Wind data was downloaded from the National Oceanic and Atmospheric Administration (NOAA) station FRWL1–8766072 located at the Freshwater Canal Locks. The NOAA weather station was located approximately 25 km to the east of the terrace site where the wave instrument was deployed.

This study identified frequent wind data events including low wind events and cold front passages, that occurred during the same months of wave data collection from November 1st, 2018, to April 9th, 2019 (159 days). Generally, the most frequent low wind events recorded had a wind speed of 3–6 m/s and a wind direction coming from the NNE and ESE (Figure 4.3).

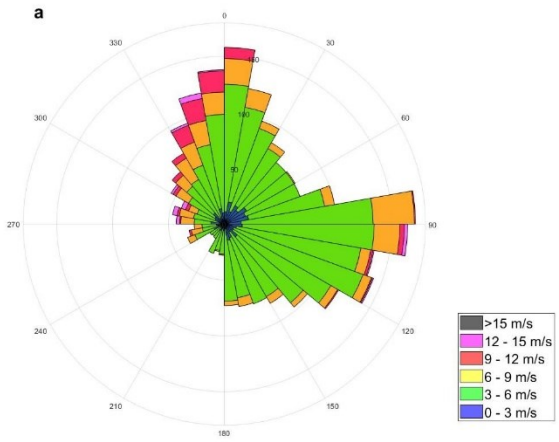

Figure 4.3 Wind rose showing average winds recorded by NOAA station FRWL1–8766072 (November 1st, 2018-April 9th, 2019) during the wave data collection time.

Similar to a previous study conducted in marsh terracing [14], cold front passages were identified from surface analysis charts produced by the NOAA weather prediction center (WPC). A total of 30 cold front passages were identified at the terrace site during the wave instrument deployment months. Wind data acquired from the FRWL1–8766072 station during cold front

passages were classified as prefrontal and postfrontal events. According to Guo et al., 2020, the wind direction suddenly changing from south to north indicates that a cold front has passed. Wind shifts were identified in the wind data obtained from the NOAA station FRWL1–8766072 to classify pre and post frontal events, based in the atmospheric charts. Prefrontal and postfrontal winds observed during the study months, showed that wind speeds ranged between 6–12 m/s with winds coming from the SE for prefrontal events and NNW for postfrontal events [13]. Wind directions observed from the weather station agree with a previous study assessing waves by atmospheric fronts in coastal Louisiana mentioning that prefrontal winds usually blow from the south and postfrontal winds blow from the north [11]. Cold front passage data was evaluated in the present study because it has been shown that one of the main sources of erosive stress in marsh terraces involves wave energy generated during these events [11, 14].

Wave Model

The current study used SWAN model version 40.85 [22] to simulate wave conditions in marsh terrace environments to find an optimal terrace design at reducing Hs. SWAN is a third-generation spectral wave model that simulates wave conditions in coastal regions. The model solves the energy balanced wave action equation for wave field evolution which has been broadly described in previous studies [23–25] . SWAN accounts for all the important wave source and dissipation processes in wave energy propagation through time and space as well as wave-wave interactions. The model solves and represent the following formulations and physical processes related with intermediate and shallow water depth: refraction, shoaling, bottom friction, depth-induced wave breaking, white capping and nonlinear wave-wave interactions such as triads and quadruplets [23]. In SWAN, breakwaters can be represented using two approaches: 1) as thin linear obstacles with specific transmission coefficients that are superimposed on top of

the bathymetry or 2) as structures that are at least one grid cell wide that are defined via the bathymetry file [15]. In the current study, marsh terraces were defined through the bathymetry file, which allowed for higher horizontal resolution. Terrace design specifics are described in the computational grid section. Some of the model limitations include the inability to simulate reflection and diffraction [26]. However, it has been demonstrated that diffraction effects are less pronounced in breakwater environments with wind driven wave conditions [27]. It is important to mention that a recent study successfully demonstrated SWAN's ability to simulate wave climates in real marsh terrace sites during frequent wind events by performing model testing [10].

Computational grids

Nine computational grids (terrace designs) were developed based on the most common terrace designs in coastal Louisiana (Figure 4.1). Each computational grid was composed of rectilinear and uniform structured grids of 500 x 500 m with a high-resolution cell size of 1 m^2 (Figure 4.4). Based on previous terracing projects and field surveys, water depth and terrace features such as length, width and slope are very uniform within the same project. Therefore, uniform parameters used in all computational grids included: water depth of 1 m, terrace width of 5 m, terrace height of 0.30 m above zero crossing, terrace slope of 3:1 set by default for all terraces by the model. Also, the orientation for all computational grids was set to 55°, which is perpendicular to the wind direction during low wind events and cold front passages associated with the most frequent and erosive wave conditions [14]. Computational grids were built and modified in Excel, saved as text files, and then imported into SWAN.

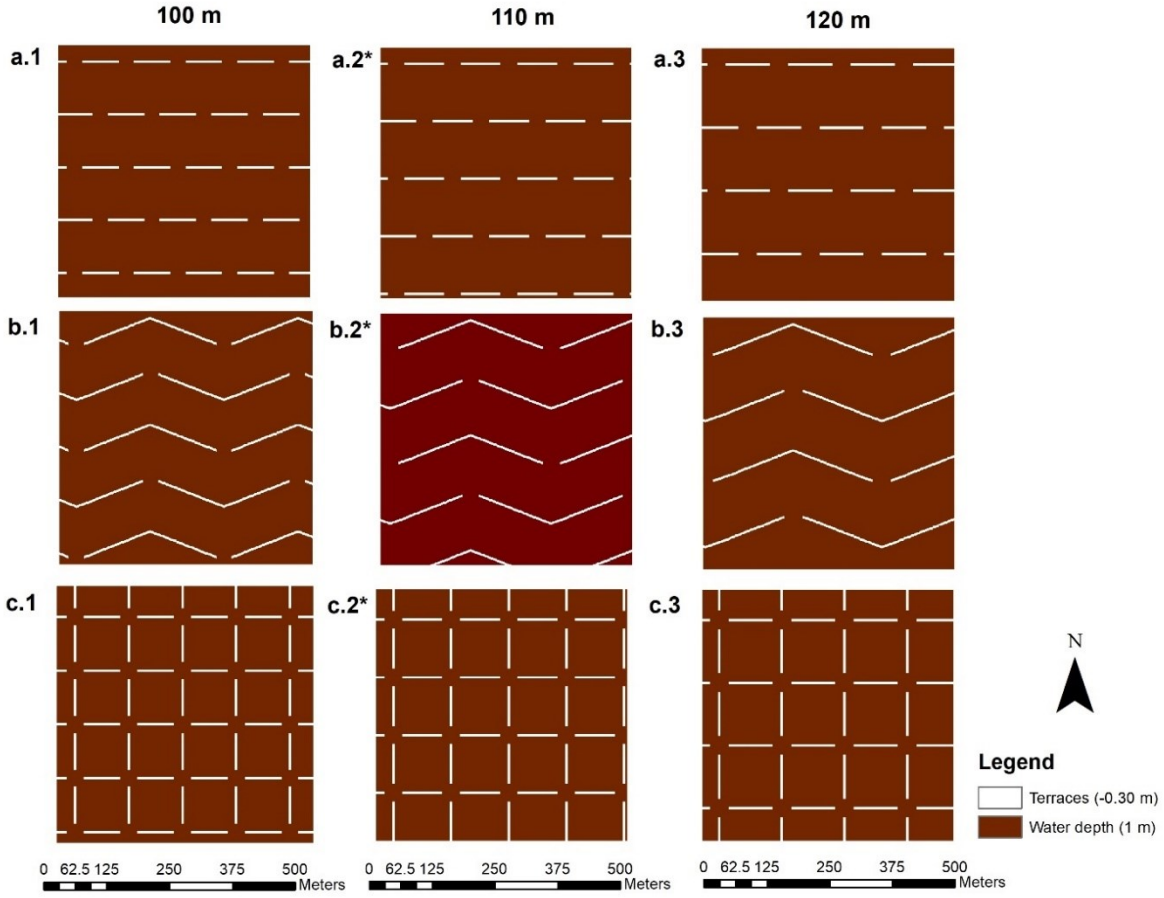

Figure 4.4 Nine terrace designs used as bathymetry in SWAN. a.1, a.2, a.3. Linear shape with terrace spacing of 100, 110 and 120 m, respectively. b.1, b.2, b.3 Chevron shape with terrace spacing of 100, 110 and 120 m, respectively. c.1, c.2, c.3 Square shape with terrace spacing of 100, 110 and 120 m, respectively. (*) indicates representative designs acquired from the most common terrace projects in the Northern Gulf of Mexico.

Three computational grids of the representative terraces (Figure 4.4 a.2, b.2, c.2) were built according to real design characteristics constructed in previous projects [6, 20]. For the representative terraces (Figure 4.4 a.2, b.2, c.2) terrace spacing was 110 m between terraces within each computational grid (Table 4.1).

Six hypothetical terrace designs (Figure 4.4 a.1, b.1, c.1 a.3, b.3, c.3) were built derived from the representative terraces. Hypothetical terrace designs were performed to evaluate the

efficacy of different terrace spacings at reducing Hs per terrace shape. Terraces modifications for the hypothetical terrace designs included terrace spacing, terrace length, and the resulting total terrace square meters per site (Figure 4.4, Table 4.1). In order to make terrace spacing and length proportional for each of the hypothetical terrace designs (Figure 4.4 a.1, b.1, c.1 a.3, b.3, c.3), the representative terraces measurements (Table 4.1) were modified by multiplying and dividing its values by 1.1. Resulting in two more sets of hypothetical terrace designs per terrace shape with the following features: 1) Hypothetical terrace designs with 100 m separation between terraces (Figure 4.4 a.1, b.1, c.1) 2) Hypothetical terrace designs with 120 m separation between terraces (Figure 4.4 a.3, b.3, c.3). Table 4.1 shows the terrace specifics for each of the terrace designs.

Table 4.1 Terrace specifics for each representative and hypothetical terrace designs. (*) Denotes representative terraces.

Terrace shape	Grid	Vertical Spacing (m)	Horizontal Spacing (m)	Individual terrace length (m)	Total terrace length (m)	Total terrace area (sq m)
	a.1	100	30	73	1,773	8,861
Linear	a.2*	110	33	80	1,746	8,727
	a3	120	36	88	1,428	7,138
	b.1	100	30	263	2,209	11,042
Chevron	b.2*	110	33	289	2,011	10,053
	b.3	120	36	318	1,820	9,097
	c.1	100	33	72	3,340	16,696
Square	c.2*	110	35	80	3,153	15,761
	c.3	120	37	88	2,824	14,116

Initial conditions, boundary conditions, and physics

The model was run in two-dimensional stationary mode. Initial conditions include spatially uniform water level of "0" throughout the model domains for all nine terrace designs

evaluated. Water level variation in marsh terraces is small enough to be neglected due to lack of tidal variation in the area.

Boundary conditions used to force the model include wave and wind data obtained from the ADCP and the NOAA weather station, respectively. Incident wave parameters include Hs (m), Tm (s), and Dirpeak (°). Wind data parameters include wind speed (m/s) and wind direction (°). Winds were also assumed to be spatially uniform throughout the model domains. Incident conditions were input at the northwestern or southeastern boundaries of the computational domains depending on the wind event used in the simulation. Incident parameters for frequent low and prefrontal events, were input at the southeastern boundary. Incident parameters for postfrontal events were input at the northwestern boundary.

SWAN default shallow water physics for lake environments were activated [28]. It is important to mention that bottom friction was not considered. Previous studies have shown that the effects of bottom friction are negligible in these reduced fetch limited conditions independent of bed material; therefore, these factors have minor influence in wave growth [25, 29].

Wind/wave scenario selection, simulations, and analysis

A stratified random sampling method was used to select single and stationary wind/wave scenarios during the data collection period (November 1st, 2018, to April 9th, 2019). First, wind data was classified in three wind events: low, prefrontal, and postfrontal winds. The most frequent low wind events recorded had a wind speed of 3–6 m/s and a wind direction coming from the NNE and ESE. Prefrontal and postfrontal winds observed during the study months, showed that wind speeds ranged between 6–12 m/s with winds coming from the SE for prefrontal events and NNW for postfrontal events [13]. Subsequently, the most constant and uniform winds during 40–60 minutes were selected under each wind event. Finally, six

wind/wave scenarios were randomly selected from each wind event, giving a total of 18 wind/wave scenarios selected. (Table 4.2). The 18 wind/wave scenarios were each used to run SWAN for each of the nine terrace designs, giving a total of 162 simulations performed in the current study. Table 4.2 depicts the wind/wave scenarios selected, and the incident wind and wave parameters input in the model.

Table 4.2 Incident wind/wave scenarios input in SWAN for all nine terrace designs assessed.

Wind event	Date / Time	Wind speed (m/s)	Wind direction (°)	Hs (m)	Tm (s)	Dirpeak (°)
Low	1. 11/16/2018 22:00	2.72	122	0.12	0.92	152
	2. 1/6/2019 14:00	2.42	88	0.14	0.96	121
	3. 1/31/2019 6:00	3.94	76	0.19	0.92	96
	4. 2/1/2019 3:00	4.48	69	0.20	0.93	97
	5. 3/11/2019 0:00	2.88	80	0.17	0.93	111
	6. 3/7/2019 12:00	4.78	82	0.16	0.90	97
Prefrontal	7. 12/8/18 14:00	7.39	97	0.20	0.95	91
	8. 12/12/18 19:00	6.02	102	0.16	0.93	108
	9. 12/27/18 17:00	6.68	140	0.22	1.07	177
	10. 1/22/19 1:00	7.3	90	0.22	0.96	107
	11. 2/20/19 9:00	6.05	149	0.21	1.15	174
	12. 2/23/19 18:00	5.84	146	0.33	1.16	174
Postfrontal	13. 11/4/18 5:00	6.17	328	0.31	1.03	358
	14. 11/26/18 2:00	10.03	337	0.33	1.13	352
	15. 12/9/18 16:00	7.31	327	0.36	1.02	344
	16. 2/8/19 10:00	10.08	350	0.36	1.17	359
	17. 2/24/19 16:00	8.21	351	0.31	1.05	360
	18. 3/26/19 20:00	7.1	338	0.31	1.00	357

To assess and compare the Hs behavior between terrace shapes and spacings for each of the nine terrace designs, the current study computed 1-D Histograms and descriptive statistics. Summary statistics calculated include minimum, maximum, mean, median, skewness, 90% upper and lower confidence interval and 90% confidence interval range.

Results

This section presents the results according to the following outline. First, simulated Hs from two wind/wave scenarios (Table 4.2, wind/wave scenario 4. and 15.) for all terrace designs. Second, the impact of different terrace spacings on Hs within each terrace shape. Third, comparison of Hs between terrace shapes. Fourth, Hs by terrace designs in different wind events. Finally, an estimation of the construction costs of the nine terrace designs evaluated in the current study.

Examples of Simulations for All Terrace Designs During Low Wind and Post Frontal Events

For demonstrative purposes, we show two figures of Hs simulations during a low wind event (Figure 4.5) and post frontal wind event (Figure 4.6) for all terrace designs assessed in the study. First, figure 4.5 shows an example of Hs simulated using wind and wave data during a low wind event occurred in 2/1/2019 at 3:00 (Table 4.2, wind/wave scenario 4.). In this example, the incident wave direction was approaching at 97° from the SE. All terrace designs clearly show reduction of Hs due to the presence of terraces. This is seen at each southeast boundary when the incident wind is reduced upon encountering the terrace structure. Hs was highly reduced in the shadow zones at the leeward side of the terraces due to fetch interruption relative to the incident wave direction. However, the chevron designs (Figure 4.5 b1, b2, b3) showed the most elongated and widest shadow zones with the smallest Hs ranging between 0–0.05 m compared to the linear (Figure 4.5 a1, a2, a3) and square designs (Figure 4.5 c1, c2, c30). It is important to note that the attenuation of Hs in the shadow zones was similar between the spacings assessed within each shape. This can also be corroborated in Appendix B (Figure B.1, B.2, B.3) showing the distribution

of Hs simulated for each terrace shape and spacing during the low wind event depicted in Figure 4.5.

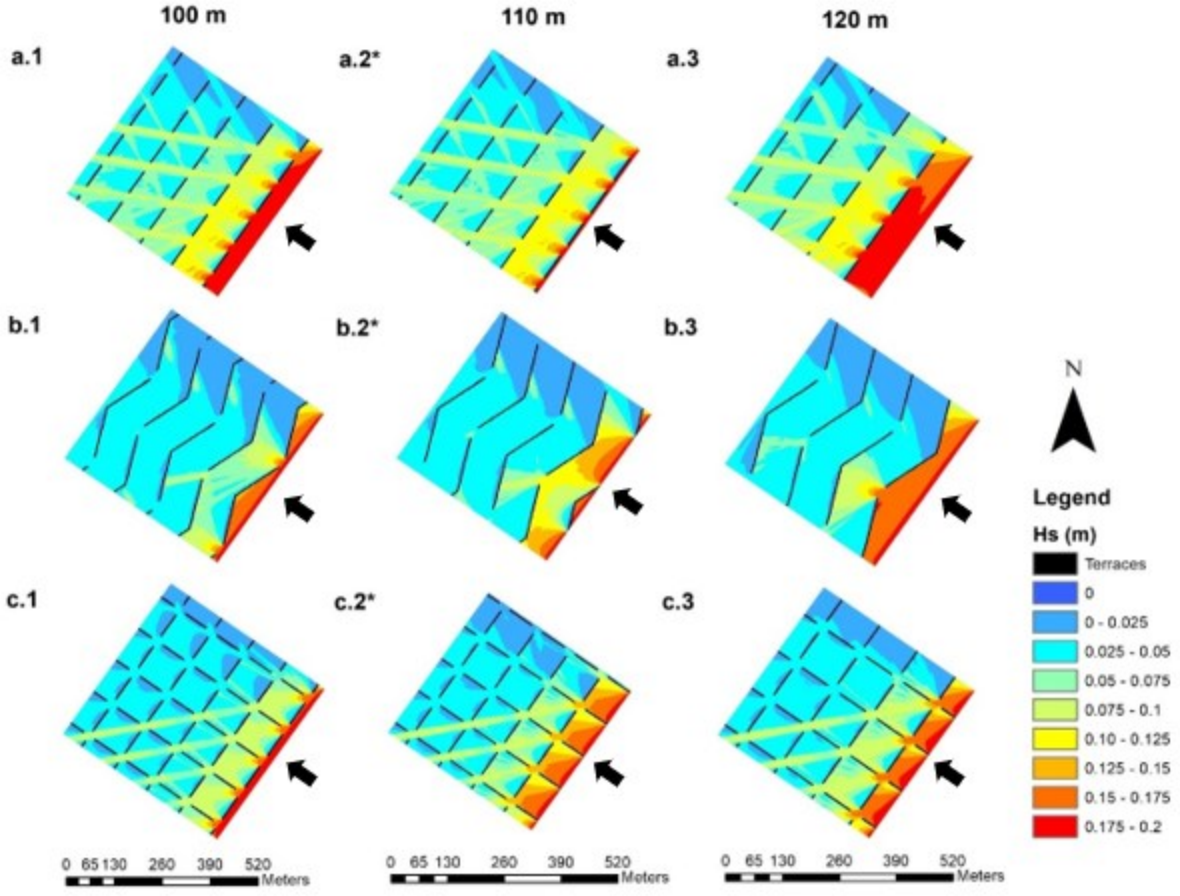

Figure 4.5 SWAN Hs simulations during a low wind event occurred in 2/1/2019 3:00. a.1, a.2, a.3. Linear designs with terrace spacing of 100, 110 and 120 m, respectively. b.1, b.2, b.3. Chevron designs with terrace spacing of 100, 110 and 120 m, respectively. c.1, c.2, c.3. Square designs with terrace spacing of 100, 110 and 120 m, respectively. Arrows indicate wind direction. (*) indicates representative terraces acquired from the most common terrace designs in the Northern Gulf of Mexico.

Figure 4.6 shows an example of Hs simulated using wind and wave data during a postfrontal wind event that occurred in 12/9/2018 at 16:00 (Table 4.2, wind/wave scenario 15.). In this example, the incident wave direction was approaching at 344° from the NE. All terrace

designs clearly showed a reduction of Hs due to the presence of terraces (Figure 4.6). Hs gradually decreased between 0.36–0 m when the wave traveled away from the northwest boundaries and encountered the terraces. Hs was highly reduced in the shadow zones at the leeward side of the terraces due to fetch interruption relative to the incident wave direction. Similar to figure 4.5, the chevron designs (Figure 4.6 b1, b2, b3) show the most elongated and widest shadow zones with the smallest Hs ranging between 0–0.05 m compared to the linear (Figure 4.6 a1, a2, a3) and square designs (Figure 4.6 c1, c2, c30). It is important to note that the attenuation of Hs represented by the shadow zones were similar between spacings assessed within each shape. This can also be corroborated in Appendix B (Figure B.4, B.5, B.6) showing the distribution of Hs simulated for each terrace shape and spacing during the postfrontal wind event depicted in Figure 4.6.

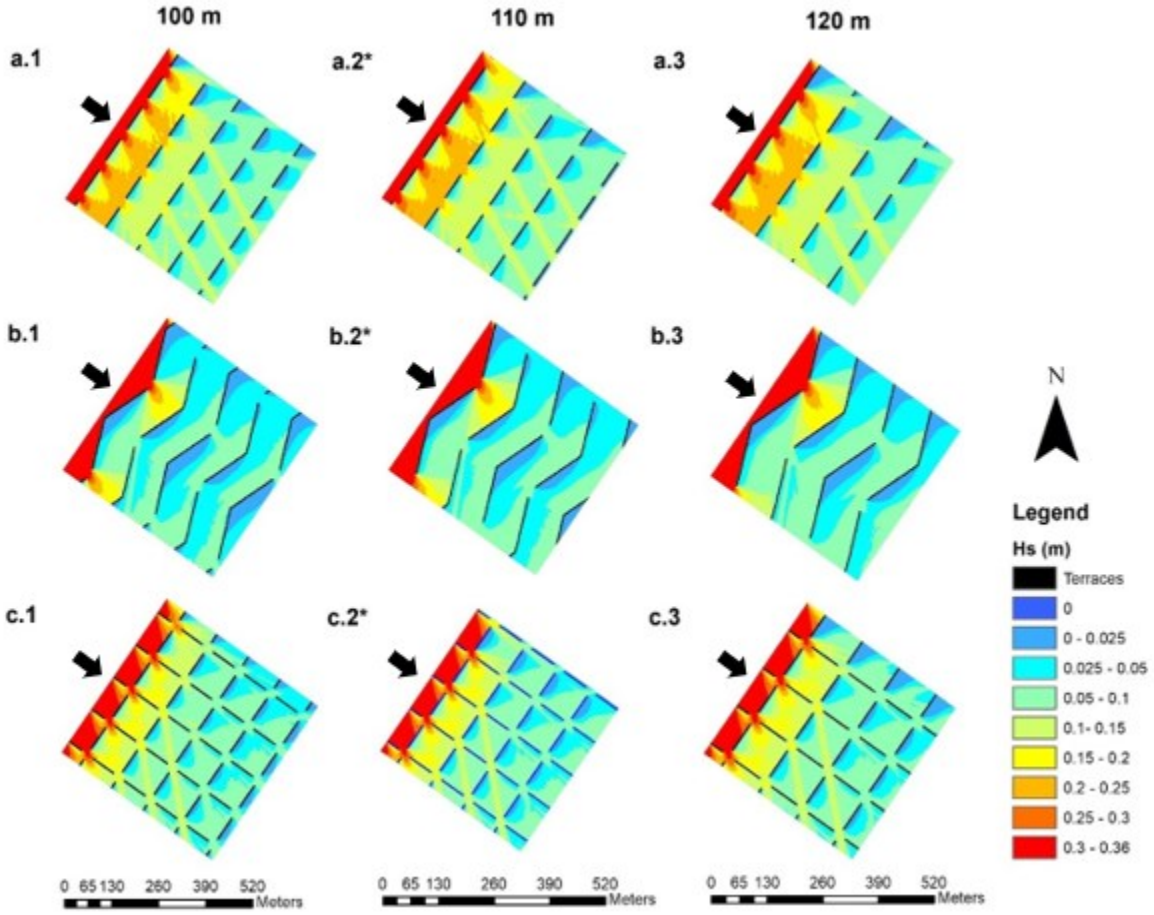

Figure 4.6 SWAN Hs simulations during a post frontal wind event occurred in 12/9/2018 16:00. a.1, a.2, a.3. Linear designs with terrace spacing of 100, 110 and 120 m, respectively. b.1, b.2, b.3. Chevron designs with terrace spacing of 100, 110 and 120 m, respectively. c.1, c.2, c.3. Square designs with terrace spacing of 100, 110 and 120 m, respectively. Arrows indicate wind direction. (*) indicates representative designs acquired from the most common terrace designs in the Northern Gulf of Mexico.

Hs Comparison Between Terrace Spacings

Appendix A shows the statistics for the simulated Hs for the linear (Table A.1), chevron (Table A.2), and square (Table A.3) designs. Statistics describe Hs conditions obtained from the 18 wind/wave scenarios simulated for each terrace spacing (100,110,120 m) evaluated per

terrace shape. A total of 54 model runs were performed per terrace shape, giving a total of 162 model runs conducted. Figure 4.7 depicts the frequency of occurrence for the mean Hs for all the simulations conducted for the three spacings evaluated.

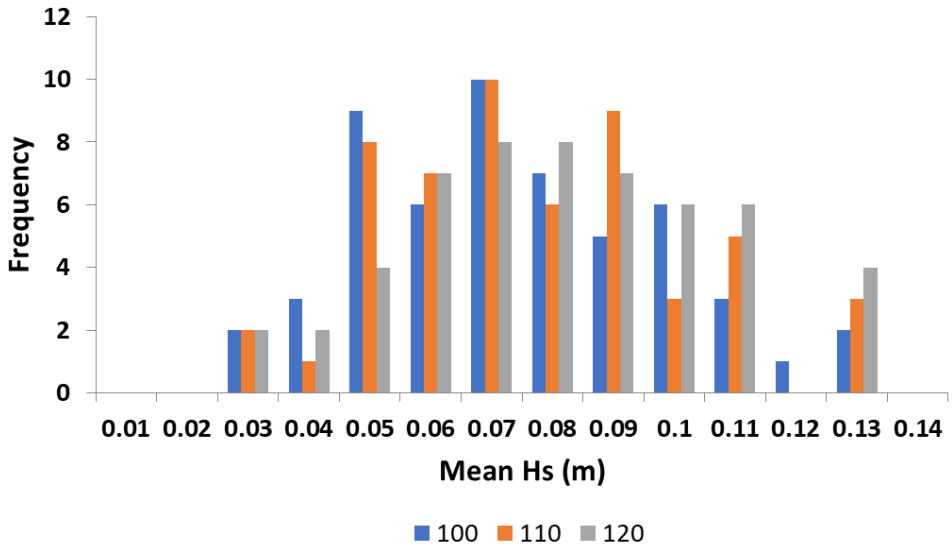

Figure 4.7 Histogram of mean Hs showing the frequency of occurrence for all the wind/wave scenarios comparing 100, 110 and 120 m spacing between terraces.

Findings from this study, show that Hs was not primarily affected by differences between the three-terrace spacings (100,110,120 m). The Hs descriptive statistics (Appendix A, Table A.1, A.2, A.3 and Figure 4.7) for all the terrace designs showed similar ranges for the three-terrace spacings evaluated within each shape. This is also reflected in the figures in Appendix B showing the distribution of Hs simulated for each terrace shape and spacing during the low and postfrontal wind event.

Overall, the statistics showed in Appendix A, Table A.1, A.2, A.3, show that the range of minimum (0 m), maximum (0.12–0.37 m) and mean (0.03–0.13 m, Figure 4.7) Hs were the same

for all the spacings under all the shapes evaluated. However, the frequency of occurrence of mean Hs (Figure 4.7) slightly varied between spacings, implying that there was a slight variation between the spacings analyzed under each shape. For the linear shape, the median ranged between 0.04–0.1 m in all spacings. For the chevron and square shape, the median ranged between 0–0.08 m in all spacings. The skewness values obtained were positive for all the terrace spacings. For the chevron shape, the 90% CI range (0.1–0.34 m) was the same between all spacings. For the linear (0.06–0.33 m) and square (0.08–0.32 m) shape, the 90% CI range was very similar between all spacings evaluated.

Hs Comparison Between Terrace Shapes

Figure 4.8 shows the frequency of occurrence for the mean Hs for the 162 model runs including the 18 wind/wave scenarios, three shapes, and three spacings. For the linear shape, the mean Hs throughout the spatial domain ranged between 0.05–0.13 m. For the chevron shape the mean Hs throughout the spatial domain ranged between 0.03–0.10 m. For the square shape, the mean Hs throughout the spatial domain ranged between 0.04–0.11 m. Also, figure 4.8 shows that in the chevron shape, most occurrences for the mean Hs were in the 0.05 m (9 wind/wave scenarios), 0.07 (10 wind/wave scenarios), and 0.08 m (9 wind/wave scenarios) classes. For the square shape, most occurrences for the mean Hs were in the 0.07 m (11 wind/wave scenarios) and 0.09 m (10 wind/wave scenarios) classes, and for the linear shape, most occurrences for mean Hs were in the 0.08 m (8 wind/wave scenarios) and 0.13 m (9 wind/wave scenarios) classes. Overall, figure 4.8 shows that the chevron shape had smaller mean Hs compared to the square and the linear shape and that the linear shape had higher mean Hs occurrences compared to the square and chevron shapes.

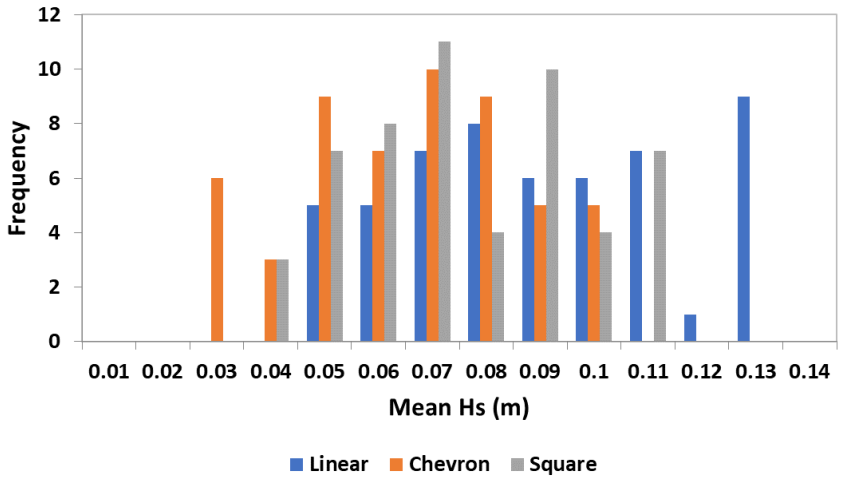

Figure 4.8 Histogram of mean Hs showing the frequency of occurrence for all the wind/wave scenarios comparing linear, chevron and square shapes.

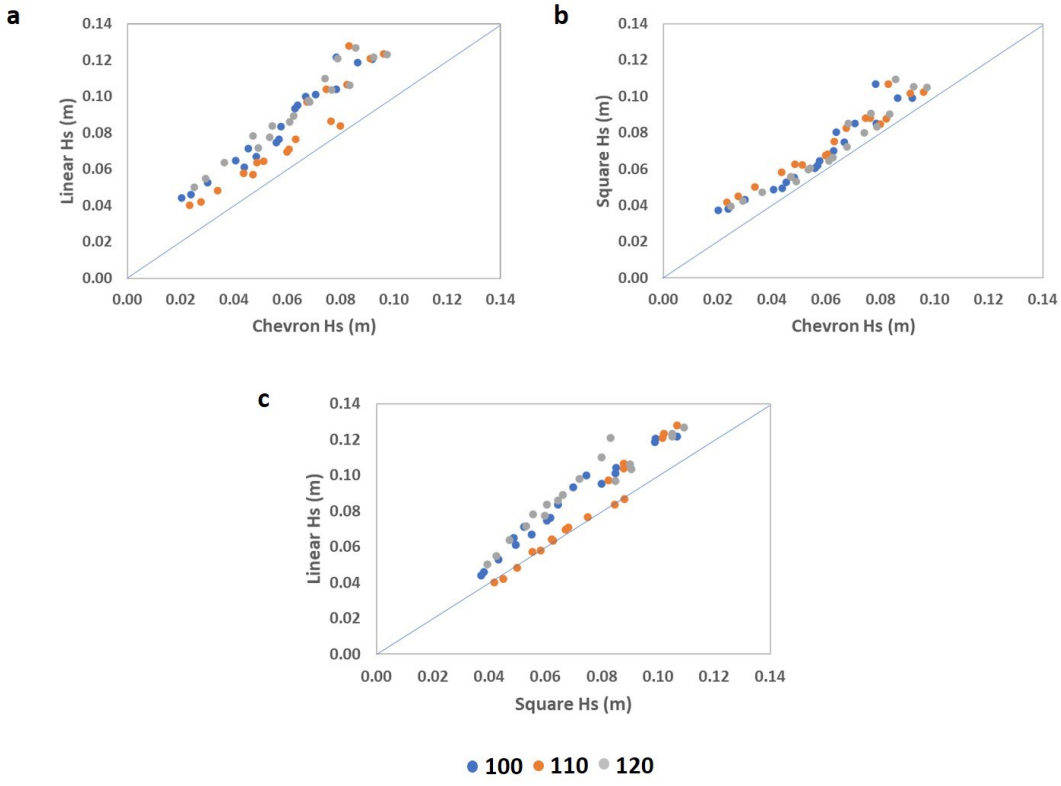

Figure 4.9 Mean Hs scatter plots comparing model simulations between terrace shapes. a) Mean Hs (m) comparison of linear vs chevron shape. b) Mean Hs (m) comparison of square vs chevron shape. c) Mean Hs (m) comparison of Linear vs square shape.

Results depicted in figure 4.9, show scatter plots comparing the mean Hs between each shape. Figure 4.9a shows the mean Hs comparison between linear vs chevron shape, figure 4.9b shows the mean Hs comparison between square vs chevron shape. Figure 4.9c shows the mean Hs comparison between linear vs square shapes. Overall, the chevron shape showed the biggest Hs reduction between all shapes evaluated.

For the comparison between linear vs chevron shape (Figure 4.9a), in all the wind/wave scenarios, the mean Hs was higher in the linear compared to the chevron shape. Overall, mean Hs reduction in the linear vs chevron shape, ranged between 0.004–0.45 m (5–54%). For the comparison between square vs chevron shape (Figure 4.9b), in all the wind/wave scenarios, the mean Hs was higher in the square compared to the chevron shape. Overall, mean Hs reduction in the square vs chevron shape, ranged between 0.004–0.028 m (5–46%). For the comparison between linear vs square shape (Figure 4.9c), in most of the wind/wave scenarios, the mean Hs was higher in the linear compared to the square shape. Overall, mean Hs reduction in the linear vs square shape, ranged between 0.001–0.038 m (1–31%).

Hs Performance of Terrace Designs During Different Wind Events

Figure 4.10 depicts the mean Hs of all terrace designs evaluated in the current study during low (Figure 4.10a), prefrontal (Figure 4.10b), and postfrontal (Figure 4.10c) wind events. Overall, for all the wind events evaluated, the terrace shape with the smallest mean Hs was the chevron shape. The terrace shape with the highest mean Hs was the linear shape (Figure 4.10).

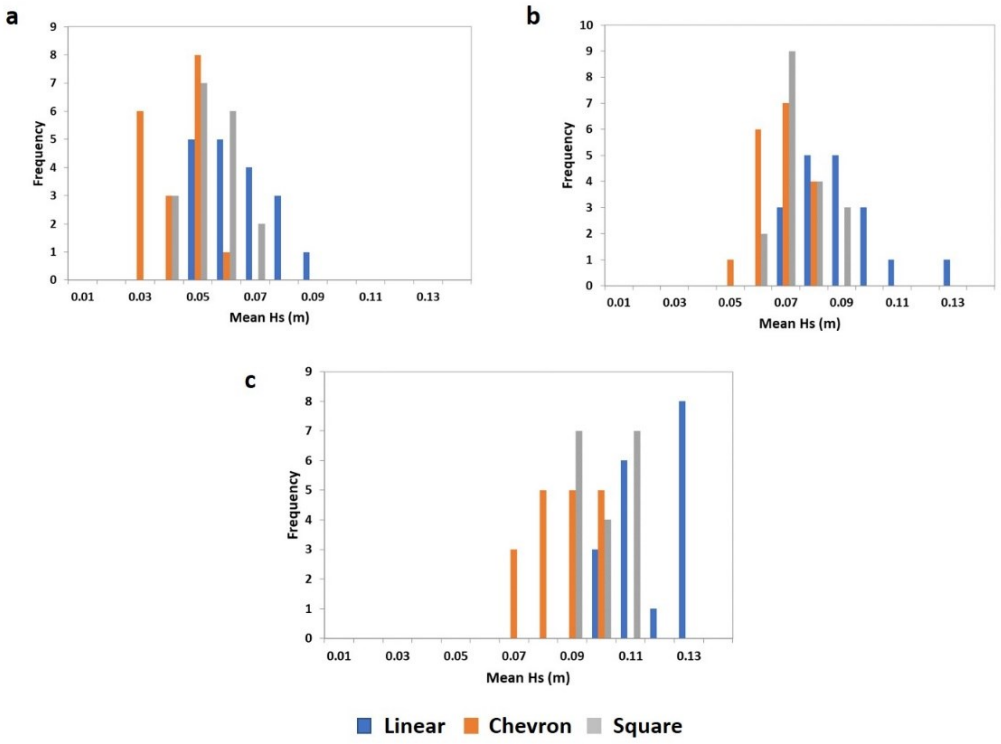

Figure 4.10 Histograms comparing mean Hs between shapes under different wind events. a) Mean Hs during low wind events. b) Mean Hs during prefrontal wind events. c) Mean Hs during postfrontal wind events.

Figure 4.10a shows the frequency of occurrence for mean Hs during frequent and low wind events. For the linear shape, the range of mean Hs was between 0.05–0.09 m and the most occurrences were in the 0.05 m (5 wind/wave scenarios) and 0.06 m (5 wind/wave scenarios) classes. For the chevron shape, the range of mean Hs was between 0.03–0.06 m and the most occurrences were in the 0.05 m (8 wind/wave scenarios) class. For the square shape, the range of mean Hs was between 0.04–0.07 m and the most occurrences were in the 0.05 m (7 wind/wave scenarios) and 0.06 m (8 wind/wave scenarios) classes.

Figure 4.10b shows the frequency of occurrence for mean Hs during prefrontal events. For the chevron shape, the range of mean Hs was between 0.05–0.08 m and the most occurrences

were in the 0.07 m (7 wind/wave scenarios) class. For the square shape, the range of mean Hs was between 0.06–0.09 m and the most occurrences were in the 0.07 m (9 wind/wave scenarios) class. For the linear shape, the range of mean Hs was between 0.07–0.13 m and the most occurrences were in the 0.08 m (5 wind/wave scenarios) and 0.09 m (5 wind/wave scenarios) classes.

Figure 4.10c shows the frequency of occurrence for mean Hs during postfrontal events. For the chevron shape, the range of mean Hs was between 0.07–0.10 m and the most occurrences were in the 0.08, 0.09 and 0.10 m (5 wind/wave scenarios each) classes. For the square shape, the range of mean Hs was between 0.09–0.11 m and the most occurrences were in the 0.09 m (7 wind/wave scenarios) and 0.11 m (7 wind/wave scenarios) classes. For the linear shape, the range of mean Hs was between 0.10–0.13 m and the most occurrences were in the 0.13 m (8 wind/wave scenarios) class.

The chevron shape reduced more Hs during low (18–54%) and postfrontal (22–35%) events than during prefrontal (5–35%) events compared to the linear and square shapes. Therefore, Hs dissipation was higher during low and high intensity wind events. The square shape reduced more Hs during prefrontal events (2–31%) and postfrontal events (12–18%) than during low events (1–29%) compared to the linear shapes. Therefore, Hs dissipation was higher during cold front events than low events. In conclusion, Hs dissipation was higher during postfrontal events (high intensity winds) by the chevron and square shapes compared to the linear shape.

Project construction costs

Project construction costs (Table 4.3) were estimated based on costs of real projects constructed in Northern Gulf of Mexico by Ducks Unlimited (DU). A terrace database including

project construction costs was provided by DU [20]. The terrace database described 16 projects built from 2009 until 2020. Total project construction costs included terrace construction, mobilization, constructions surveys and planting. According to the database provided, the cost per meter range between $39.15–$124.46 [20] and the cost per meter of terrace constructed varied depending on water depth and sediment material. It was also mentioned by DU that terrace shape is not a factor that affects construction costs [6].

As mentioned before, the current study considered uniform water depth (1 m), and sediment material for all the terrace designs. Therefore, for all terrace designs, the cost per meter of terrace constructed (Table 4.3) was considered the same. A cost per meter of constructed terrace was estimated to be $86.98 based on an average of the costs between projects implemented by DU during the last 10 years.

Table 4.3 Project constructions of all terrace designs assessed in the current study. (*) Denotes representative terraces.

Terrace Shape	Grids	Terrace Spacing	Total terrace length (m)	Total terrace area (sq m)	Total terrace field area (sq m)	Cost per m	Cost per sq m	Project construction cost
Linear	a.1	100	1,773	8,861	250,000	$86.98	$0.62	$154,207
	a.2*	110	1,746	8,727	250,000	$86.98	$0.61	$151,858
	a3	120	1,428	7,138	250,000	$86.98	$0.50	$124,200
Chevron	b.1	100	2,209	11,042	250,000	$86.98	$0.77	$192,128
	b.2*	110	2,011	10,053	250,000	$86.98	$0.70	$174,907
	b.3	120	1,820	9,097	250,000	$86.98	$0.63	$158,295
Square	c.1	100	3,340	16,696	250,000	$86.98	$1.16	$290,497
	c.2*	110	3,153	15,761	250,000	$86.98	$1.10	$274,232
	c.3	120	2,824	14,116	250,000	$86.98	$0.98	$245,618

Overall, the most economically terrace shape to construct are any of the linear shapes ($124,200.39–$154,206.79), followed by the chevron shapes ($158,294.62–$192,127.92). The

most expensive terrace shape to construct are the square shapes ($245,617.59–$290,496.72). The estimated constructions costs are directly related with the total terrace length constructed in each of the terrace designs. Terrace shapes with more length constructed such as the square shapes (2,824–3,340 m) are the most expensive compared to the terrace shapes with less terrace length such as the chevron (1,820–2,209 m) and linear (1,428–1,773 m) shapes.

Discussion

Hs Comparison Between Terrace Spacings

Overall, in the current study it was determined that the spacing between terraces is not a design factor primarily affecting Hs behavior. Hs ranges show very little variation between the spacings evaluated under each shape. Therefore, an optimal terrace spacing to minimize fetch and reduce Hs could be any of the three spacings evaluated (100,110,120 m). These results agree with previous research mentioning that any breakwater design contributes to Hs reduction, stating that emerged breakwaters are the most optimal at reducing Hs [17].

For all the terrace spacings, the Hs was reduced to 0 m in the zone immediately behind the terraces (protected zone) due to breakwater shadow effects (Figure 4.5, 4.6). This agrees with previous studies showing that most of the Hs attenuation occurs instantly behind the sheltered zone of a breakwater structure [30]. The range of maximum Hs in all spacings correspond to the incident wave conditions used to force the model. Therefore, higher waves mainly occurred close to the boundaries where the incident waves originated from (Figure 4.5, 4.6).

It is important to note, that the shadow zone at the protected side of the terraces slightly varies spatially between each terrace spacing as shown in figures 4.5 and 4.6. Terrace designs with a 120 m spacing between terraces showed elongated and wider shadow zones behind the terraces compared to the 110 and 100 m spacing for all shapes. This agrees with Mathews (2020)

and Chan et al., (2007) finding that larger gap areas between individual terraces produced elongated shadow zones in the area immediately behind the terraces due to bleed flow through the field. Therefore, the 120 m spacing may reduce Hs for a longer distance until it approaches to the next fetch disruption corresponding to the marsh platform shoreline or to the presence of terraces as observed in the current study. Further research is encouraged to assess wider terrace spacings within the common range of terrace construction (90 to 152 m) [6] to find a maximum or optimal spacing at reducing Hs.

Hs Comparison Between Terrace Shapes

An important finding from the current study was that reduction of Hs is mostly affected by terrace shape. The chevron was the best shape for reducing Hs.

The overall range of Hs reduction (31-54%) in all the designs agree with several recent studies. The reduction in Hs (up to 54%) for the chevron shape in this study was similar to a study comparing two break water designs protecting a Harbor in Lake Ontario [15]. In the Cooper and Mulligan (2016) study, it was found that an L-shaped breakwater provided an additional reduction of Hs of 54% compared to the original breakwater. Wiberg et al., (2019) also found an average Hs attenuation between 30-50% by oyster reefs in water depths similar to our study (0.5- 1.0 m). Vona et al., (2020) showed that the average Hs reduction by breakwaters ranged between 10-50% in a shallow coastal bay using Delf3D and SWAN.

Overall, the Hs ranges obtained in this study agree with previous studies conducted in fetch limited conditions where wave climates were influenced by breakwaters [10, 32, 33]. A recent study that observed and modeled waves in real marsh terrace fields found that the mean Hs range between 0.03–0.14 m in a chevron and in a rectangular terrace site using SWAN [10].

The results from the current study agree with Mathews (2020) and French et al., (2020) concluding that a chevron design constructed perpendicular to directions associated with erosive wave conditions is the most effective at disrupting fetch, and reducing total shear stress and water flow velocities, respectively. However, Mathews (2020) and French et al., (2020) did not evaluated the reduction of Hs by terraces. Mathews (2020) only evaluated sediment dynamics and circulation patterns such as current and flow in a hypothetical basin with terraces. French et al., (2020) evaluated the spatiotemporal relationship between wind conditions, wave observations, and soil measurements in two marsh terrace sites at Louisiana.

In the current study, the chevron shaped terraces produced wider shadow zones with smaller Hs compared to the linear and square shapes. This may be due to the chevron shapes having the longest terrace lines. According to Chan et al (2007) permeable structures with high gaps to structure ratios produce less effective and smaller shadow zones. In this study, the gaps between terraces were higher in the linear and square shapes compared with the chevron, therefore smaller shadow zones were found in the linear and square shapes. It is also important to mention that optimal terrace shape at reducing Hs is a function of the incident wind and wave direction in the area of study [15]. In the current study, terrace design orientation was perpendicular to the wind direction (NW, SE) that produces the most erosive waves based on a previous study [13].

Hs Performance of Terrace Designs During Different Wind Events

In this study, the chevron shape was the most optimal at reducing Hs in all the wind events evaluated. The linear shape had the highest mean Hs ranges in all wind events evaluated. The mean Hs reduced in all shapes varied based on different wind and wave conditions that were the input in the model. Similar to previous studies assessing breakwater environments, Hs

reduction by terraces was found to be very dependent on the incident wind/wave direction, related with terrace orientation [10, 13, 15].

Overall, the current study found that Hs dissipation was higher during cold front events (most intense wind events) by the chevron and square shapes compared to the linear shapes. This finding is significant because it proves the success of marsh terraces at reducing erosive waves originated by the most frequent high intensity wind events (cold fronts) [14]. Therefore, this restoration technique effectively achieves the main goal for the design of coastal structures by reducing maximum wave heights during the most intense wind events [34].

A limitation of the current study was that the incident wind and wave conditions were input perpendicular (NW, SE) to terrace designs orientation, therefore the effectiveness of terrace designs at reducing Hs may vary if the direction of the incident wind and wave conditions are input parallel to terrace orientation. Future research should assess terrace design effectiveness under the influence of different wind directions and hurricane conditions to complement the results of the current study.

The Most Optimal Terrace Designs Based on Shape, Spacing, Costs, and Marsh Increase.

Based on the results of the current study showing that Hs reduction is primarily affected by terrace shape and not by terrace spacing, and according to the construction costs estimated, the most optimal terrace design to construct is the chevron shape with a 120 m terrace spacing with an estimated project construction cost of $158,294.62. The least optimal terrace design to construct is the square shape at 100 m with an estimated construction cost of $290,496.72. Any of the square designs are the least optimal to construct because of the following reasons: 1) higher costs of implementation compared to other shapes. 2) the mean Hs ranges simulated are

similar between the linear and square shapes. 3) the Hs reduction of the square shapes (up to 31%), is less than the Hs reduction of the chevron shapes (up to 54%).

The current study did not simulate sediment and flow dynamics affecting erosion and deposition of the marsh terrace designs, however, based on a previous study [12] the chevron shape also seems to be optimal at enhancing marsh deposition within the terrace footprint. In this same study, out of 20 marsh sites analyzed, five out of seven chevron sites of study showed depositional trends. For the linear shape, five out of 10 linear sites of study showed depositional trends. Finally, one out of three square (or rectangular) terrace sites resulted in depositional trends. It is also important to mention that Hs is not a direct and unique indicator for marsh erosion. Generally, lower Hs might result in less marsh erosion. However, at a fundamental physical level, Tm is also a critical parameter in calculating the stress that a wave can impart. Moreover, there is a specific threshold energy for erosion based on the physical properties of the sediment, grain cohesion, and the presence of vegetation in marshes. Below that specific threshold, no erosion will occur regardless of differences in Hs. This is important to consider for conducting cost effectiveness analysis of marsh terraces. Future studies should also relate sediment properties with sediment and wave hydrodynamics to determine marsh erosion trends in terrace environments.

Conclusions

The effectiveness of nine terrace designs at reducing Hs during low and cold front wind events were assessed in the current study using the numerical wave model SWAN. Terrace design factors evaluated in this study included: 1) The most common terrace shapes (linear, chevron, square) constructed in the northern Gulf of Mexico [6, 8], and 2) Three commonly used terrace spacings (100, 110,120 m) [6, 20]. All terrace designs were oriented perpendicular to the

most frequent wind direction in low wind and cold front passages responsible of the most erosive waves in marsh terrace sites [13, 14].

Overall, findings from the current study conclude that 1) the most optimal terrace shape is the chevron shape compared to the square and linear shape. The chevron terraces reduced Hs by up to 54%. 2) Hs reduction is not primarily affected by the terrace spacings (100,110,120 m). The Hs ranges obtained were very similar for all terrace spacings within each terrace shape. 3) The chevron shape is the most optimal at reducing Hs during low and cold front events compared to the linear and square shape. 4) Based on the estimation of the construction costs and the reduction of Hs primarily affected by terrace shape, the most optimal terrace design to construct is a chevron shape with a 120 m terrace spacing with an estimated construction cost of $158,294.62.

To our knowledge, this is the first study assessing Hs reduction evaluating terrace design factors such as shape and spacing during low and cold front wind events using a numerical wave model. Future research should assess more terrace designs aspects including different terrace shapes, width, orientation and spacings under the influence of different wind directions and hurricane conditions to complement the results of the current study. Also, future research should develop a hydrodynamic model focused on sediment transport to identify the most effective terrace design at reducing erosion and enhancing terrace deposition. Results from this study aim to help restoration and conservation agencies to optimize marsh terracing implementation at reducing Hs to address the accelerated rates of wetland erosion occurring due to climate change and subsidence in coastal Louisiana.

REFERENCES

[1] Brasher, M. G. Review of the Benefits of Marsh Terraces in the Northern Gulf of Mexico. **2015**, No. May.

[2] Rozas, L. P.; Minello, T. J. Marsh Terracing as a Wetland Restoration Tool for Creating Fishery Habitat. *Wetlands*, **2001**, *21* (3), 327–341.

[3] Vinent, O. D.; Herbert, E. R.; Coleman, D. J.; Himmelstein, J. D.; Kirwan, M. L. Onset of Runaway Fragmentation of Salt Marshes. *One Earth*, **2021**.

[4] Smith, J. M.; Cialone, M. A.; Wamsley, T. V.; McAlpin, T. O. Potential Impact of Sea Level Rise on Coastal Surges in Southeast Louisiana. *Ocean Eng.*, **2010**, *37* (1), 37–47. https://doi.org/10.1016/J.OCEANENG.2009.07.008.

[5] Turner, R. E.; Streever, B. *Approaches to Coastal Wetland Restoration: Northern Gulf of Mexico*; Kugler Publications, 2002.

[6] Brasher, M. G.; Hetherwick, J.; Cenac, W. Personal Communication, 2021.

[7] Westphal, K. A.; Nakashima, L. D.; National Audubon Society. Louisiana Terrace Inventory GIS Application and Resource (LTIGAR) https://www.arcgis.com/home/item.html?id=8076d77c64a643c4b5c53c14d5328640.

[8] Ducks Unlimited. Geodatabase of Existing Marsh Terraces, 2015.

[9] O'Connell, J. L.; Nyman, J. A. Marsh Terraces in Coastal Louisiana Increase Marsh Edge and Densities of Waterbirds. *Wetlands*, **2010**, *30* (1), 125–135.

[10] Osorio, R. J.; Linhoss, A.; Skarke, A.; Brasher, M. G.; French, J.; Baghbani, R. *Modeling Wave Climates for Optimal Design of Marsh Terraces for Wetland Restoration*; Starkville, 2021.

[11] Guo, B.; Subrahmanyam, M. V; Li, C. Waves on Louisiana Continental Shelf Influenced by Atmospheric Fronts. *Sci. Rep.*, **2020**, *10* (1), 1–9.

[12] Osorio, R. J.; Linhoss, A. Evaluation of Marsh Terraces for Wetland Restoration: A Remote Sensing Approach. *Water*, **2020**, *12* (2), 336.

[13] Mathews, M. C. Geomorphic Effectiveness of Marsh Terracing as a Coastal Restoration Technique in Southern Louisiana. Tulane University School of Science and Engineering 2020.

[14] French, J.; Skarke, A. Optimization of Marsh Terracing as a Wetland Restoration Technique: Mitigation of Cohesive Sediment Erosion by Waves Associated with Frontal Passage, Mississippi State University, 2020.

[15] Cooper, A. H.; Mulligan, R. P. Application of a Spectral Wave Model to Assess Breakwater Configurations at a Small Craft Harbour on Lake Ontario. *J. Mar. Sci. Eng.*, **2016**, *4* (3), 46.

[16] Vona, I.; Gray, M. W.; Nardin, W. The Impact of Submerged Breakwaters on Sediment Distribution along Marsh Boundaries. *Water*, **2020**, *12* (4), 1016.

[17] Vieira, B. F. V; Pinho, J. L. S.; Barros, J. A. O.; Antunes do Carmo, J. S. Hydrodynamics and Morphodynamics Performance Assessment of Three Coastal Protection Structures. *J. Mar. Sci. Eng.*, **2020**, *8* (3), 175.

[18] Leonardi, N.; Ganju, N. K.; Fagherazzi, S. A Linear Relationship between Wave Power and Erosion Determines Salt-Marsh Resilience to Violent Storms and Hurricanes. *Proc. Natl. Acad. Sci.*, **2016**, *113* (1), 64–68.

[19] Google LLC. Google Earth Pro. Google 2021.

[20] Ducks Unlimited. *Terrace Costs Database*; John D. Hetherwick: U.S., 2020.

[21] Ocean Illumination Ltd. Ocean Contour Acoustic Doppler Data Proccesing.

[22] SWAN team. SWAN User Manual. Delft University of Technology 2012, p 94.

[23] Booij, N.; Ris, R. C.; Holthuijsen, L. H. A Third-generation Wave Model for Coastal Regions: 1. Model Description and Validation. *J. Geophys. Res. Ocean.*, **1999**, *104* (C4), 7649–7666.

[24] Ris, R. C.; Holthuijsen, L. H.; Booij, N. A Third-generation Wave Model for Coastal Regions: 2. Verification. *J. Geophys. Res. Ocean.*, **1999**, *104* (C4), 7667–7681.

[25] Breugem, W. A.; Holthuijsen, L. H. Generalized Shallow Water Wave Growth from Lake George. *J. Waterw. port, coastal, Ocean Eng.*, **2007**, *133* (3), 173–182.

[26] Gonçalves, M.; Rusu, E.; Soares, C. G. Evaluation of the Wave Models SWAN and STWAVE in Shallow Water Using Nested Schemes. *Marit. Eng. Technol.*, **2012**, *481*, 178–185.

[27] Ilic, S.; Van Der WESTHUYSEN, A. J.; Roelvink, J. A.; Chadwick, A. J. Multidirectional Wave Transformation around Detached Breakwaters. *Coast. Eng.*, **2007**, *54* (10), 775–789.

[28] TUDelft. SWAN model features.

[29] Young, I. R.; Verhagen, L. A. The Growth of Fetch Limited Waves in Water of Finite Depth. Part 1. Total Energy and Peak Frequency. *Coast. Eng.*, **1996**, *29* (1–2), 47–78.

[30] Ti, Z.; Wei, K.; Qin, S.; Li, Y.; Mei, D. Numerical Simulation of Wave Conditions in Nearshore Island Area for Sea-Crossing Bridge Using Spectral Wave Model. *Adv. Struct. Eng.*, **2018**, *21* (5), 756–768.

[31] Chan, H.-C.; Leu, J.-M.; Lai, C.-J. Velocity and Turbulence Field around Permeable Structure: Comparisons between Laboratory and Numerical Experiments. *J. Hydraul. Res.*, **2007**, *45* (2), 216–226.

[32] Wiberg, P. L.; Taube, S. R.; Ferguson, A. E.; Kremer, M. R.; Reidenbach, M. A. Wave Attenuation by Oyster Reefs in Shallow Coastal Bays. *Estuaries and Coasts*, **2019**, *42* (2), 331–347.

[33] Siemes, R. W. A.; Borsje, B. W.; Daggenvoorde, R. J.; Hulscher, S. J. M. H. Artificial Structures Steer Morphological Development of Salt Marshes: A Model Study. *J. Mar. Sci. Eng.*, **2020**, *8* (5), 326.

[34] Mai, S.; Wilhelmi, J.; Barjenbruch, U. Wave Height Distributions in Shallow Waters. *Coast. Eng.*, **2010**, 2.

CHAPTER V

CONCLUSIONS

The main objectives of this dissertation were to 1) assess terrace performance over time related with erosional and depositional processes using a remote sensing approach; 2) simulate wave climates in marsh terrace sites, conduct wave model validation, determine the effectiveness of marsh terraces for the reduction of significant wave height using SWAN; and 3) assess the effectiveness of different terrace designs at reducing significant wave height during low winds and cold front passages in coastal Louisiana using SWAN. This study found that marsh terrace performance over time shows more predominant deposition that erosion in the 20 terrace fields of study analyzed. This result is important in the face of subsidence and sea level rise in coastal Louisiana. According to previous studies the rate of subsidence and sea level rise in a 14 year period could reach 70-140 mm and 168 ± 8 mm, respectively [3–5]. Therefore, marsh terraces effectively achieved marsh creation within a 14-year span, achieving one of the main goals for the implementation of this restoration technique. It was also found that the high density of channels surrounding or adjacent to the terrace fields of study were potential drivers encouraging terrace deposition by potentially supplying sediment loading.

The current study also characterized wave climates in two marsh terraces fields in coastal Louisiana. Waves in the marsh terraces were small in amplitude with high frequencies, which is characteristic of low energy and sheltered environments. Model validation showed an agreement between simulated and measured data, particularly for significant wave height (RMSE: 0.01–

0.02 m; R: 0.97 for R2, 0.79 for C2 and 0.42 for C1) and wave direction (RMSE: 8.29–26.03º; R: 0.76 for R2, 0.73 for C2, and 0.59 for C1,), indicating that SWAN was appropriate for use in marsh terrace systems. Similarly, this study demonstrated that marsh terraces are effective at reducing average significant wave height up to 84% compared to unterraced sites.

This study found that the chevron shape is the most optimal terrace shape at reducing significant wave height compared to the other shapes. The mean Hs reduction in the chevron shape ranged between 5–54% compared to the linear shape and 5–46% compared to the square shape. The chevron shape is also the most optimal at reducing Hs during low (18–54%) and cold front events (5–35%) compared to the linear and square shapes. Similarly, this research found that significant wave height reduction is not primarily affected by the terrace spacings evaluated (100,110,120 m). Finally, based on the estimation of construction costs and the reduction of significant wave height, it was concluded that the most optimal terrace design to implement is the chevron shape with a 120 m terrace spacing. However, future studies should assess wider spacings between terraces to find an optimal or maximum spacing at reducing Hs.

Recommendations to engineers and restoration agencies in charge of the construction of marsh terraces are the following: 1) Terracing projects should be built in ponds surrounding or connected to channels in order to increase the sediment supply entering the sites. Based on our results, a high density of channels surrounding or adjacent to the terrace fields, and an external source of sediment loading are likely important drivers encouraging terrace deposition. Moreover, river diversion projects along with marsh terraces might promote marsh deposition in the terrace sites. 2) Terraces should be built perpendicular to the most frequent and strong winds which are also responsible for producing the most erosive waves in the area. 3) Based on Hs reduction and construction costs, the most optimal terrace shape is the chevron terrace shape

oriented perpendicular to the most frequent wind direction occurring in the area. Chevron designs generally have less gaps between terraces compared to linear and square shapes. Therefore, chevron designs produce more elongated and wider shadow zones with lower Hs compared to linear and square shapes. However, the square shape might also be optimal at reducing Hs in areas where winds are coming from different directions, interrupting fetch from four different sides.

Overall, the outcomes of this dissertation are very important given the lack of previous research on the performance of multiple terrace projects over time using remote sensing and numerical modeling. To our knowledge, this is the first study evaluating real wind wave climates in terrace fields, assessing significant wave height reduction by terraces, and evaluating different terrace design factors such as shape and spacing during a variety of wind conditions. The results of this dissertation are expected to help restoration agencies to implement terrace designs more effectively in order to address wetland erosion in the Gulf of Mexico, in the U.S. and other coastal areas facing similar environmental problems. Future studies should utilize remote sensing to quantify shoreline erosion, terrace longevity and its variability in marsh environments. Results obtained from those analysis should be related with design and environmental factors to identify the primary factors that influence terrace longevity and shoreline erosion. Future studies should also conduct model validation utilizing wind conditions from cold front passages and hurricanes. Storm conditions are more likely to result in erosive waves based on previous studies. Therefore, utilizing higher wind conditions and greater Hs values as an input in SWAN could potentially strength and improve model validation results. Finally, future research should also develop a hydrodynamic model focused on sediment transport and flow dynamics assessing different terrace designs. The results of the hydrodynamic model will help to identify environmental

factors such as sediment type, sediment load, soil strength and submerged aquatic vegetation (SAV) affecting marsh terrace performance relative to geological processes and the attenuation of wave energy.

APPENDIX A

SUPPLEMENTARY TABLE

Table A.1 Descriptive statistics of Hs simulated for the linear shape wind/wave scenarios.

Wind condition	Wind/wave scenario	Mesh	Terrace Spacing	Min.	Max.	Mean	Med.	Skew.	Lower CI.(90%)	Upper CI.(90%)	Range CI.90%
Low	11/16/2018 22 00	a.1	100	0.0010	0.1207	0.0441	0.0390	1.1709	0.0079	0.1120	0.1041
		a.2*	110	0.0010	0.1207	0.0401	0.0385	0.8318	0.0077	0.0707	0.0630
		a.3	120	0.0014	0.1207	0.0501	0.0422	0.7577	0.0071	0.1120	0.1049
	1/31/2019 6 00	a.1	100	0.0000	0.1930	0.0649	0.0520	1.1820	0.0077	0.1759	0.1682
		a.2*	110	0.0000	0.1911	0.0578	0.0519	1.0130	0.0100	0.1089	0.0989
		a.3	120	0.0000	0.1928	0.0782	0.0646	0.7854	0.0122	0.1777	0.1655
	2/1/2019 3 00	a.1	100	0.0000	0.2034	0.0712	0.0577	1.1558	0.0102	0.1852	0.1750
		a.2*	110	0.0000	0.2012	0.0635	0.0569	0.9531	0.0113	0.1198	0.1085
		a.3	120	0.0000	0.2029	0.0838	0.0697	0.7699	0.0166	0.1838	0.1672
	1/6/2019 14 00	a.1	100	0.0000	0.1408	0.0459	0.0385	1.1721	0.0024	0.1310	0.1286
		a.2*	110	0.0000	0.1408	0.0420	0.0390	0.8986	0.0029	0.0821	0.0792
		a.3	120	0.0000	0.1408	0.0547	0.0449	0.8077	0.0039	0.1309	0.1270
	3/7/2019 12 00	a.1	100	0.0000	0.1617	0.0611	0.0520	1.0875	0.0155	0.1461	0.1306
		a.2*	110	0.0000	0.1609	0.0570	0.0545	0.6913	0.0161	0.0955	0.0794
		a.3	120	0.0001	0.1619	0.0717	0.0624	0.7012	0.0195	0.1500	0.1305
	3/11/2019 00	a.1	100	0.0000	0.1716	0.0527	0.0438	1.2908	0.0036	0.1474	0.1438
		a.2*	110	0.0000	0.1714	0.0484	0.0448	1.0854	0.0043	0.0930	0.0887
		a.3	120	0.0000	0.1716	0.0636	0.0521	0.8176	0.0054	0.1499	0.1445
Prefrontal	12/8/18 14:08	a.1	100	0.0003	0.2030	0.0835	0.0728	1.0466	0.0259	0.1942	0.1684
		a.2*	110	0.0005	0.2010	0.0764	0.0733	0.6527	0.0265	0.1269	0.1004
		a.3	120	0.0005	0.2038	0.0978	0.0868	0.6375	0.0282	0.1965	0.1683
	12/12/18 19:08	a.1	100	0.0003	0.1615	0.0674	0.0620	0.9091	0.0187	0.1503	0.1317
		a.2*	110	0.0005	0.1614	0.0643	0.0639	0.4288	0.0197	0.1031	0.0834
		a.3	120	0.0003	0.1616	0.0774	0.0699	0.5316	0.0189	0.1514	0.1325
	12/27/18 17:08	a.1	100	0.0007	0.2207	0.0764	0.0634	1.2260	0.0172	0.1944	0.1772
		a.2*	110	0.0008	0.2207	0.0710	0.0651	0.8022	0.0184	0.1233	0.1049
		a.3	120	0.0009	0.2207	0.0892	0.0760	0.7865	0.0175	0.1976	0.1801
	1/22/19 1:08	a.1	100	0.0003	0.2235	0.0933	0.0824	0.9887	0.0304	0.2118	0.1814
		a.2*	110	0.0003	0.2214	0.0837	0.0794	0.7697	0.0301	0.1439	0.1138
		a.3	120	0.0003	0.2336	0.1100	0.0962	0.6623	0.0319	0.2252	0.1933
	2/20/19 9:08	a.1	100	0.0004	0.2106	0.0748	0.0610	1.1741	0.0190	0.1872	0.1682
		a.2*	110	0.0004	0.2106	0.0695	0.0622	0.8028	0.0198	0.1240	0.1043
		a.3	120	0.0004	0.2106	0.0860	0.0738	0.7470	0.0196	0.1872	0.1676

Table A.1 (continued)

Wind condition	Wind/wave scenario	Mesh	Terrace Spacing	Min.	Max.	Mean	Med.	Skew.	Lower CI.(90%)	Upper CI.(90%)	Range CI.90%
Prefrontal	**2/23/19 18:08**	a.1	100	0.0005	0.3310	0.0997	0.0705	1.4156	0.0177	0.3029	0.2852
		a.2*	110	0.0004	0.3310	0.0865	0.0688	1.2310	0.0173	0.1808	0.1635
		a.3	120	0.0006	0.3310	0.1208	0.0928	0.9429	0.0180	0.3083	0.2903
Postfrontal	**11/4/18 5:00**	a.1	100	0.0006	0.3112	0.0952	0.0702	1.4814	0.0215	0.2919	0.2704
		a.2*	110	0.0007	0.3112	0.0971	0.0751	1.5069	0.0220	0.2920	0.2700
		a.3	120	0.0005	0.3112	0.0969	0.0700	1.4138	0.0214	0.2920	0.2706
	11/26/18 2:00	a.1	100	0.0006	0.3307	0.1185	0.1010	1.3625	0.0426	0.3025	0.2599
		a.2*	110	0.0007	0.3307	0.1209	0.1051	1.3785	0.0427	0.3037	0.2610
		a.3	120	0.0007	0.3307	0.1216	0.1027	1.2864	0.0442	0.3026	0.2584
	12/9/18 16:08	a.1	100	0.0010	0.3662	0.1216	0.0976	1.3499	0.0266	0.3546	0.3280
		a.2*	110	0.0011	0.3673	0.1279	0.1070	1.2920	0.0281	0.3557	0.3276
		a.3	120	0.0015	0.3674	0.1268	0.1008	1.2480	0.0280	0.3557	0.3278
	2/8/19 10:08	a.1	100	0.0001	0.3612	0.1204	0.1019	1.4935	0.0443	0.3193	0.2750
		a.2*	110	0.0001	0.3612	0.1233	0.1065	1.5063	0.0460	0.3194	0.2734
		a.3	120	0.0001	0.3612	0.1231	0.1026	1.4186	0.0463	0.3193	0.2730
	2/24/19 16:08	a.1	100	0.0000	0.3109	0.1041	0.0875	1.4444	0.0363	0.2829	0.2466
		a.2*	110	0.0001	0.3109	0.1064	0.0912	1.4629	0.0378	0.2830	0.2452
		a.3	120	0.0001	0.3109	0.1062	0.0881	1.3657	0.0383	0.2830	0.2447
	3/26/19 20:08	a.1	100	0.0002	0.3114	0.1012	0.0788	1.4576	0.0291	0.2941	0.2650
		a.2*	110	0.0003	0.3114	0.1039	0.0846	1.4683	0.0300	0.2942	0.2642
		a.3	120	0.0004	0.3114	0.1036	0.0800	1.3729	0.0299	0.2941	0.2642

Table A.2 Descriptive statistics of Hs simulated for the chevron shape wind/wave scenarios.

Wind condition	Wind/wave scenario	Mesh	Terrace Spacing	Min.	Max.	Mean	Med.	Skew.	Lower CI.(90%)	Upper CI.(90%)	Range CI.90%
Low	11/16/2018 22 00	b.1	100	0E+00	0.1211	0.0212	0.0031	1.7683	0.0000	0.1106	0.1106
		b.2*	110	0E+00	0.1207	0.0234	0.0039	1.3997	0.0000	0.1012	0.1012
		b.3	120	0E+00	0.1207	0.0250	0.0049	1.5523	0.0000	0.1119	0.1119
	1/31/2019 6 00	b.1	100	1E-13	0.1917	0.0414	0.0331	2.0496	0.0007	0.1513	0.1506
		b.2*	110	1E-18	0.1911	0.0436	0.0347	1.4885	0.0000	0.1370	0.1370
		b.3	120	7E-21	0.1919	0.0471	0.0355	1.4967	0.0000	0.1552	0.1552
	2/1/2019 3 00	b.1	100	1E-16	0.2021	0.0463	0.0385	1.8961	0.0004	0.1585	0.1581
		b.2*	110	3E-19	0.2015	0.0485	0.0391	1.4016	0.0001	0.1437	0.1436
		b.3	120	6E-20	0.2025	0.0543	0.0408	1.4071	0.0002	0.1715	0.1713
	1/6/2019 14 00	b.1	100	8E-22	0.1409	0.0250	0.0084	1.8872	0.0000	0.1297	0.1297
		b.2*	110	0E+00	0.1407	0.0276	0.0074	1.4852	0.0000	0.1190	0.1190
		b.3	120	0E+00	0.1408	0.0292	0.0041	1.5274	0.0000	0.1310	0.1310
	3/7/2019 12 00	b.1	100	1E-08	0.1615	0.0447	0.0389	1.8302	0.0073	0.1366	0.1293
		b.2*	110	1E-06	0.1611	0.0470	0.0396	1.3157	0.0019	0.1255	0.1236
		b.3	120	8E-07	0.1617	0.0491	0.0411	1.2251	0.0001	0.1400	0.1399
	3/11/2019 00	b.1	100	2E-22	0.1715	0.0300	0.0212	1.9337	0.0000	0.1437	0.1437
		b.2*	110	8E-22	0.1714	0.0338	0.0210	1.4370	0.0000	0.1314	0.1314
		b.3	120	6E-22	0.1716	0.0364	0.0204	1.4668	0.0000	0.1468	0.1468
Prefrontal	12/8/18 14:08	b.1	100	1E-05	0.2016	0.059	0.0500	1.7572	0.0084	0.1808	0.1724
		b.2*	110	6E-05	0.2010	0.063	0.0498	1.2677	0.0041	0.1724	0.1683
		b.3	120	5E-05	0.2037	0.068	0.0507	1.3470	0.0025	0.1927	0.1902
	12/12/18 19:08	b.1	100	6E-05	0.1616	0.049	0.0442	1.6352	0.0092	0.1461	0.1369
		b.2*	110	1E-04	0.1615	0.051	0.0451	1.1405	0.0021	0.1359	0.1338
		b.3	120	7E-05	0.1616	0.053	0.0445	1.1878	0.0004	0.1481	0.1477
	12/27/18 17:08	b.1	100	2E-04	0.2207	0.058	0.0474	1.8575	0.0095	0.1818	0.1723
		b.2*	110	8E-05	0.2207	0.061	0.0453	1.3812	0.0094	0.1689	0.1595
		b.3	120	7E-05	0.2207	0.062	0.0443	1.5706	0.0090	0.1946	0.1856
	1/22/19 1:08	b.1	100	4E-06	0.2219	0.064	0.0509	1.8986	0.0130	0.2057	0.1927
		b.2*	110	9E-05	0.2762	0.080	0.0549	1.7558	0.0074	0.2714	0.2640
		b.3	120	3E-05	0.2326	0.074	0.0514	1.4189	0.0031	0.2179	0.2148
	2/20/19 9:08	b.1	100	2E-05	0.2106	0.057	0.0453	1.9233	0.0102	0.1841	0.1739
		b.2*	110	1E-05	0.2106	0.060	0.0438	1.4126	0.0112	0.1672	0.1560
		b.3	120	2E-05	0.2106	0.061	0.0429	1.5763	0.0109	0.1873	0.1764
	2/23/19 18:08	b.1	100	9E-06	0.3310	0.069	0.0429	2.2081	0.0092	0.2935	0.2843
		b.2*	110	6E-06	0.3310	0.076	0.0413	1.5412	0.0097	0.2722	0.2625
		b.3	120	2E-05	0.3310	0.079	0.0418	1.7157	0.0091	0.3054	0.2963

Table A.2. (continued)

Wind condition	Wind/wave scenario	Mesh	Terrace Spacing	Min.	Max.	Mean	Med.	Skew.	Lower CI.(90%)	Upper CI.(90%)	Range CI.90%
Postfrontal	**11/4/18 5:00**	b.1	100	4E-10	0.3061	0.0536	0.0417	3.0617	0.0043	0.1768	0.1725
		b.2*	110	2E-11	0.3112	0.0674	0.0431	2.2775	0.0106	0.2930	0.2825
		b.3	120	1E-05	0.3112	0.0682	0.0440	2.2015	0.0093	0.2931	0.2838
	11/26/18 2:00	b.1	100	1E-06	0.3158	0.0764	0.0658	2.8650	0.0242	0.1914	0.1672
		b.2*	110	1E-07	0.3307	0.0911	0.0704	2.1754	0.0290	0.3050	0.2760
		b.3	120	1E-07	0.3307	0.0923	0.0712	2.1143	0.0279	0.3051	0.2772
	12/9/18 16:08	b.1	100	7E-11	0.3647	0.0657	0.0481	2.9688	0.0100	0.2237	0.2137
		b.2*	110	3E-11	0.3670	0.0831	0.0513	2.2148	0.0136	0.3547	0.3412
		b.3	120	1E-05	0.3683	0.0857	0.0526	2.1332	0.0129	0.3562	0.3433
	2/8/19 10:08	b.1	100	3E-07	0.3320	0.0814	0.0710	2.9376	0.0325	0.1989	0.1664
		b.2*	110	1E-07	0.3612	0.0961	0.0755	2.2380	0.0351	0.3182	0.2831
		b.3	120	1E-07	0.3612	0.0974	0.0766	2.1775	0.0343	0.3183	0.2840
	2/24/19 16:08	b.1	100	3E-12	0.2965	0.0691	0.0592	2.9501	0.0263	0.1747	0.1484
		b.2*	110	7E-11	0.3109	0.0823	0.0630	2.2318	0.0298	0.2831	0.2533
		b.3	120	7E-11	0.3109	0.0833	0.0634	2.1689	0.0286	0.2833	0.2547
	3/26/19 20:08	b.1	100	2E-10	0.3050	0.0605	0.0482	3.0610	0.0147	0.1781	0.1634
		b.2*	110	3E-11	0.3114	0.0746	0.0511	2.2751	0.0195	0.2941	0.2746
		b.3	120	9E-12	0.3114	0.0765	0.0523	2.1971	0.0184	0.2957	0.2773

Table A.3 Descriptive statistics of Hs simulated for the square shape wind/wave scenarios.

Wind condition	Wind/wave scenario	Mesh	Terrace Spacing	Min.	Max.	Mean	Med.	Skew.	Lower CI.(90%)	Upper CI.(90%)	Range CI.90%
Common	11/16/2018 22 00	c.1	100	0.0010	0.1207	0.0373	0.0320	1.8695	0.0098	0.0876	0.0778
		c.2*	110	0.0009	0.1207	0.0418	0.0327	1.1731	0.0077	0.1042	0.0965
		c.3	120	0.0008	0.1207	0.0394	0.0319	1.4269	0.0069	0.1047	0.0978
	1/31/2019 6 00	c.1	100	0.0001	0.1915	0.0487	0.0381	1.9783	0.0140	0.1232	0.1092
		c.2*	110	0.0000	0.1911	0.0584	0.0389	1.1493	0.0098	0.1560	0.1462
		c.3	120	0.0001	0.1911	0.0556	0.0387	1.3977	0.0120	0.1558	0.1438
	2/1/2019 3 00	c.1	100	0.0000	0.2020	0.0526	0.0401	1.9144	0.0141	0.1361	0.1220
		c.2*	110	0.0000	0.2012	0.0628	0.0430	1.1092	0.0106	0.1630	0.1524
		c.3	120	0.0000	0.2012	0.0606	0.0415	1.3265	0.0107	0.1694	0.1587
	1/6/2019 14 00	c.1	100	0.0002	0.1408	0.0382	0.0312	1.8514	0.0076	0.1046	0.0970
		c.2*	110	0.0001	0.1407	0.0451	0.0327	1.1868	0.0067	0.1235	0.1168
		c.3	120	0.0001	0.1407	0.0426	0.0319	1.4395	0.0060	0.1241	0.1181
	3/7/2019 12 00	c.1	100	0.0003	0.1613	0.0495	0.0408	1.8578	0.0189	0.1095	0.0907
		c.2*	110	0.0000	0.1608	0.0555	0.0426	1.0770	0.0144	0.1313	0.1169
		c.3	120	0.0000	0.1608	0.0531	0.0421	1.2245	0.0114	0.1321	0.1208
	3/11/2019 00	c.1	100	0.0001	0.1715	0.0433	0.0347	2.0111	0.0102	0.1162	0.1060
		c.2*	110	0.0001	0.1714	0.0500	0.0350	1.2539	0.0072	0.1382	0.1310
		c.3	120	0.0001	0.1714	0.0472	0.0344	1.4890	0.0058	0.1388	0.1330
Prefrontal	12/8/18 14:08	c.1	100	0.0005	0.2014	0.0644	0.0517	1.7543	0.0233	0.1465	0.1232
		c.2*	110	0.0005	0.2010	0.0752	0.0566	1.0804	0.0240	0.1728	0.1488
		c.3	120	0.0006	0.2010	0.0722	0.0562	1.2091	0.0208	0.1762	0.1554
	12/12/18 19:08	c.1	100	0.0006	0.1614	0.0552	0.0467	1.6155	0.0183	0.1188	0.1005
		c.2*	110	0.0005	0.1613	0.0622	0.0484	0.9884	0.0151	0.1412	0.1261
		c.3	120	0.0005	0.1613	0.0598	0.0486	1.1472	0.0136	0.1412	0.1276
	12/27/18 17:08	c.1	100	0.0008	0.2207	0.0619	0.0491	1.8415	0.0176	0.1397	0.1221
		c.2*	110	0.0012	0.2207	0.0682	0.0494	1.2731	0.0167	0.1719	0.1552
		c.3	120	0.0014	0.2207	0.0662	0.0505	1.4885	0.0173	0.1724	0.1551
	1/22/19 1:08	c.1	100	0.0003	0.2217	0.0699	0.0533	1.7476	0.0276	0.1708	0.1432
		c.2*	110	0.0002	0.2214	0.0848	0.0606	1.0704	0.0280	0.1990	0.1710
		c.3	120	0.0002	0.2215	0.0799	0.0593	1.2236	0.0241	0.2004	0.1763
	2/20/19 9:08	c.1	100	0.0005	0.2106	0.0606	0.0462	1.8285	0.0192	0.1415	0.1223
		c.2*	110	0.0006	0.2106	0.0673	0.0475	1.2664	0.0186	0.1700	0.1514
		c.3	120	0.0006	0.2106	0.0645	0.0475	1.5210	0.0193	0.1714	0.1521
	2/23/19 18:08	c.1	100	0.0006	0.3310	0.0747	0.0449	2.0163	0.0170	0.2206	0.2036
		c.2*	110	0.0008	0.3310	0.0881	0.0488	1.3771	0.0170	0.2684	0.2514
		c.3	120	0.0009	0.3310	0.0832	0.0473	1.6203	0.0171	0.2733	0.2562

Table A.3 (continued)

Posfrontal	**11/4/18 5:00**	c.1	100	0.0005	0.3112	0.0801	0.0496	1.7247	0.0183	0.2582	0.2399
		c.2*	110	0.0005	0.3112	0.0824	0.0499	1.6738	0.0172	0.2656	0.2484
		c.3	120	0.0005	0.3112	0.0850	0.0534	1.5549	0.0137	0.2685	0.2548
	11/26/18 2:00	c.1	100	0.0004	0.3307	0.0990	0.0725	1.6710	0.0362	0.2713	0.2352
		c.2*	110	0.0026	0.3307	0.1017	0.0737	1.6627	0.0389	0.2789	0.2400
		c.3	120	0.0004	0.3307	0.1052	0.0781	1.4985	0.0372	0.2802	0.2430
	12/9/18 16:08	c.1	100	0.0008	0.3632	0.1067	0.0666	1.5854	0.0247	0.3351	0.3104
		c.2*	110	0.0010	0.3626	0.1069	0.0645	1.5953	0.0246	0.3376	0.3130
		c.3	120	0.0010	0.3635	0.1093	0.0689	1.5011	0.0208	0.3379	0.3171
	2/8/19 10:08	c.1	100	0.0001	0.3612	0.0992	0.0712	1.7657	0.0395	0.2792	0.2397
		c.2*	110	0.0046	0.3612	0.1022	0.0727	1.7535	0.0419	0.2895	0.2476
		c.3	120	0.0000	0.3612	0.1051	0.0756	1.6183	0.0400	0.2923	0.2524
	2/24/19 16:08	c.1	100	0.0001	0.3109	0.0851	0.0595	1.7644	0.0325	0.2474	0.2149
		c.2*	110	0.0007	0.3109	0.0878	0.0601	1.7528	0.0352	0.2558	0.2207
		c.3	120	0.0000	0.3109	0.0902	0.0634	1.5881	0.0307	0.2589	0.2282
	3/26/19 20:08	c.1	100	0.0002	0.3114	0.0849	0.0551	1.7281	0.0251	0.2620	0.2369
		c.2*	110	0.0002	0.3114	0.0879	0.0557	1.6878	0.0270	0.2703	0.2433
		c.3	120	0.0002	0.3114	0.0905	0.0598	1.5451	0.0209	0.2731	0.2522

APPENDIX B

SUPPLEMENTARY FIGURES

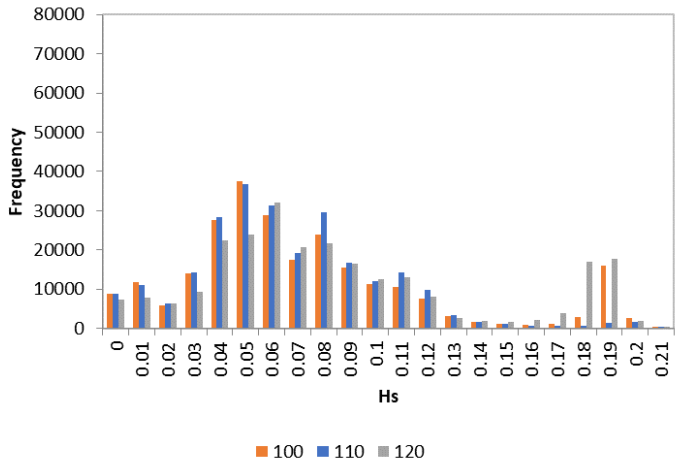

Figure B.1 Distribution of Hs for linear shape with 110 100 120 distances during a low event occurred in 2/1/19-3:00

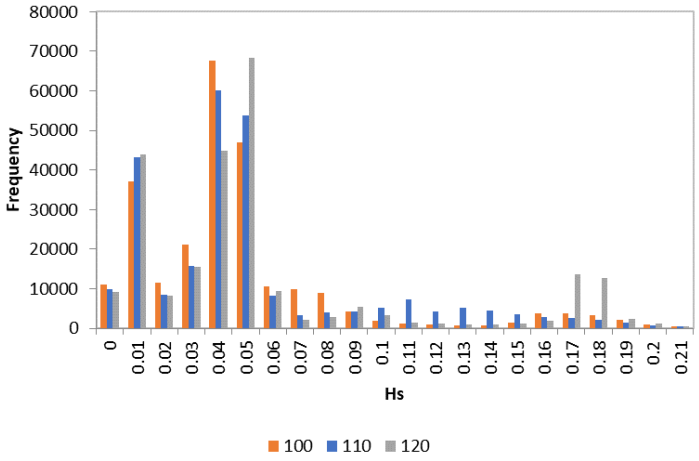

Figure B.2 Distribution of Hs for chevron shape with 110 100 120 distances during a low event occurred in 2/1/19-3:00

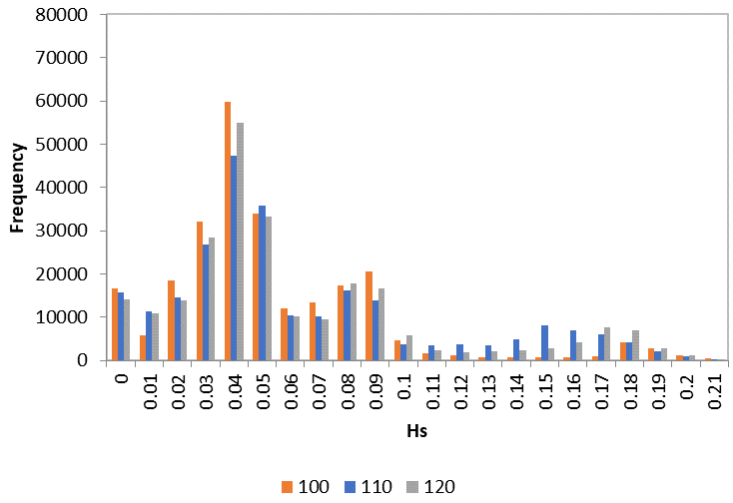

Figure B.3 Distribution of Hs for square shape with 110 100 120 distances during a low event occurred in 2/1/19-3:00

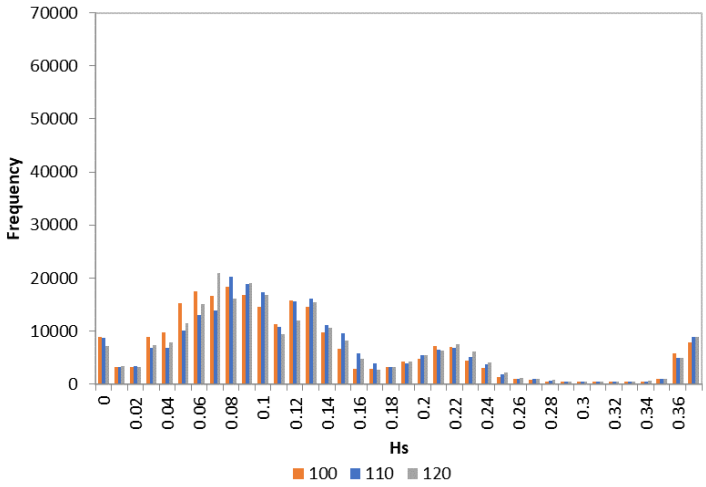

Figure B.4 Distribution of Hs for Linear shape with 110 100 120 distances during a post frontal event occurred in 12/9/18-16:00

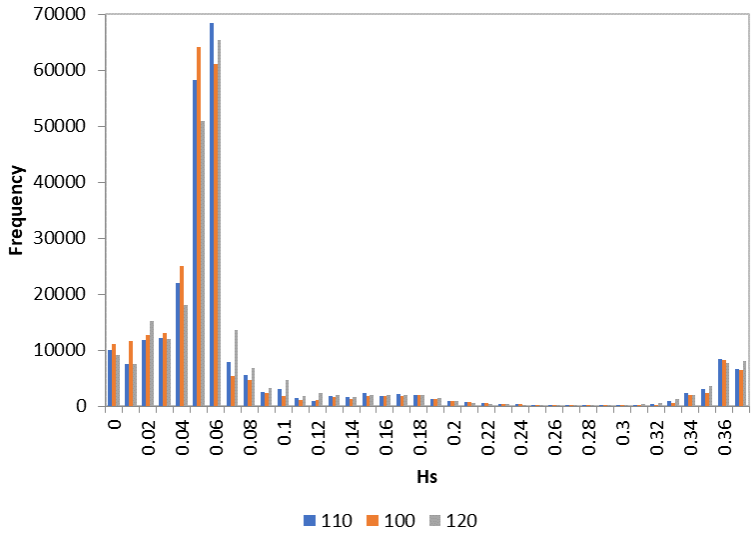

Figure B.5 Distribution of Hs for Chevron shape with 110 100 120 distances during a post frontal event occurred in 12/9/18-16:00

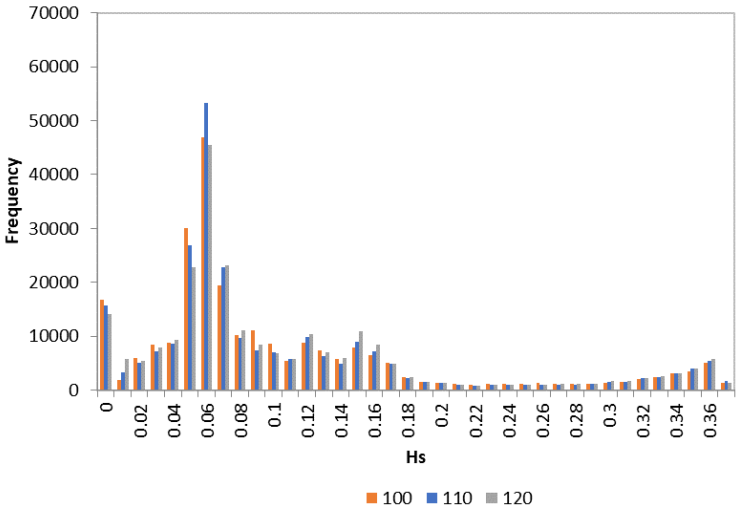

Figure B.6 Distribution of Hs for square shape with 110 100 120 distances during a post frontal event occurred in 12/9/18-16:00